

Stress Assessments of Browns Ferry Nuclear
Unit 2 Steam Dryer with Tie Bar and Hood Modifications

Revision 0

Prepared by

Continuum Dynamics, Inc.
34 Lexington Avenue
Ewing, NJ 08618

Prepared under Purchase Order No. 00053157 for

TVA / Browns Ferry Nuclear Plant
Nuclear Plant Road, P. O. Box 2000 PAB-2M
Decatur, AL 35609

Approved by



Alan J. Bilanin
Reviewed by



Milton E. Teske
June 2008

This report complies with Continuum Dynamics, Inc. Nuclear Quality Assurance Program currently in effect.

Executive Summary

The finite element model and analysis methodology, used to assess stresses induced by the flow of steam through the steam dryer at Brown Ferry Nuclear Unit 2 (BFN2), are described and applied to obtain stresses at CLTP conditions. The resulting stresses are assessed for compliance with the ASME B&PV Code, Section III, subsection NG, for the load combination corresponding to normal operation (the Level A Service Condition). The results presented herein account for proposed modifications to the BFN2 steam dryer designed to improve stress margins under EPU operation. In particular, changes to the tie bars, hood and steam dam gussets have been incorporated to promote alternating stress ratios above 2.0 at EPU conditions.

The analysis is carried out in the frequency domain, which confers a number of useful computational advantages over a time-accurate transient analysis including the ability to assess the effects of frequency scalings in the loads without the need for additional finite element calculations. [[

^{(3)]} The analysis develops a series of unit stress solutions corresponding to the application of a unit pressure at a MSL at specified frequency, f . Each unit solution is obtained by first calculating the associated acoustic pressure field using a separate analysis that solves the damped Helmholtz equation within the steam dryer [1]. This pressure field is then applied to a finite element structural model of the steam dryer and the harmonic stress response at frequency, f , is calculated using the commercial ANSYS 10.0 finite element analysis software. This stress response constitutes the unit solution and is stored as a file for subsequent processing. Once all unit solutions have been computed, the stress response for any combination of MSL pressure spectrums (obtained by Fast Fourier Transform of the pressure histories in the MSLs) is determined by a simple matrix multiplication of these spectrums with the unit solutions.

Results obtained from application of the methodology to the BFN2 steam dryer prior to the installation of acoustic side branches (ASBs) show that at nominal CLTP operation the minimum alternating stress ratio (SR-a) anywhere on the steam dryer is $SR-a=2.91$. The loads used to obtain this value account for all the end-to-end biases and uncertainties in the loads model [2] and finite element analysis. In order to account for uncertainties in the modal frequency predictions of the finite element model, the stresses are also computed for loads that are shifted in the frequency domain by $\pm 2.5\%$, $\pm 5\%$, $\pm 7.5\%$ and $\pm 10\%$. The minimum alternating stress ratio encountered at any frequency shift is found to be $SR-a=2.59$ occurring at the $+7.5\%$ shift. The stress ratio due to maximum stresses (SR-P) is dominated by static loads and is $SR-P=1.88$ without frequency shifts and $SR-P=1.81$ when frequency shifts are considered.

These values do *not* account for the ASBs that will be installed as part of the extended power uprate modifications for BFN2. When ASBs are installed, the smallest alternating stress ratio increases to $SR-a=2.81$ at CLTP. This corresponds to a value of $SR-a=2.13$ at EPU conditions which is expected to qualify the Unit 2 dryer for EPU operation.

Table of Contents

Section	Page
Executive Summary	i
Table of Contents	ii
1. Introduction and Purpose	1
2. Methodology	3
2.1 Overview	3
2.2 [[..... ⁽³⁾]]	5
2.3 Computational Considerations	6
3. Finite Element Model Description	9
3.1 Steam Dryer Geometry	9
3.2 Material Properties	14
3.3 Model Simplifications	14
3.4 Perforated Plate Model	15
3.5 Vane Bank Model	16
3.6 Water Inertia Effect on Submerged Panels	17
3.7 Structural Damping	17
3.8 Mesh Details and Element Types	17
3.9 Connections Between Structural Components	18
3.10 Pressure Loading	29
4. Structural Analysis	32
4.1 Static Analysis	32
4.2 Harmonic Analysis	32
4.3 Post-Processing	37
4.4 Computation of Stress Ratios for Structural Assessment	37
5. Results	41
5.1 General Stress Distribution and High Stress Locations	43
5.2 Load Combinations and Allowable Stress Intensities	56
5.3 Frequency Content and Filtering of the Stress Signals	74
6. Conclusions	80
7. References	81
Appendix A. Local Stress Corrections Resulting from Finalized Modification Designs	83

1. Introduction and Purpose

Plans to qualify the Browns Ferry nuclear plant for operation at Extended Power Uprate (EPU) operating condition require an assessment of the steam dryer stresses experienced under the increased loads. The steam dryer loads due to pressure fluctuations in the main steam lines (MSLs) are potentially damaging and the cyclic stresses from these loads can produce fatigue cracking if loads are sufficiently high. The industry has addressed this problem with physical modifications to the dryers, as well as a program to define steam dryer loads and their resulting stresses. The purpose of the stress analysis discussed here is to calculate the maximum and alternating stresses generated during Current Licensed Thermal Power (CLTP) and determine the margins that exist when compared to stresses that comply with the ASME Code (ASME B&PV Code, Section III, subsection NG).

The stress analysis considered here incorporates proposed design changes to the Browns Ferry Unit 2 (BFN2) steam dryer. In a previous stress analysis of the BFN2 steam dryer [3] using the same methodology, it was determined that the limiting alternating stress was $SR-a=1.65$ at CLTP which, when extrapolated to EPU conditions, arrives significantly below the desired $SR-a=2.0$ EPU target. Virtually all of the high stress regions occurred where the tie bars connect to the top cover plates of the vane banks. This prompted a redesign of the tie bars to alleviate these stresses. Using the frequency-based stress analysis described herein it was possible to rapidly analyze proposed modifications and thus arrive at a successful tie bar design with tapered and widened ends that brings the alternating stress ratios at the tie bar/top cover plate connections to well above 3.0 at CLTP operation. Since the outermost tie bars on the existing configuration also help support the steam dam, it was found necessary to add additional steam dam gussets. The final design of the modified steam dam and associated gussets is also included in the present analysis.

The stress analysis of the modified BFN2 steam dryer establishes whether the existing and proposed modifications are adequate for sustaining structural integrity and preventing future weld cracking under planned EPU operating conditions. The load combination considered here corresponds to normal operation (the Level A Service Condition) and includes fluctuating pressure loads developed from BFN2 main steam line data, and weight. The fluctuating pressure loads, induced by the flowing steam, are predicted using a separate acoustic circuit analysis of the steam dome and main steam lines [4]. Level B service conditions, which include seismic loads, are not included in this evaluation.

[[

(3)]]

[[⁽³⁾]] This approach also affords a number of additional computational advantages over transient simulations including: [[

⁽³⁾]] This last advantage is realized through the use of “unit” solutions representing the stress distribution resulting from the application of a unit fluctuating pressure at one of the MSLs at a particular frequency. [[⁽³⁾]]

This report describes the overall methodology used to obtain the unit solutions in the frequency domain and how to assemble them into a stress response for a given combination of pressure signals in the MSLs. This is followed by details of the BFN2 steam dryer finite element model including the elements used and overall resolution, treatment of connections between elements, the hydrodynamic model, the implementation of structural damping and key idealizations/assumptions inherent to the model. Post-processing procedures are also reviewed including the computation of maximum and alternating stress intensities, identification of high stress locations, adjustments to stress intensities at welds and evaluation of stress ratios used to establish compliance with the ASME Code. The results in terms of stress intensity distributions and stress ratios are presented next together with PSDs of the dominant stress components.

2. Methodology

2.1 Overview

Based on previous analysis undertaken at Quad Cities Units 1 and 2, the steam dryer can experience strong acoustic loads due to the fluctuating pressures in the MSLS connected to the steam dome containing the dryer. C.D.I. has developed an acoustic circuit model (ACM) that, given a collection of strain gage measurements [5] of the fluctuating pressures in the MSLS, predicts the acoustic pressure field anywhere inside the steam dome and on the steam dryer [1,2,4]. The ACM is formulated in frequency space and contains two major components that are directly relevant to the ensuing stress analysis of concern here. [[

(1)

(2)

⁽³⁾]]

[[

(3)

(4)

(5)

⁽³⁾]]

[[

(6)

⁽³⁾]]

2.2 [[
[[

⁽³⁾]]

⁽³⁾]]

[[

(3)]]

2.3 Computational Considerations

Focusing on the structural computational aspects of the overall approach, there are a number of numerical and computational considerations requiring attention. The first concerns the transfer of the acoustic forces onto the structure, particularly the spatial and frequency resolutions. The ANSYS finite element program inputs general distributed pressure differences using a table format. This consists of regular 3D rectangular (i.e., block) $n_x \times n_y \times n_z$ mesh where n_α is the number of mesh points in the i -th Cartesian direction and the pressure difference is provided at each mesh point (see Section 3.10). These tables are generated separately using a program that reads the loads provided from the ACM software, distributes these loads onto the finite element mesh using a combination of interpolation procedures on the surface and simple diffusion schemes off the surface (off-surface loads are required by ANSYS to ensure proper interpolation of forces), and written to ASCII files for input to ANSYS. A separate load file is written at each frequency for the real and imaginary component of the complex force.

The acoustic field is stored at 5 Hz intervals from 0 to 250 Hz. While a 5 Hz resolution is sufficient to capture frequency dependence of the acoustic field (i.e., the pressure at a point varies gradually with frequency), it is too coarse for representing the structural response especially at low frequencies. For 1% critical structural damping, one can show that the frequency spacing needed to resolve a damped resonant peak at natural frequency, f_n , to within 5% accuracy is $\Delta f = 0.0064 \times f_n$. Thus for $f_n = 10$ Hz where the lowest structural response modes occur, a frequency interval of 0.064 Hz or less is required. In our calculations we require that 5% maximum error be maintained over the range from $f_n = 5$ Hz to 250 Hz resulting in a finest frequency interval of 0.0321 Hz at the low frequency end (this adequately resolves all structural modes up to 250 Hz). Since there are no structural modes between 0 to 5 Hz, a 0.5 Hz spacing is used over this range with minimal (less than 5%) error. The unit load, $\hat{f}_n(\omega, \mathbf{R})$, at any frequency, ω_k , is obtained by linear interpolation of the acoustic solutions at the two nearest frequencies, ω_i and ω_{i+1} , spaced 5 Hz apart. Linear interpolation is sufficient since the pressure load varies slowly over the 5 Hz range (linear interpolation of the structural response would not be acceptable over this range since it varies much more rapidly over the same interval).

Solution Management

[[

(3)]]

[[

(3)]]

Structural Damping

In harmonic analysis one has a broader selection of damping models than in transient simulations. A damping factor, z , of 1% critical damping is used in the structural analysis. In transient simulations, this damping can only be enforced exactly at two frequencies (where the damping model is “pinned”). Between these two frequencies the damping factor can be considerably smaller, for example 0.5% or less depending on the pinning frequencies. Outside the pinning frequencies, damping is higher. With harmonic analysis it is straightforward to enforce very close to 1% damping over the entire frequency range. In this damping model, the damping matrix, \mathbf{D} , is set to

$$\mathbf{D} = \frac{2z}{\omega} \mathbf{K} \quad (7)$$

where \mathbf{K} is the stiffness matrix and ω the forcing frequency. One can show that with this model the damping factor varies between 0.995% and 1.005% which is a much smaller variation than using the pinned model required in transient simulation.

Load Frequency Rescaling

One way to evaluate the sensitivity of the stress results to approximations in the structural modeling and applied loads is to rescale the frequency content of the applied loads. In this procedure the nominal frequencies, ω_k , are shifted to $(1+\lambda)\omega_k$, where the frequency shift, λ , ranges between $\pm 10\%$, and the response recomputed for the shifted loads. The objective of the frequency shifting can be explained by way of example. Suppose that in the actual dryer a strong structural-acoustic coupling exists at a particular frequency, ω^* . This means that the following conditions hold simultaneously: (i) the acoustic signal contains a significant signal at ω^* ; (ii) the structural model contains a resonant mode of natural frequency, ω_n , that is near ω^* ; and (iii) the associated structural mode shape is strongly coupled to the acoustic load (i.e., integrating the product of the mode shape and the surface pressure over the steam dryer surface produces a significant modal force). Suppose now that because of discretization errors and modeling idealizations that the predicted resonance frequency differs from ω^* by a small amount (e.g., 1.5%). Then condition (ii) will be violated and the response amplitude therefore significantly

diminished. By shifting the load frequencies one re-establishes condition (ii) when $(1 + \lambda)\omega^*$ is near ω_n . The other two requirements also hold and a strong structural acoustic interaction is restored.

[[(6)

(3)]]

Evaluation of Maximum and Alternating Stress Intensities

Once the unit solutions have been obtained, the most intensive computational steps in the generation of stress intensities are: (i) the FFTs to evaluate stress time histories from (5); and (ii) the calculation of alternating stress intensities. [[

(3)]]

The high computational penalty incurred in calculating the alternating stress intensities is due to the fact that this calculation involves comparing the stress tensors at every pair of points in the stress history. This comparison is necessary since in general the principal stress directions can vary during the response, thus for N samples in the stress history, there will be $(N-1)N/2$ such pairs or, for $N=64K$ (the number required to accurately resolve the spectrum up to 250 Hz in 0.01 Hz intervals), 2.1×10^9 calculations per node each requiring the determination of the roots to a cubic polynomial. [[

(3)]]

3. Finite Element Model Description

A description of the ANSYS model of the Browns Ferry Unit 2 steam dryer follows.

3.1 Steam Dryer Geometry

A geometric representation of the Browns Ferry Unit 2 steam dryer was developed from available drawings (provided by TVA and included in the design record file, DRF-TVA-250B) within the Workbench module of ANSYS. The completed model is shown in Figure 1. This model includes anticipated modifications to the Browns Ferry Unit 2 steam dryer site and additional modifications proposed for EPU operation. These are as follows.

On-Site Modifications

- (i) The top tie rods are replaced with thicker new ones installed on Unit 1. The gussets on the top of the outer hoods supporting the steam dam plate are cut away to facilitate installation of the new tie bars and possibly alleviate local stresses.

Previous analysis [3] showed significant stresses at the welds where the thicker tie bars connect to the top cover plates which would result in alternating stress ratios at EPU below the target level of 2.0. Therefore, additional design modifications were proposed to reduce these stresses to target levels. These changes, which effectively paralleled similar modifications to the BFN1 dryer were implemented in Model 1 described below and a complete stress analysis carried out. As discussed in Appendix A, this first redesign, while improving overall stress margins, did not reach target levels at two locations (the front end of the gusset pads and the outermost tie bars). As a result, a final modification resulting in FEA Model 2 was implemented. To facilitate schedule while ensuring accuracy, calculations using Model 2 were conducted over a limited frequency range (70.45 - 95.11 Hz) which is responsible for most of the stress contributions at those locations that were modified in proceeding from Model 1 to Model 2. Additional details of this modification improvement process and conservative calculation of the stresses at these sites using the Model 2 analysis are given in Appendix A.

The additional changes were as follows:

Additional Modifications Proposed For EPU Operation – Model 1

- (ii) Remove the thicker tie bars connecting to the inner hoods (i.e., those connecting the inner to inner hoods and those connecting the inner to middle hoods) and replace them with ones having tapered and flared ends to more evenly distribute loads at the end connections.
- (iii) Similarly, replace the thicker tie bars connecting to the outer hoods with the modified ones having flared and tapered ends. However, rather than completely removing the existing tie bars, part of it is retained to support the lock gusset and restrain motion of the steam dam. The portion extending between the steam dam to the middle hood is removed.
- (iv) Add three additional gussets to support each of the two steam dams.

Further Modifications Proposed For EPU Operation – Model 2

- (v) Further modify the outermost tie bars at the location where they land on the top of the middle vane bank. Specifically, they are widened locally to a 3" width and a vertical tapered and flared pad added to distribute some of the loads into the thicker middle hood.
- (vi) The gusset bases in (iv) extend all the way to the outer hood. This was found to produce high stresses at the gusset pad/outer hood junction. Therefore they were retracted by 3". Also 3" wide reinforcement strips were placed on the outer hood top cover plates along the hood edge.
- (vii) The tie bar/lock gusset assemblies in (iii) above were removed from the model (they do not exist in the actual BFN2 unit at this point in time) and replaced by gussets identical to those in (vi) so that a total of five new gussets are installed to support the steam dam. These are in addition to the existing ones at the ends of the steam dam.

These additional modifications have been incorporated into the BFN2 steam dryer model and are reflected in the results presented in this report. The modified areas using Model 2 are shown in Figure 2. As indicated above, the dryer was analyzed for the complete 0-250 Hz frequency range using Model 1. The resulting stresses prompted redesign at three locations (v)-(vii) above resulting in Model 2. Stress results were then obtained at locations (v) to (vii) using Model 2 with a reduced frequency range signal. The stresses were readjusted on the basis of the Model 1 predictions to account for the contributions from the neglected frequency components. In the results and Tables in Section 5, locations that have been adjusted using Model 2 are indicated. Everywhere else, the Model 1 stress predictions are reported.



Figure 1. Overall geometry of the Browns Ferry Unit 2 steam dryer model.

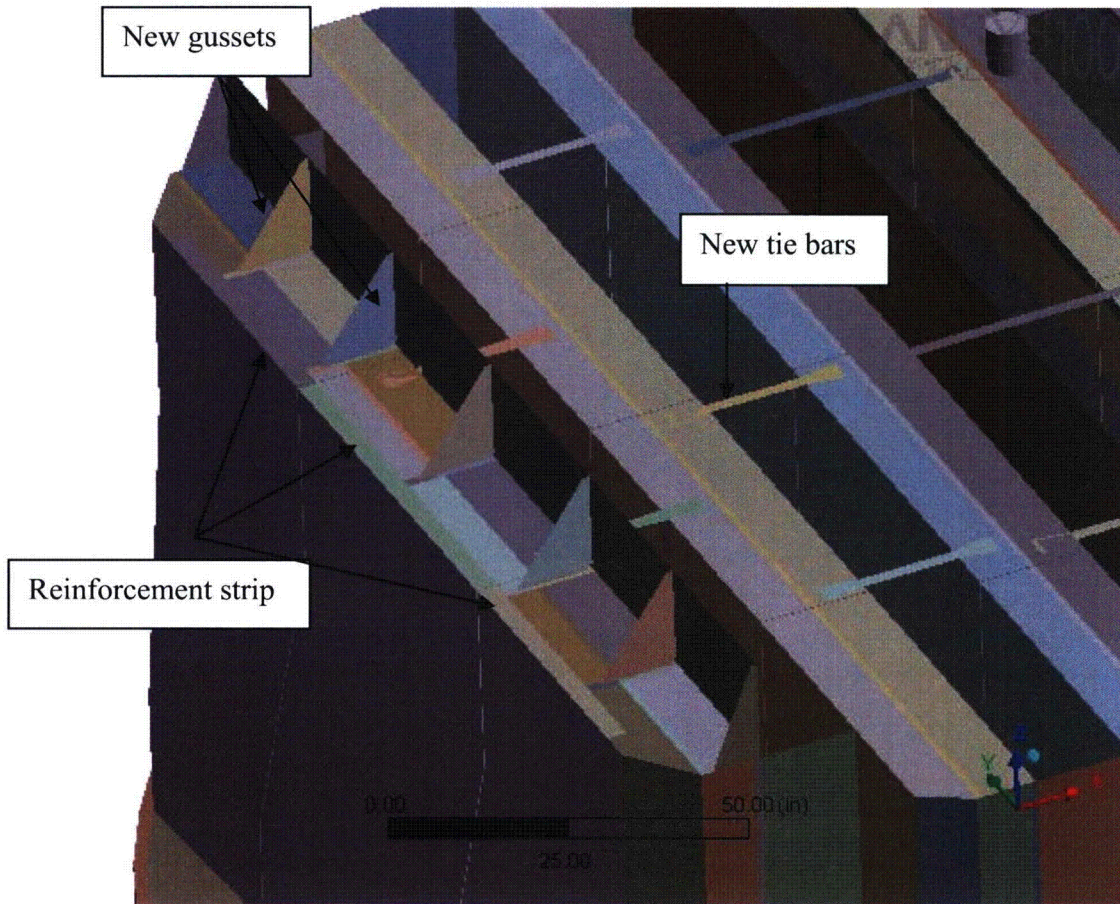


Figure 2a. Anticipated modifications accounted for in the model and associated geometrical details.



Figure 2b. Vertical plate (or pad) additions to tie bars at middle hood junction.

3.2 Material Properties

The steam dryer is constructed from Type 304 stainless steel and has an operating temperature of 550°F. Properties used in the analysis are summarized below in Table 1.

Table 1. Material properties.

	Young's Modulus (10 ⁶ psi)	Density (lbm/in ³)	Poisson Ratio
Structural Steel	25.55	0.284	0.3
Structural Steel with Added Water Inertia Effect	25.55	1.055	0.3

The structural steel modulus is taken from Appendix A of the ASME Code for Type 304 Stainless Steel at an operating temperature 550°F. The effective properties of perforated plates and submerged parts are discussed in Sections 3.4 and 3.6. Note that the increased effective density for submerged components is only used in the harmonic analysis. When calculating the stress distribution due to the static dead weight load, the unmodified density of steel (0.284 lbm/in³) is used throughout.

3.3 Model Simplifications

The following simplifications were made to achieve reasonable model size while maintaining good modeling fidelity for key structural properties:

- Perforated plates were approximated as continuous plates using modified elastic properties designed to match the static and modal behaviors of the perforated plates. The perforated plate structural modeling is summarized in Section 3.4 and Appendix C of [8].
- The drying vanes were replaced by point masses attached to the corresponding trough bottom plates and vane bank top covers (Figure 4). The bounding perforated plates, vane bank end plates, and vane bank top covers were explicitly modeled (see Section 3.5).
- The added mass properties of the lower part of the skirt below the reactor water level were obtained using a separate hydrodynamic analysis (see Section 3.6).
- [[⁽³⁾]]
- Four steam dryer support brackets that are located on the reactor vessel and spaced at 90° intervals were explicitly modeled (see Section 3.9).
- Most welds were replaced by node-to-node connections; interconnected parts share common nodes along the welds. In other locations the constraint equations between nodal degrees of freedom were introduced as described in Section 3.9.

3.4 Perforated Plate Model

The perforated plates were modeled as solid plates with adjusted elastic and dynamic properties. Properties of the perforated plates were assigned according to the type and size of perforation. Based on [10], for an equilateral square pattern with given hole size and spacing, the effective moduli of elasticity were found.

The adjusted properties for the perforated plates are shown in Table 2 as ratios to material properties of structural steel, provided in Table 1. Locations of perforated plates are classified by steam entry / exit vane bank side and vertical position.

Tests were carried out to verify that this representation of perforated plates by continuous ones with modified elastic properties preserves the modal properties of the structure. These tests are summarized in Appendix C of [8] and compare the predicted first modal frequency for a cantilevered perforated plate against an experimentally measured value. The prediction was obtained for a 40% open area plate (the maximum open area ratio of the perforated plates at BFN2, as seen in Table 2) using the analytical formula for a cantilevered plate and the modified Young's modulus and Poisson's ratio given by O'Donnell [10]. The measured and predicted frequencies are in close agreement, differing by less than 3%.

[[

(see Figure 3).

Table 2

⁽³⁾]]

[[

(3)]]

Figure 3. [[

(3)]]

Table 2. Material properties of perforated plates.

[[

(3)]]

3.5 Vane Bank Model

The vane bank assemblies consist of many vertical angled plates that are computationally expensive to model explicitly, since a prohibitive number of elements would be required. These parts have significant weight which is transmitted through the surrounding structure, so it is important to capture their gross inertial properties. Here the vane banks are modeled as a collection of point masses located at the center of mass for each vane bank section (Figure 4). The following masses were used for the vane bank sections, based on data found on provided drawings:

inner banks, 1575 lbm, 4 sections per bank;

middle banks, 1450 lbm, total 4 sections per bank; and
outer banks, 1515 lbm, 3 sections per bank.

These masses were applied to the base plates and vane top covers using the standard ANSYS point mass modeling option, element MASS21. ANSYS automatically distributes the point mass inertial loads to the nodes of the selected structure. The distribution algorithm minimizes the sum of the squares of the nodal inertial forces, while ensuring that the net forces and moments are conserved. Vane banks are not exposed to main steam lines directly, but rather shielded by the hoods.

The collective stiffness of the vane banks is expected to be small compared to the surrounding support structure and is neglected in the model. In the static case it is reasonable to expect that this constitutes a conservative approach, since neglecting the stiffness of the vane banks implies that the entire weight is transmitted through the adjacent vane bank walls and supports. In the dynamic case the vane banks exhibit only a weak response since (i) they have large inertia so that the characteristic acoustically-induced forces divided by the vane masses and inertias yield small amplitude motions, velocities and accelerations; and (ii) they are shielded from acoustic loads by the hoods, which transfer dynamic loads to the rest of the structure. Thus, compared to the hoods, less motion is anticipated on the vane banks so that approximating their inertial properties with equivalent point masses is justified. Nevertheless, the bounding parts, such as perforated plates, side panels, and top covers, are retained in the model. Errors associated with the point mass representation of the vane banks are compensated for by frequency shifting of the applied loads.

3.6 Water Inertia Effect on Submerged Panels

Water inertia was modeled by an increase in density of the submerged structure to account for the added hydrodynamic mass. This added mass was found by a separate hydrodynamic analysis (included in DRF-TVA-250B supporting this report) to be 0.1928 lbm/in^2 on the submerged skirt area. This is modeled by effectively increasing the material density for the submerged portions of the skirt. Since the skirt is 0.25 inches thick, the added mass is equivalent to a density increase of 0.771 lbm/in^3 . This added water mass was included in the ANSYS model by appropriately modifying the density of the submerged structural elements when computing harmonic response. For the static stresses, the unmodified density of steel is used throughout.

3.7 Structural Damping

Structural damping was defined as 1% of critical damping for all frequencies. This damping is consistent with guidance given on pg. 10 of NRC RG-1.20 [14].

3.8 Mesh Details and Element Types

Shell elements were employed to model the skirt, hoods, perforated plates, side and end plates, trough bottom plates, reinforcements, base plates and cover plates. Specifically, the four-node, Shell Element SHELL63, was selected to model these structural components. This element models bending and membrane stresses, but omits transverse shear. The use of shell elements is appropriate for most of the structure where the characteristic thickness is small compared to the other plate dimensions. For thicker structures, such as the upper and lower

support rings, solid brick elements were used to provide the full 3D stress. Tie bars were modeled with BEAM188 beam elements. The elements SURF154 are used to assure proper application of pressure loading to the structure. Mesh details and element types are shown in Table 3 and Table 4.

The mesh is generated automatically by ANSYS with refinement near edges. The maximum allowable mesh spacing is specified by the user. Here a 2.5 inch maximum allowable spacing is specified everywhere except in the following areas: drain pipes (1.5 inch maximum spacing); base plates (2 inches); tie rods (0.5 inches); and the curved portions of the drain channels (1 inch). Details of the finite element mesh are shown in Figure 5. Numerical experiments carried out using the ANSYS code applied to simple analytically tractable plate structures with dimensions and mesh spacings similar to the ones used for the steam dryer, confirm that the natural frequencies are accurately recovered (less than 1% errors for the first modes). These errors are compensated for by the use of frequency shifting.

3.9 Connections Between Structural Components

Most connections between parts are modeled as node-to-node connections. This is the correct manner (i.e., within the finite element framework) of joining elements away from discontinuities. At joints between shells, this approach omits the additional stiffness provided by the extra weld material. Also, locally 3D effects are more pronounced. The latter effect is accounted for using weld factors. The deviation in stiffness due to weld material is negligible, since weld dimensions are on the order of the shell thickness. The consequences upon modal frequencies and amplitude are, to first order, proportional to t/L where t is the thickness and L a characteristic shell length. The errors committed by ignoring additional weld stiffness are thus small and readily compensated for by performing frequency shifts.

When joining shell and solid elements, however, the problem arises of properly constraining the rotations, since shell element nodes contain both displacement and rotational degrees of freedom at every node whereas solid elements model only the translations. A node-to-node connection would effectively appear to the shell element as a simply supported, rather than (the correct) cantilevered restraint and significantly alter the dynamic response of the shell structure.

To address this problem, constraint equations are used to properly connect adjacent shell- and solid-element modeled structures. Basically, all such constraints express the deflection (and rotation for shell elements) of a node, \mathbf{R}_1 , on one structural component in terms of the deflections/rotations of the corresponding point, \mathbf{P}_2 , on the other connected component. Specifically, the element containing \mathbf{P}_2 is identified and the deformations at \mathbf{P}_2 determined by interpolation between the element nodes. The following types of shell-solid element connections are used in the steam dryer model including the following:

1. Connections of shell faces to solid faces (Figure 6a). While only displacement degrees of freedom are explicitly constrained, this approach also implicitly constrains the rotational degrees of freedom when multiple shell nodes on a sufficiently dense grid are connected to the same solid face.
2. Connections of shell edges to solids (e.g., connection of the bottom of closure plates with the upper ring). Since solid elements do not have rotational degrees of freedom, the

coupling approach consisted of having the shell penetrate into the solid by one shell thickness and then constraining both the embedded shell element nodes (inside the solid) and the ones located on the surface of the solid structure (see Figure 6b). Numerical tests involving simple structures showed that this approach and penetration depth reproduce both the deflections and stresses of the same structure modeled using only solid elements or ANSYS' bonded contact technology. Continuity of rotations and displacements is achieved.

The use of constraint conditions rather than the bonded contacts advocated by ANSYS for connecting independently meshed structural components confers better accuracy and useful numerical advantages to the structural analysis of the steam dryer including better conditioned and smaller matrices. The smaller size results from the fact that equations and degrees of freedom are eliminated rather than augmented (in Lagrange multiplier-based methods) by additional degrees of freedom. Also, the implementation of contact elements relies on the use of very high stiffness elements (in penalty function-based implementations) or results in indefinite matrices (Lagrange multiplier implementations) with poorer convergence behavior compared to positive definite matrices.

The upper support ring rests on four support blocks which resist vertical and lateral displacement. Because the contact region between the blocks and upper support ring is small, the ring is considered free to rotate about the radial axis. Specifically nodal constraints (zero relative displacement) are imposed over the contact area between the steam dryer upper support ring and the support blocks. Two nodes on each support block are fixed as indicated in Figure 7. One node is at the center of the support block surface facing the vessel and the other node is 0.5" offset inside the block towards the steam dryer, half way to the nearest upper support ring node. This arrangement approximates the nonlinear contact condition where the ring can tip about the block.

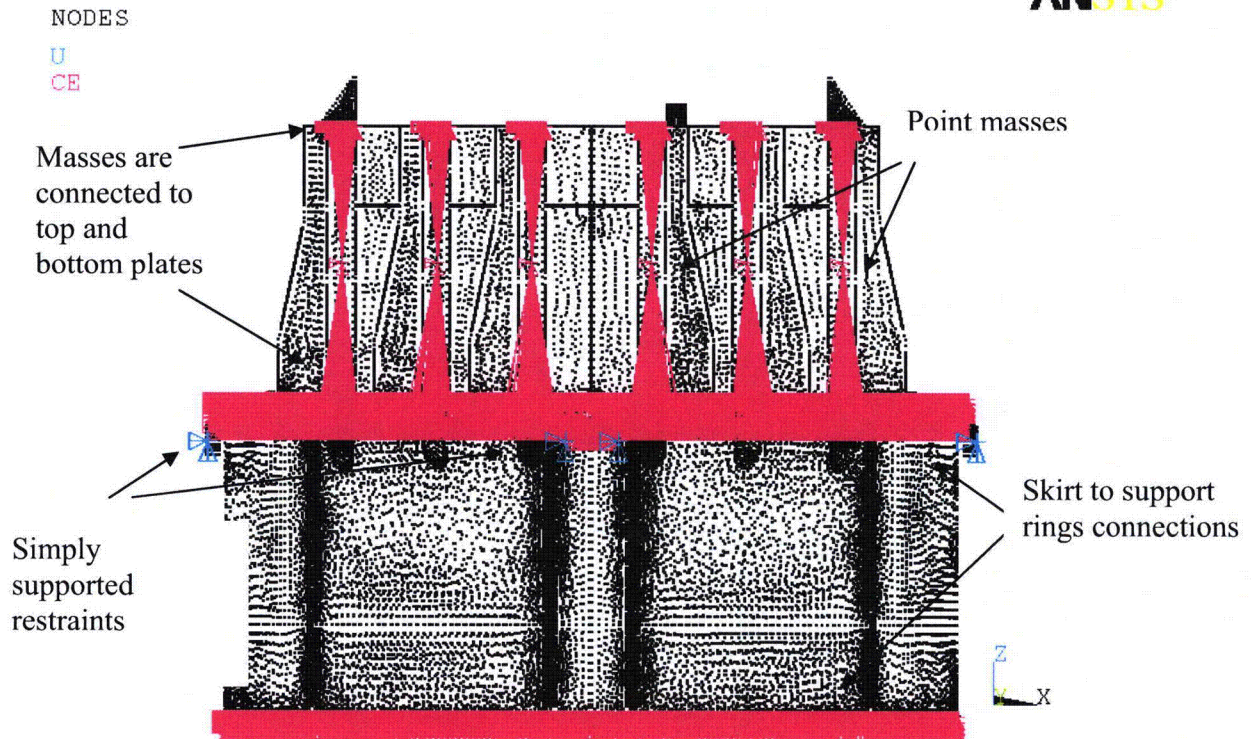


Figure 4. Point masses representing the vanes. The pink shading represents where constraint equations between nodes are applied.

Table 3. FE Model Summary.

Description	Quantity
Total Nodes ¹	137,080
Total Elements	120,557

1. Not including additional damper nodes and elements.

Table 4. Listing of Element Types.

Generic Element Type Name	Element Name	ANSYS Name
20-Node Quadratic Hexahedron	SOLID186	20-Node Hexahedral Structural Solid
10-Node Quadratic Tetrahedron	SOLID187	10-Node Tetrahedral Structural Solid
4-Node Elastic Shell	SHELL63	4-Node Elastic Shell
Mass Element	MASS21	Structural Mass
Pressure Surface Definition	SURF154	3D Structural Surface Effect
Beam element	BEAM188	3-D Finite Strain Beam
Damper element	COMBIN14	Spring-Damper

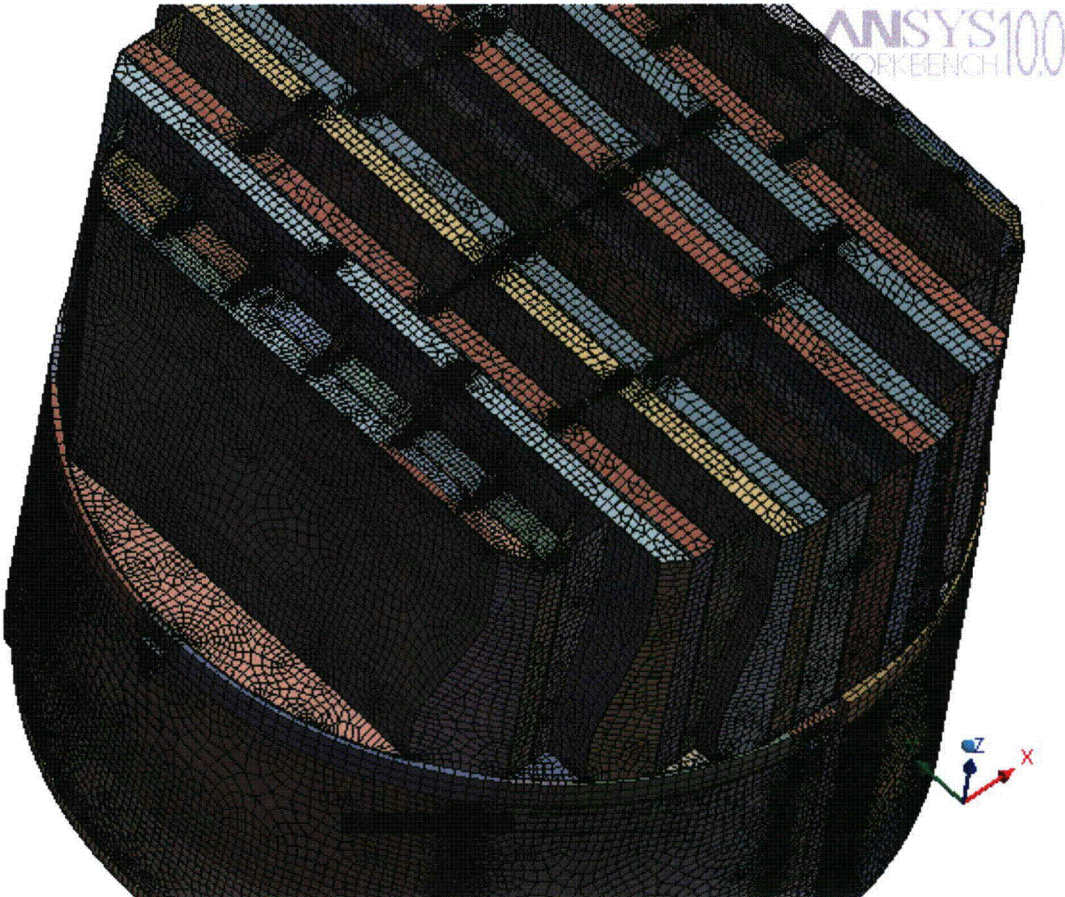


Figure 5a. Mesh overview.

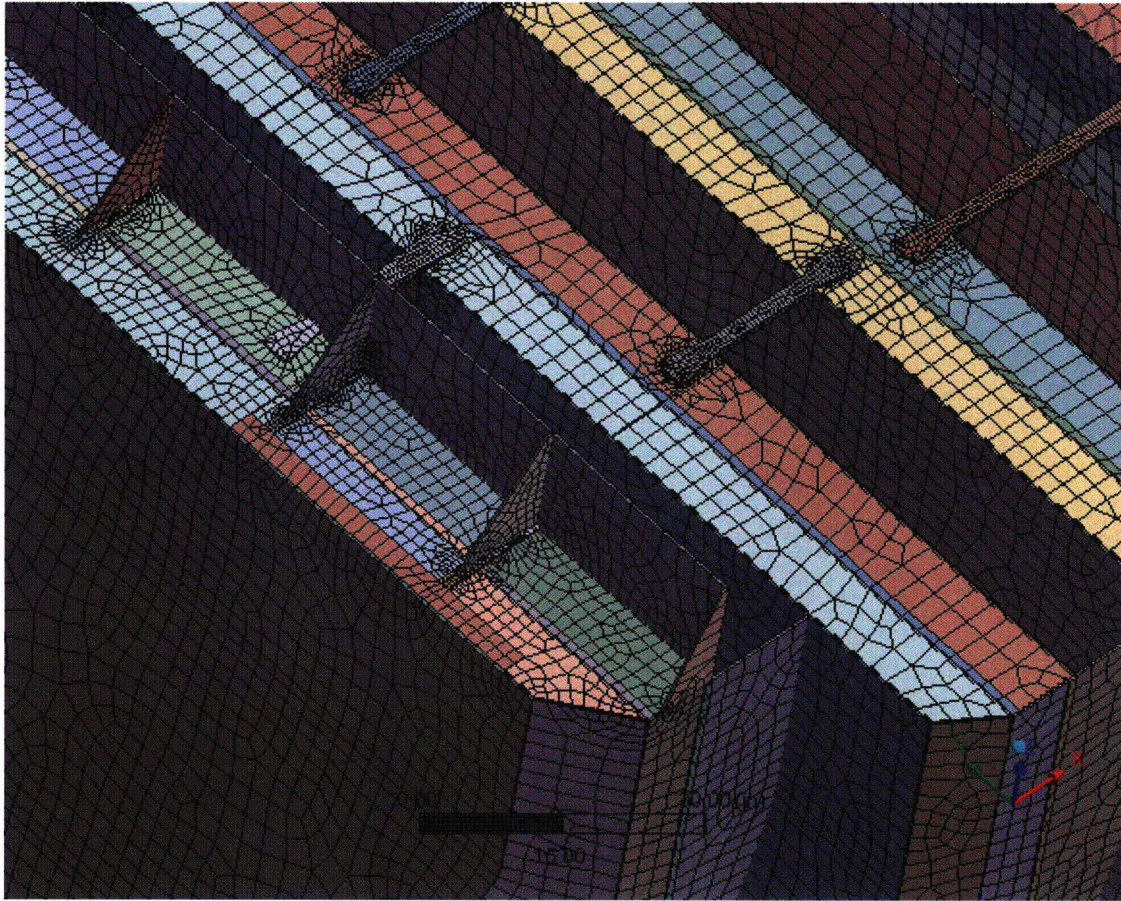


Figure 5b. Close up of mesh showing modified tie bars.

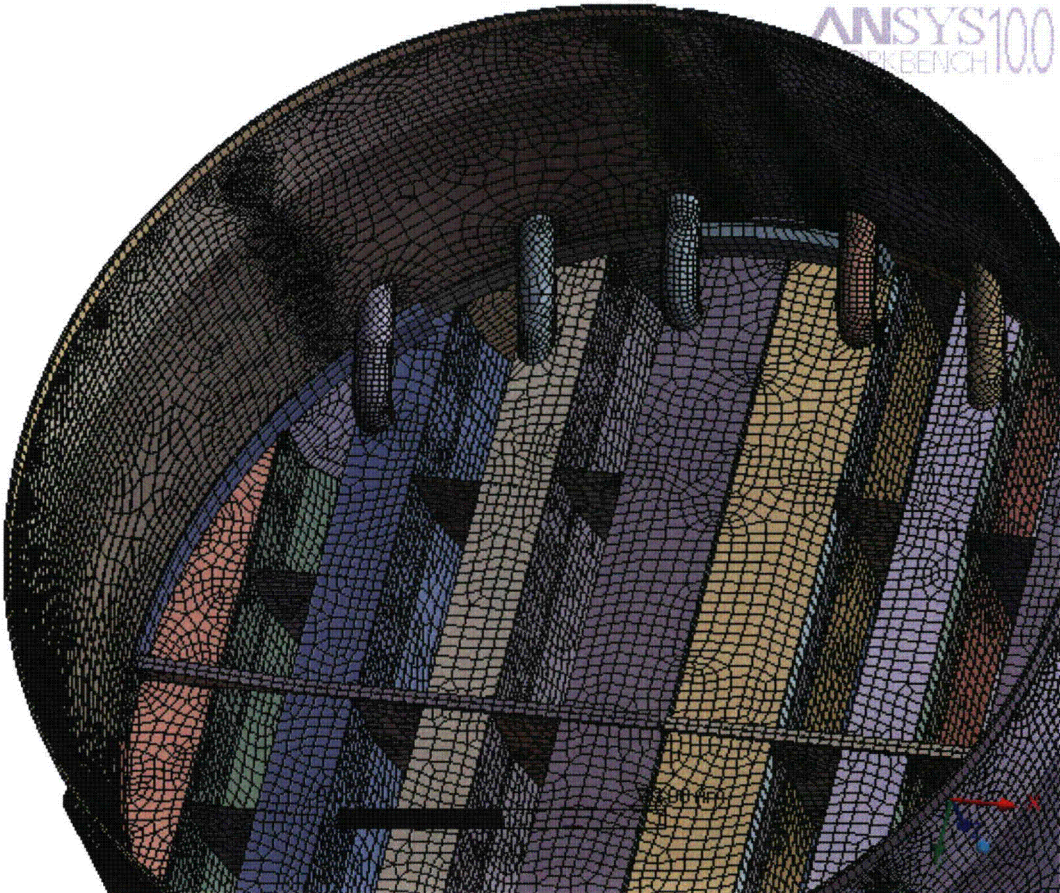


Figure 5c. Close up of mesh showing drain pipes and hood supports.

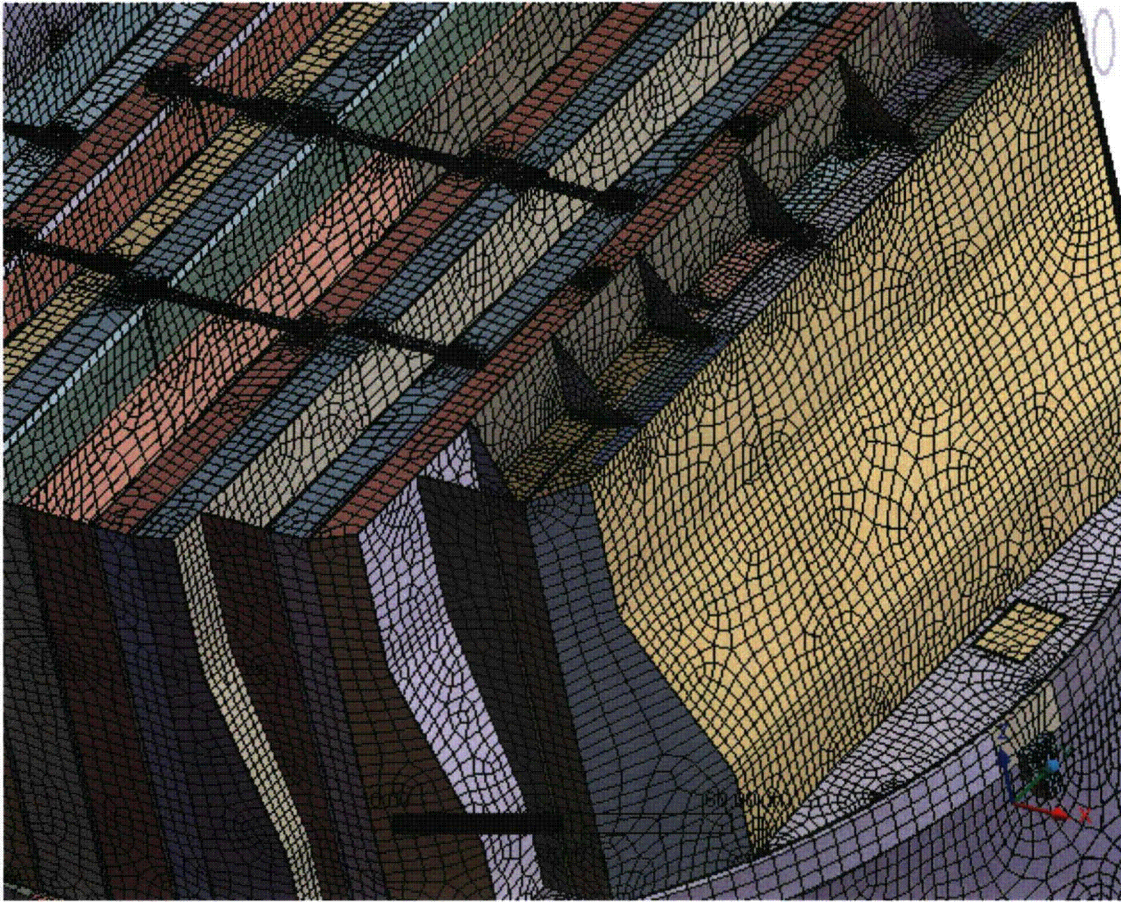


Figure 5d. Close up of mesh showing node-to-node connections between various plates.

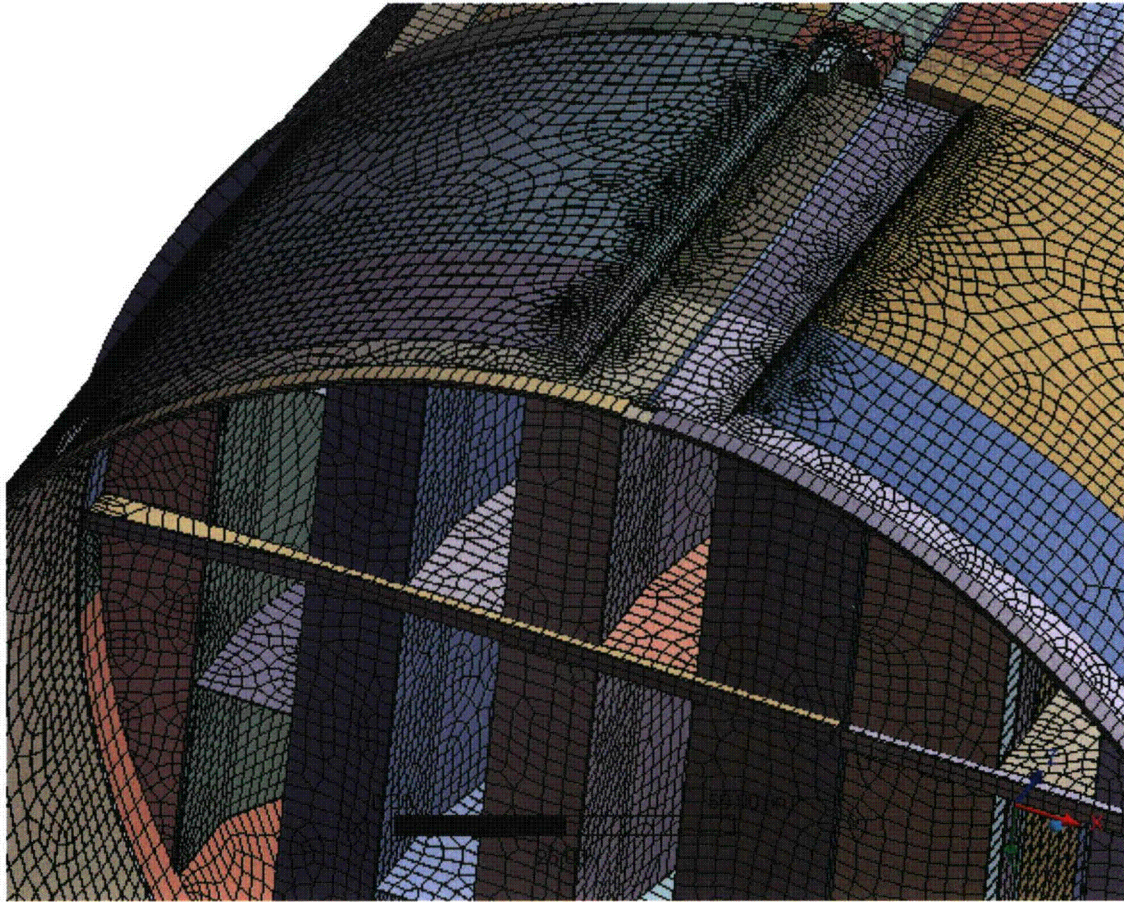


Figure 5e. Close up of mesh showing node-to-node connections between the skirt and drain channels; supporting beams and base plates; hood supports and hoods.

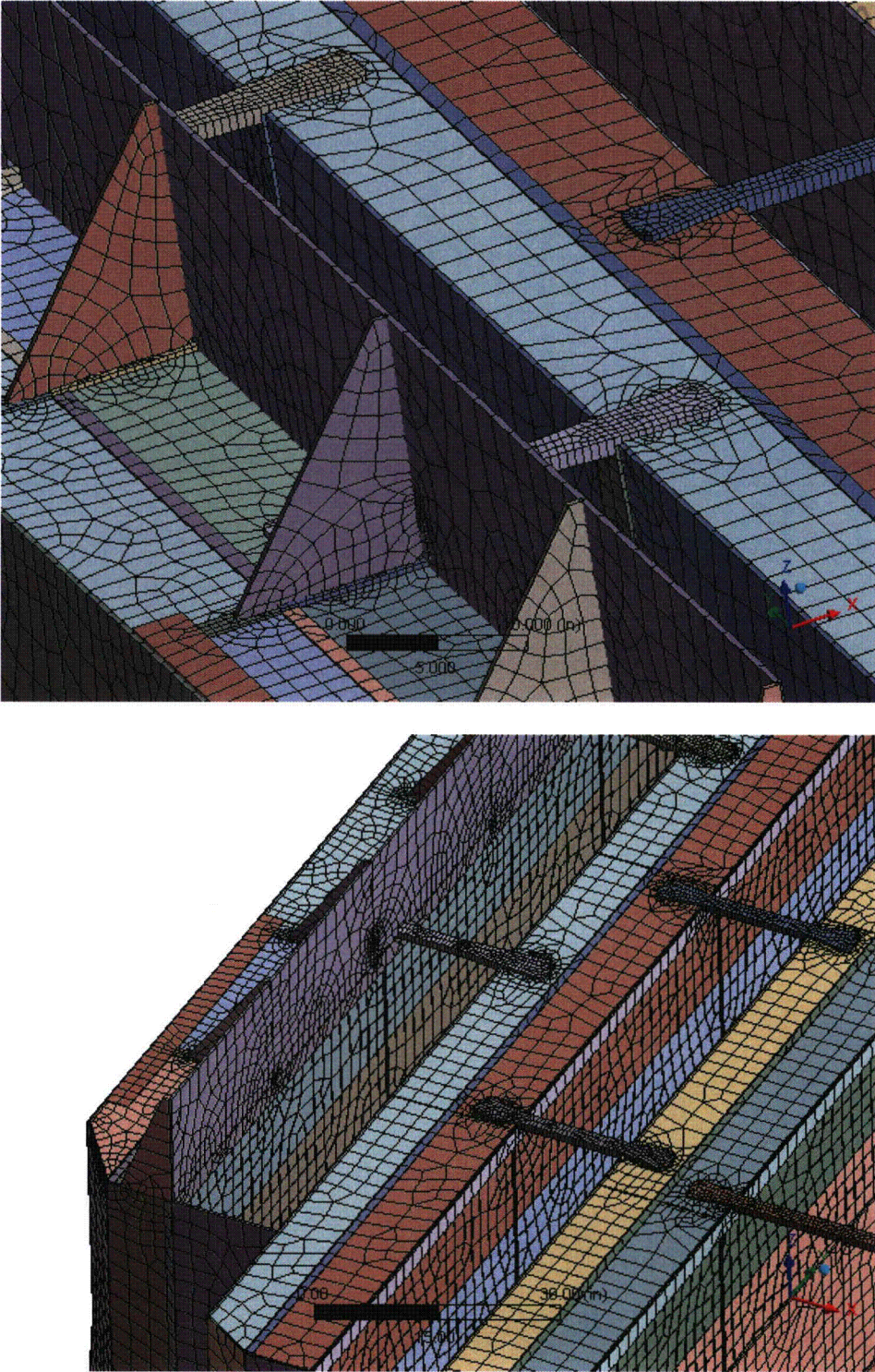


Figure 5f. Close up view of tie bars connecting vane cover plates and adjacent to the steam dam.

Shell nodes DOF are related to solid element shape functions

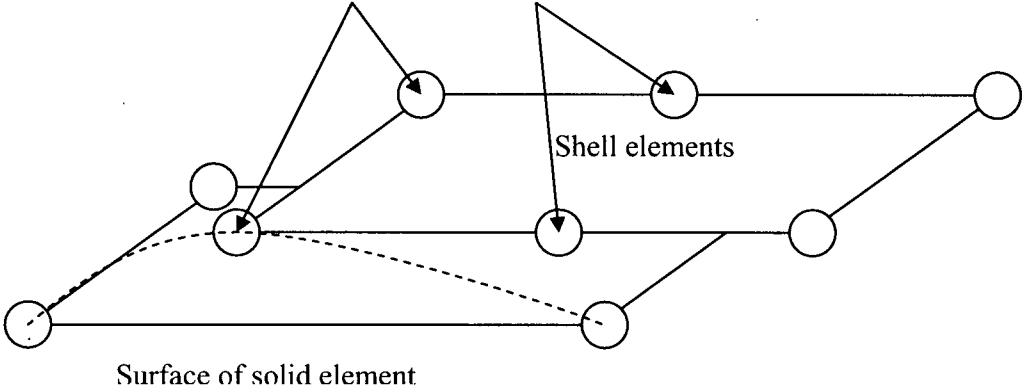


Figure 6a. Face-to-face shell to solid connection.

Shell nodes DOF are related to solid element shape functions

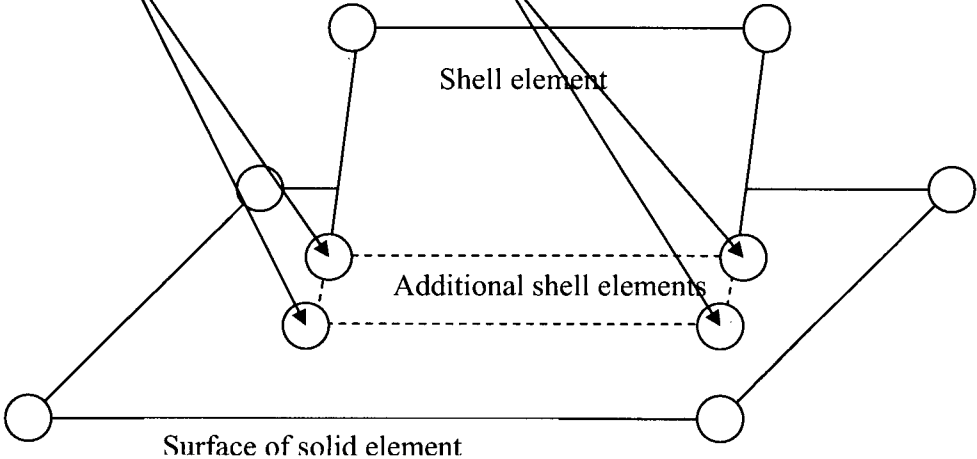


Figure 6b. Shell edge-to-solid face connection.

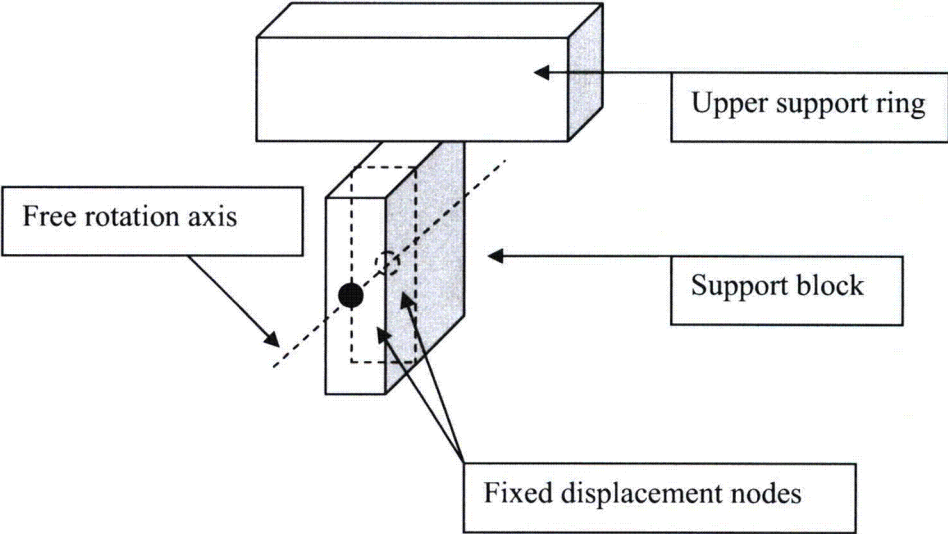


Figure 7. Boundary conditions. Inside node is half way between outer surface of support block and upper support ring.

3.10 Pressure Loading

The harmonic loads are produced by the pressures acting on the exposed surfaces of the steam dryer. At every frequency and for each MSL, the pressure distribution corresponding to a unit pressure at the MSL inlet is represented on a three-inch grid lattice grid (i.e., a mesh whose lines are aligned with the x-, y- and z-directions) that is superimposed over the steam dryer surface. This grid is compatible with the 'Table' format used by ANSYS to 'paint' general pressure distributions upon structural surfaces. The pressures are obtained from the Helmholtz solver routine in the acoustic analysis [1].

In general, the lattice nodes do not lie on the surface so that to obtain the pressure differences at the surface it is necessary to interpolate the pressure differences stored at the lattice nodes. This is done using simple linear interpolation between the 8 forming nodes of the lattice cell containing the surface point of interest. Inspection of the resulting pressures at selected nodes shows that these pressures vary in a well-behaved manner between the nodes with prescribed pressures. Graphical depictions of the resulting pressures and comparisons between the peak pressures in the original nodal histories and those in the final surface load distributions produced in ANSYS, all confirm that the load data are interpolated accurately and transferred correctly to ANSYS.

The harmonic pressure loads are only applied to surfaces above the water level, as indicated in Figure 8. In addition to the pressure load, the static loading induced by the weight of the steam dryer is analyzed separately. The resulting static and harmonic stresses are linearly combined to obtain total values which are then processed to calculate maximum and alternating stress intensities for assessment in Section 5.

[[

⁽³⁾]] This is useful since revisions in the loads model do not necessitate recalculation of the unit stresses.

NODES
PRES-NORM

ANSYS

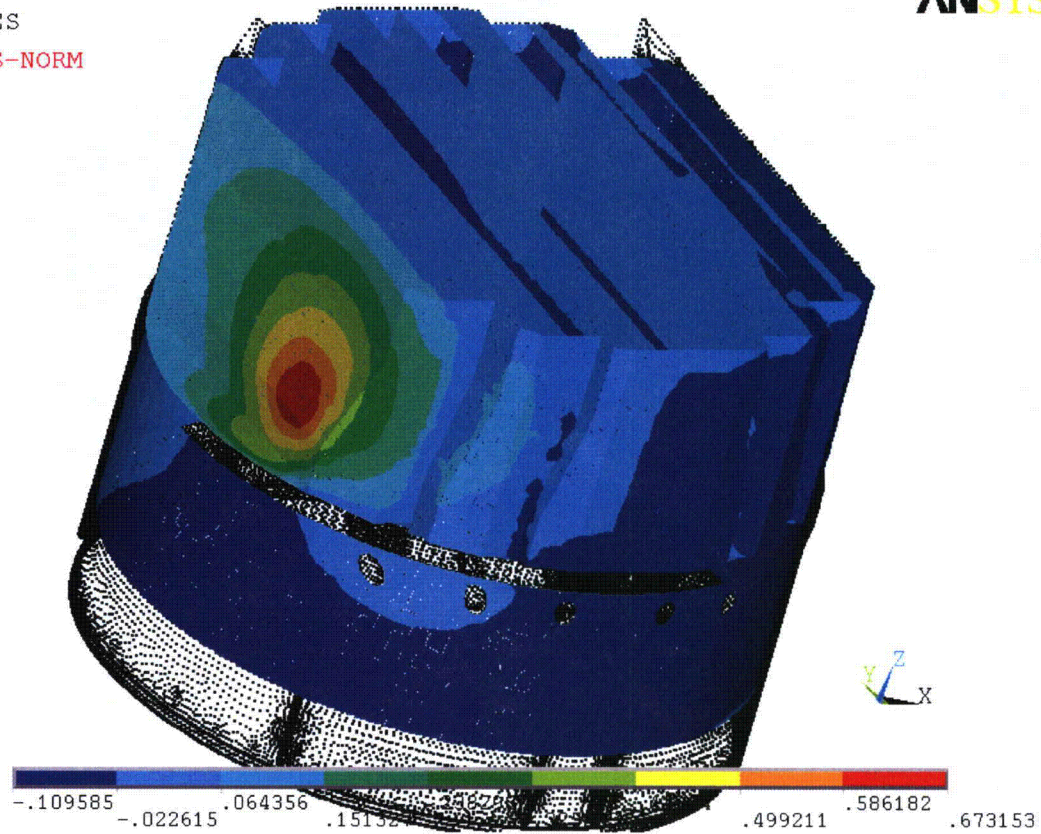


Figure 8a. Real part of unit pressure loading MSL C (in psid) on the steam dryer at 50.2 Hz. No loading is applied to the submerged transparent surface.



NODES
PRES-NORM

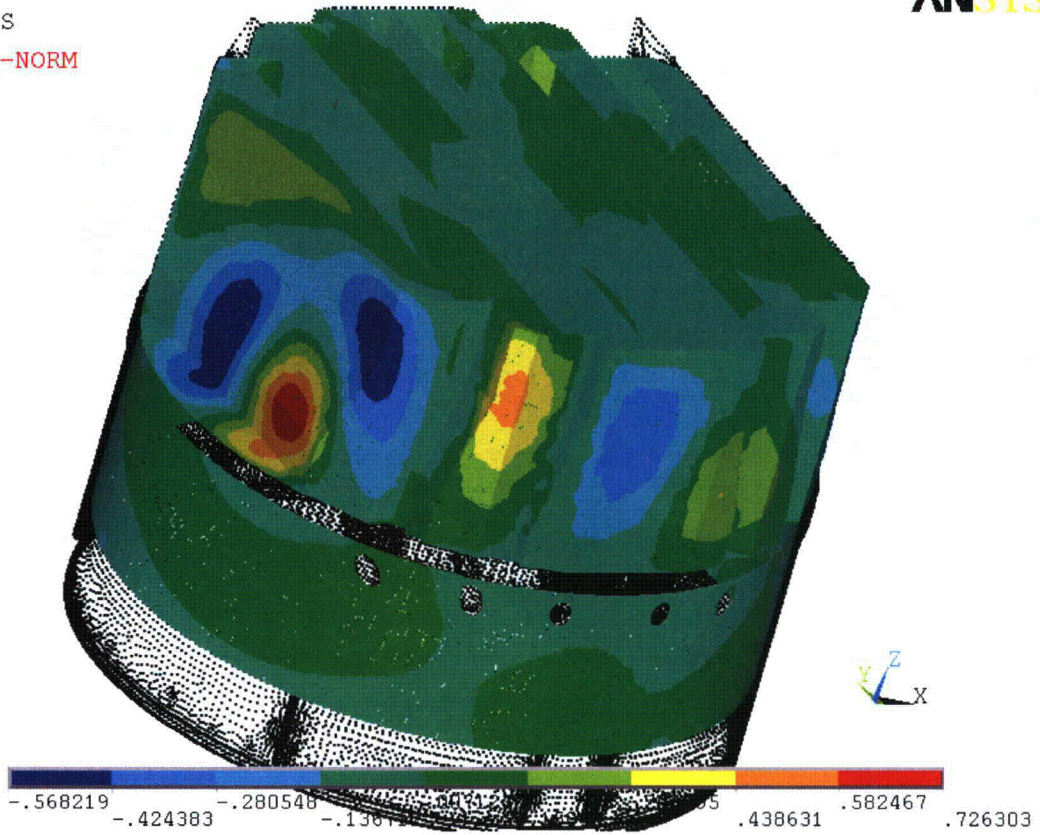


Figure 8b. Real part of unit pressure loading MSL C (in psid) on the steam dryer at 200.89 Hz. No loading is applied to the submerged transparent surface.

4. Structural Analysis

The solution is decomposed into static and harmonic parts, where the static solution produces the stress field induced by the supported structure subjected to its own weight and the harmonic solution accounts for the harmonic stress field due to the unit pressure of given frequency in one of the main steam lines. All solutions are linearly combined, with amplitudes provided by signal measurements in each steam line, to obtain the final displacement and stress time histories. This decomposition facilitates the prescription of the added mass model accounting for hydrodynamic interaction and allows one to compare the stress contributions arising from static and harmonic loads separately. Proper evaluation of the maximum membrane and membrane+bending stresses requires that the static loads due to weight be accounted for. Hence both static and harmonic analyses are carried out.

4.1 Static Analysis

The results of the static analysis are shown in Figure 9. The locations with highest stress include the upper support ring areas near support brackets with stress intensity 5,491 psi.

4.2 Harmonic Analysis

The harmonic pressure loads were applied to the structural model at all surface nodes described in Section 3.10. Typical stress intensity distributions over the structure are shown in Figure 10. Stresses were calculated for each frequency, and results from static and harmonic calculations were combined.

To evaluate maximum stresses, the stress harmonics including the static component are transformed into a time history using FFT, and the maximum and alternating stress intensities for the response, evaluated. According to ASME B&PV Code, Section III, Subsection NG-3216.2 the following procedure was established to calculate alternating stresses. For every node, the stress difference tensors, $\sigma'_{nm} = \sigma_n - \sigma_m$, are considered for all possible pairs of the stresses σ_n and σ_m at different time levels, t_n and t_m . Note that all possible pairs require consideration since there are no "obvious" extrema in the stress responses. However, in order to contain computational cost, extensive screening of the pairs takes place (see Section 2.3) so that pairs known to produce alternating stress intensities less than 500 psi are rejected. For each remaining stress difference tensor, the principal stresses S_1, S_2, S_3 are computed and the maximum absolute value among principal stress differences, $S_{nm} = \max\{|S_1 - S_2|, |S_1 - S_3|, |S_2 - S_3|\}$, obtained. The alternating stress at the node is then one-half the maximum value of S_{nm} taken over all combinations (n,m), i.e., $S_{alt} = \frac{1}{2} \max_{n,m} \{S_{nm}\}$. This alternating stress is compared against allowable values, depending on the node location with respect to welds.



NODAL SOLUTION

STEP=1

SUB =1

TIME=1

USUM (AVG)

RSYS=0

DMX =.061779

SMN =.754E-03

SMX =.061779

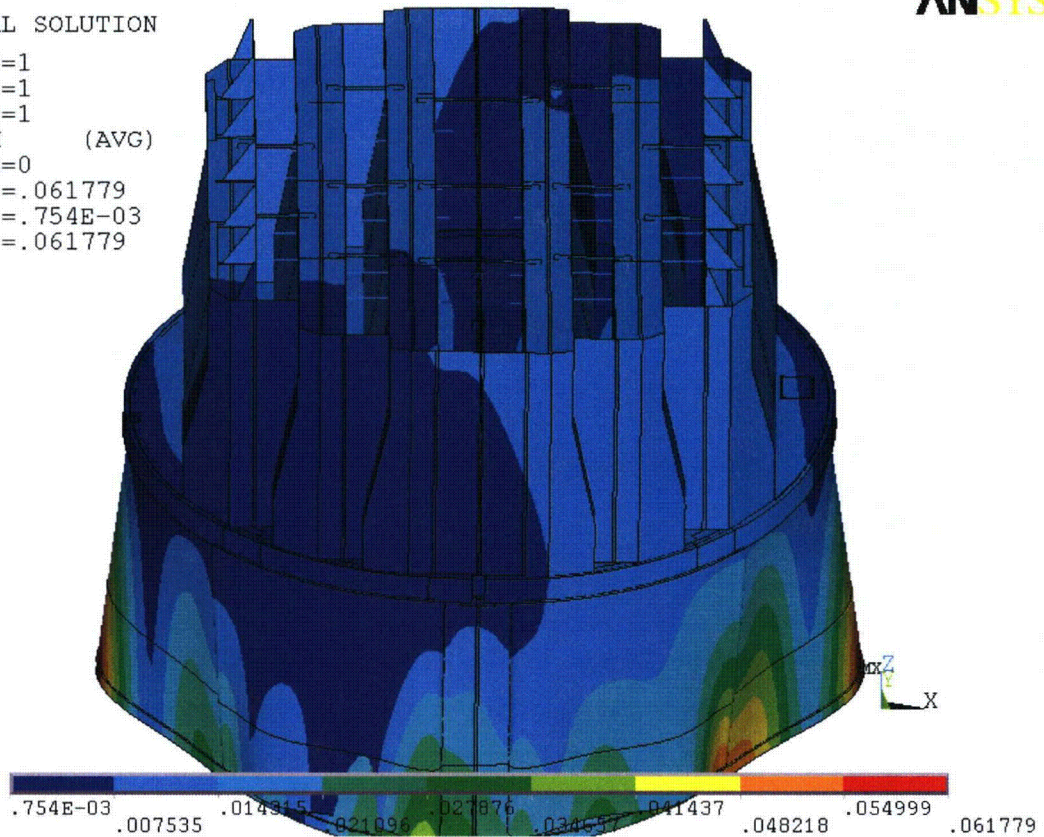


Figure 9a. Overview of static calculations showing displacements (in inches). Maximum displacement (DMX) is 0.062". Note that displacements are amplified for visualization.



```
NODAL SOLUTION
STEP=1
SUB =1
TIME=1
SINT      (AVG)
DMX =.061779
SMN =.488763
SMX =5491
```

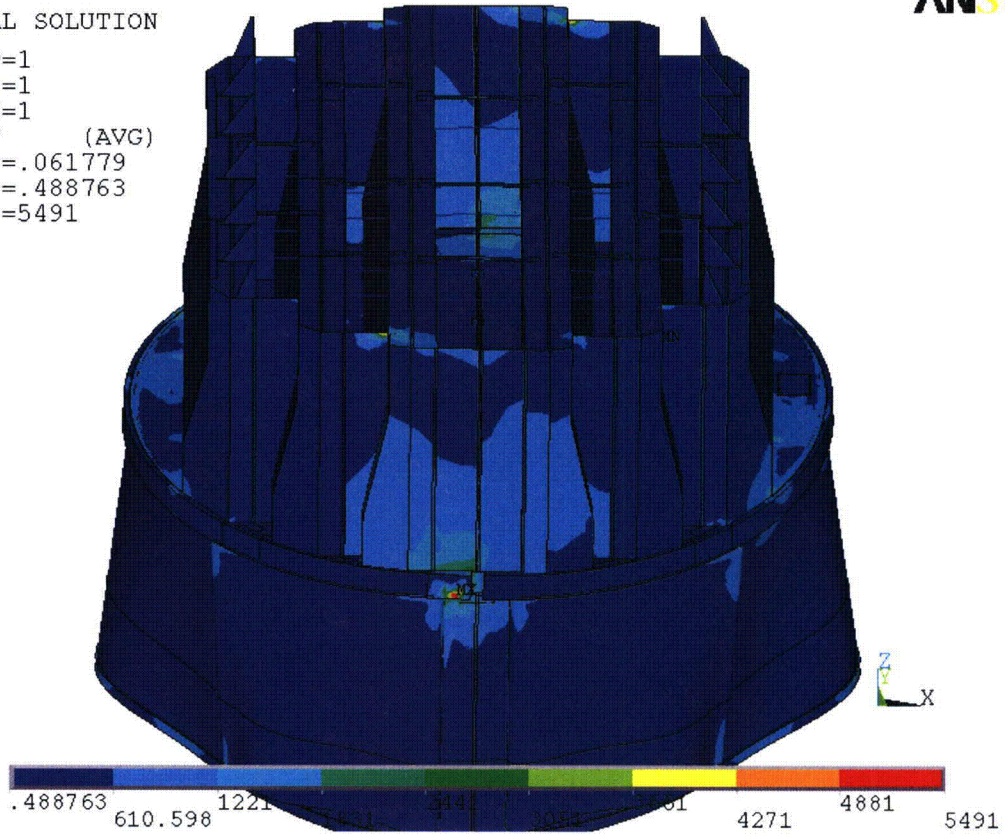


Figure 9b. Overview of static calculations showing stress intensities (in psi). Maximum stress intensity (SMX) is 5491 psi. Note that displacements are amplified for visualization



NODAL SOLUTION

STEP=3
SUB =1
FREQ=50.207
REAL ONLY
SINT (AVG)
DMX =.21313
SMN =.421228
SMX =10888

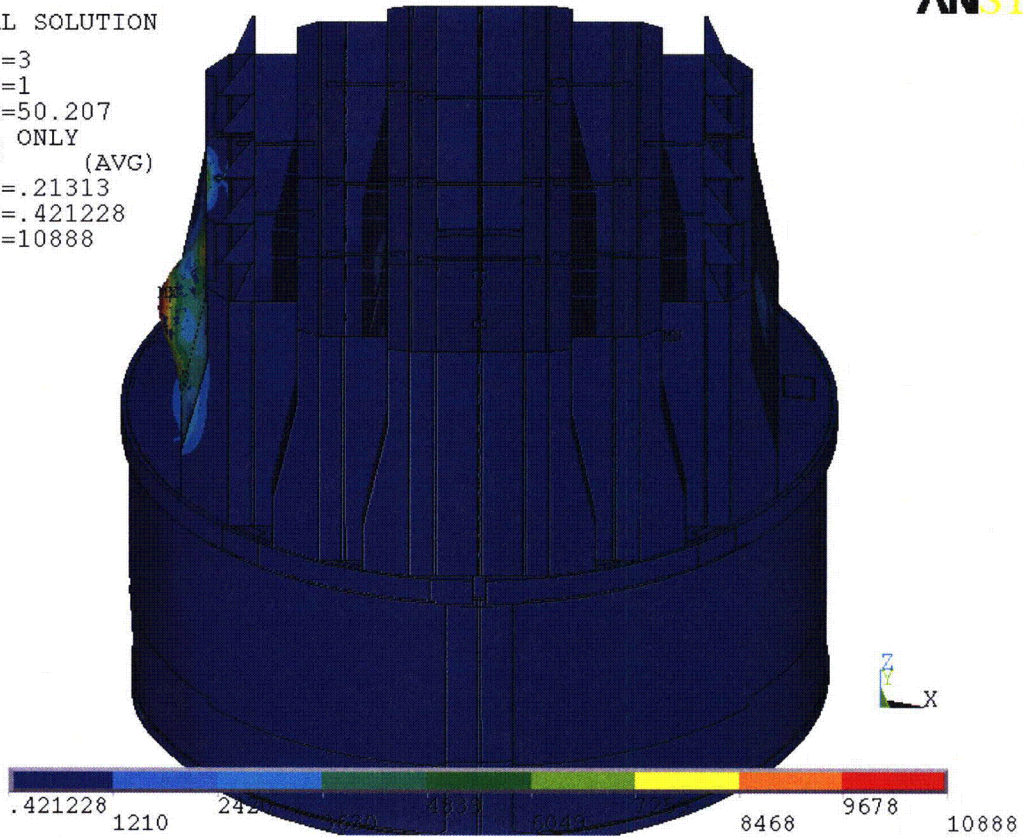


Figure 10a. Overview of harmonic calculations showing real part of stress intensities (in psi) along with displacements. Unit loading MSL C at 50.2 Hz (oriented to show high stress locations).

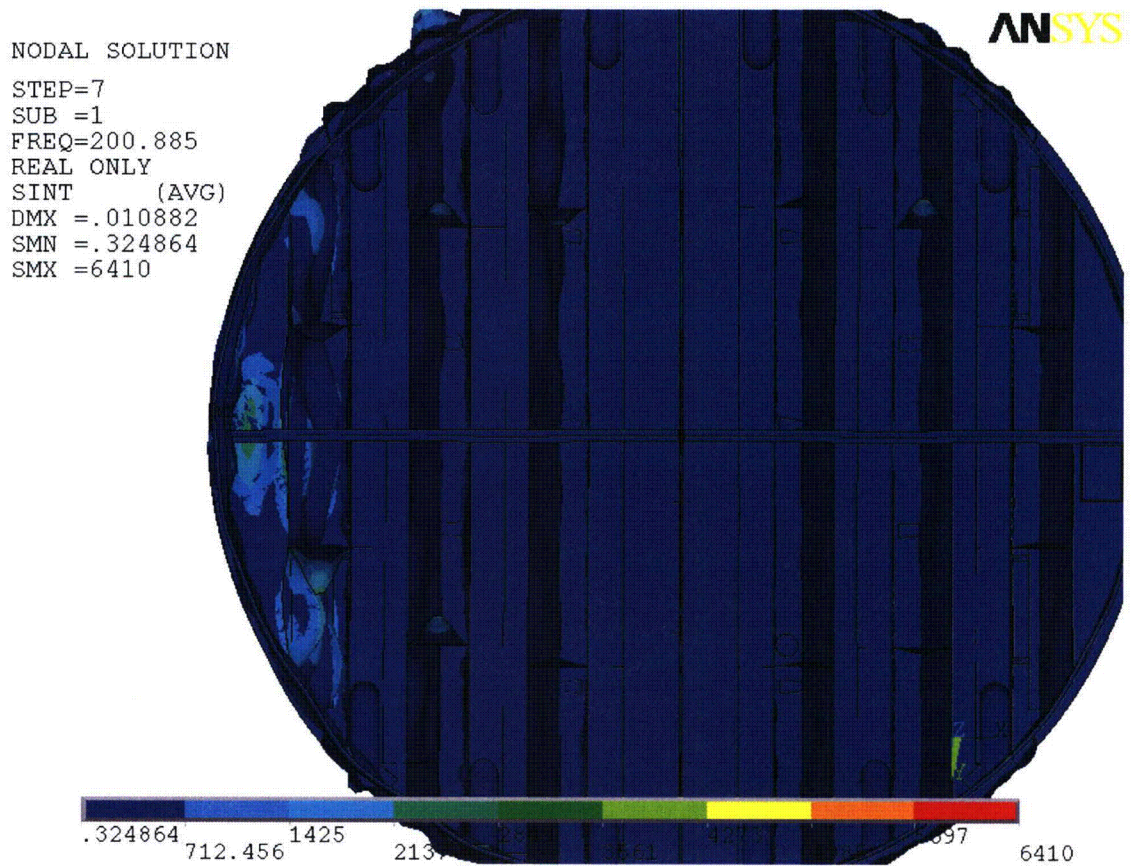


Figure 10b. Overview of harmonic calculations showing real part of stress intensities (in psi) along with displacements. Unit loading MSL C at 200.9 Hz (oriented to show high stress locations).

4.3 Post-Processing

The static and transient stresses computed at every node with ANSYS were exported into files for subsequent post-processing. These files were then read into separate customized software to compute the maximum and alternating stresses at every node. The maximum stress was defined for each node as the largest stress intensity occurring during the time history. Alternating stresses were calculated according to the ASME standard described above. For shell elements the maximum stresses were calculated separately at the mid-plane, where only membrane stress is present, and at top/bottom of the shell, where bending stresses are also present.

For nodes that are shared between several structural components or lie on junctions, the maximum and alternating stress intensities are calculated as follows. First, the nodal stress tensor is computed separately for each individual component by averaging over all finite elements meeting at the node and belonging to the same structural component. The time histories of these stress tensors are then processed to deduce the maximum and alternating stress intensities for each structural component. Finally for nodes shared across multiple components the highest of the component-wise maximum and alternating stresses is recorded as the "nodal" stress. This approach prevents averaging of stresses across components and thus yields conservative estimates for nodal stresses at the weld locations where several components are joined together.

The maximum stresses are compared against allowable values which depend upon the stress type (membrane, membrane+bending, alternating – P_m , P_m+P_b , S_{alt}) and location (at a weld or away from welds). These allowables are specified in the following section. For solid elements the most conservative allowable for membrane stress, P_m , is used, although bending stresses are nearly always present also. The structure is then assessed in terms of stress ratios formed by dividing allowables by the computed stresses at every node. Stress ratios less than unity imply that the associated maximum and/or alternating stress intensities exceed the allowable levels. Post-processing tools calculate the stress ratios, identifying the nodes with low stress ratios and generating files formatted for input to the 3D graphics program, TecPlot, which provides more general and sophisticated plotting options than currently available in ANSYS.

4.4 Computation of Stress Ratios for Structural Assessment

The ASME B&PV Code, Section III, subsection NG provides different allowable stresses for different load combinations and plant conditions. The stress levels of interest in this analysis are for the normal operating condition, which is the Level A service condition. The load combination for this condition is:

$$\text{Normal Operating Load Combination} = \text{Weight} + \text{Pressure} + \text{Thermal}$$

The weight and fluctuating pressure contributions have been calculated in this analysis and are included in the stress results. The static pressure differences and thermal expansion stresses are small, since the entire steam dryer is suspended inside the reactor vessel and all surfaces are exposed to the same conditions. Seismic loads only occur in Level B and C cases, and are not considered in this analysis.

Allowable Stress Intensities

The ASME B&PV Code, Section III, subsection NG shows the following (Table 5) for the maximum allowable stress intensity (S_m) and alternating stress intensity (S_a) for the Level A service condition. The allowable stress intensity values for type 304 stainless steel at operating temperature 550°F are taken from Table I-1.2 and Fig. I-9.2.2 of Appendix I of Section III, in the ASME B&PV Code. The calculation for different stress categories is performed in accordance with Fig. NG-3221-1 of Division I, Section III, subsection NG.

Table 5. Maximum Allowable Stress Intensity and Alternating Stress Intensity for all areas other than welds. The notation P_m represents membrane stress; P_b represents stress due to bending; Q represents secondary stresses (from thermal effects and gross structural discontinuities, for example); and F represents additional stress increments (due to local structural discontinuities, for example).

Type	Notation	Service Limit	Allowable Value (psi)
<i>Maximum Stress Allowables:</i>			
General Membrane	P_m	S_m	18,300
Membrane + Bending	$P_m + P_b$	$1.5 S_m$	27,450
Primary + Secondary	$P_m + P_b + Q$	$3.0 S_m$	54,900
<i>Alternating Stress Allowable:</i>			
Peak = Primary + Secondary + F	S_{alt}	S_a	13,600

When evaluating welds, either the calculated or allowable stress was adjusted, to account for stress concentration factor and weld quality. Specifically:

- For maximum allowable stress intensity, the allowable value is decreased by multiplying its value in Table 5 by 0.55.
- For alternating stress intensity, the calculated weld stress intensity is multiplied by a weld stress intensity (fatigue) factor of 1.8, before comparison to the S_a value given above.

The weld factors of 0.55 and 1.8 were selected based on the observable quality of the shop welds and liquid penetrant NDE testing of all welds (excluding tack and intermittent welds, which were subject to 5X visual inspection) during fabrication. These factors are consistent with fatigue strength reduction factors recommended by the Welding Research Council, [15], and stress concentration factors at welds, provided in [16] and [17]. In addition, critical welds are subject to periodical visual inspections in accordance with the requirements of GE SIL 644 SIL and BWR VIP-139 [18]. Therefore, for weld stress intensities, the allowable values are shown in Table 6.

These factors (0.55 and 1.8) also conservatively presume that the structure is joined using fillet welds unless specified otherwise. Since fillet welds correspond to larger stress concentration factors than other types of welds, this assumption is a conservative one.

Table 6. Weld Stress Intensities.

Type	Notation	Service Limit	Allowable Value (psi)
<i>Maximum Stress Allowables:</i>			
General Membrane	Pm	0.55 Sm	10,065
Membrane + Bending	Pm + Pb	0.825 Sm	15,098
Primary + Secondary	Pm + Pb + Q	1.65 Sm	30,195
<i>Alternating Stress Allowables:</i>			
Peak = Primary + Secondary + F	S _{alt}	Sa	13,600

Comparison of Calculated and Allowable Stress Intensities

The classification of stresses into general membrane or membrane + bending types was made according to the exact location, where the stress intensity was calculated; namely, general membrane, Pm, for middle surface of shell element, and membrane + bending, Pm + Pb, for other locations. For solid elements the most conservative, general membrane, Pm, allowable is used.

The structural assessment is carried out by computing stress ratios between the computed maximum and alternating stress intensities, and the allowable levels. Locations where any of the stresses exceed allowable levels will have stress ratios less than unity. Since computation of stress ratios and related quantities within ANSYS is time-consuming and awkward, a separate FORTRAN code was developed to compute the necessary maximum and alternating stress intensities, Pm, Pm+Pb, and S_{alt}, and then compare it to allowables. Specifically, the following quantities were computed at every node:

1. The maximum membrane stress intensity, Pm (evaluated at the mid-thickness location for shells),
2. The maximum membrane+bending stress intensity, Pm+Pb, (taken as the largest of the maximum stress intensity values at the bottom, top, and mid thickness locations, for shells),
3. The alternating stress, S_{alt}, (the maximum value over the three thickness locations is taken).
4. The stress ratio due to a maximum stress intensity assuming the node lies at a non-weld location (note that this is the minimum ratio obtained considering both membrane stresses and membrane+bending stresses):

$$SR-P(nw) = \min \{ Sm/Pm, 1.5 * Sm/(Pm+Pb) \}.$$
5. The alternating stress ratio assuming the node lies at a non-weld location,

$$SR-a(nw) = Sa / (1.1 * S_{alt}),$$
6. The same as 4, but assuming the node lies on a weld,

$$SR-P(w) = SR-P(nw) * f_{sw} * 0.55$$
7. The same as 5, but assuming the node lies on a weld,

$$SR-a(w) = SR-a(nw) * f_{sw} / 1.8.$$

where $f_{sw}=1$ at all welds (when justified, f_{sw} can be adjusted to reflect different weld types). Note that in steps 4 and 6, the minimum of the stress ratios based on P_m and P_m+P_b , is taken. The allowables listed in Table 6, $S_m=18,300$ psi and $S_a=13,600$ psi. The factors, 0.55 and 1.8, are the weld factors discussed above. The factor of 1.1 accounts for the differences in Young's moduli for the steel used in the steam dryer and the values assumed in alternating stress allowable. According to NG-3222.4 in subsection NG of Section III of the ASME Code, the effect of elastic modulus upon alternating stresses is taken into account by multiplying alternating stress S_{alt} at all locations by the ratio, $E/E_{model}=1.1$, where:

$$E = 28.3 \cdot 10^6 \text{ psi, as shown on Fig. I-9.2.2. ASME BP\&V Code}$$
$$E_{model} = 25.55 \cdot 10^6 \text{ psi (Table 1)}$$

The nodes with stress ratios lower than 4 are plotted in TecPlot (a 3D graphics plotting program widely used in engineering communities [19]) to establish whether they lie on a weld or not. The appropriate maximum and alternating stress ratios, SR-P and SR-a, are thus determined and a final listing of nodes having the smallest stress ratios is generated. These nodes are tabulated and depicted in the Results Sections.

5. Results

The stress intensities and associated stress ratios resulting from the Rev. 4 acoustic/hydrodynamic loads [2] with associated biases and uncertainties factored in, are presented below. The bias due to finite frequency discretization and uncertainty associated with the finite element model itself, are also factored in. In the following sections the highest maximum and alternating stress intensities are presented to indicate which points on the dryer experience significant stress concentration and/or modal response (Section 5.1). The lowest stress ratios obtained by comparing the stresses against allowable values, accounting for stress type (maximum and alternating) and location (on or away from a weld), are also reported (Section 5.2). Finally the frequency dependence of the stresses at nodes experiencing the lowest stress ratios is depicted in the form of accumulative PSDs (Section 5.3).

In each section results are presented both at nominal conditions (no frequency shift) and with frequency shift included. Unless specified otherwise, frequency shifts are generally performed at 2.5% increments. The tabulated stresses and stress ratios are obtained using a 'blanking' procedure that is designed to prevent reporting a large number of high stress nodes from essentially the same location on the structure. In the case of stress intensities this procedure is as follows. The relevant stress intensities are first computed at every node and then nodes sorted according to stress level. The highest stress node is noted and all neighboring nodes within 10 inches of the highest stress node and its symmetric images (i.e., reflections across the $x=0$ and $y=0$ planes) are "blanked" (i.e., excluded from the search for subsequent high stress locations). Of the remaining nodes, the next highest stress node is identified and its neighbors (closer than 10 inches) blanked. The third highest stress node is similarly located and the search continued in this fashion until all nodes are either blanked or have stresses less than half the highest value on the structure. For stress ratios, an analogous blanking procedure is applied. Thus the lowest stress ratio of a particular type in a 10" neighborhood and its symmetric images is identified and all other nodes in these regions excluded from listing in the table. Of the remaining nodes, the one with the lowest stress ratio is reported and its neighboring points similarly excluded, and so on until all nodes are either blanked or have a stress ratio higher than 4.

The measured CLTP strain gage signals contain significant contributions from non-acoustic sources such as sensor noise, MSL turbulence and pipe bending vibration that contribute to the hoop strain measurements. The ACM analysis does not distinguish between the acoustic and non-acoustic fluctuations in the MSL signals that could lead to sizeable, but fictitious acoustic loads and resulting stresses on the dryer. One way to remove these fictitious loads is to collect data with the system maintained at operating pressure (1000 psi) and temperature, but low (less than 20% of CLTP) flow. By operating the recirculation pumps at this condition, the background plant noise and vibrations remain present. At these conditions the acoustic loads are known to be negligible so that collected data, referred to as the 1000 psig data, originate entirely from non-acoustic sources such as sensor noise and mechanical vibrations. This information is valuable since it allows one to now distinguish between the acoustic and non-acoustic content in the CLTP signal and therefore modify the CLTP loads so that only the acoustic component is retained. For consistency, the 1000 psig strain gage signals are filtered in the same manner as the CLTP data and are fed into the ACM model to obtain the monopole and dipole signals at the MSL inlets. Since there is negligible flow, these signals are fictitious, i.e., the hoop strains

measured by the strain gages are not due to pressure fluctuations, but rather due to noise. However, under the supposition that these signals are acoustic in origin the hypothetical stresses due to these signals can nevertheless be computed.

The contribution of background noise in the Browns Ferry Unit 2 steam dryer was quantified by taking strain gage measurements at 19% power. Measurements taken for the BFN1 unit at increasing power levels indicate that the 19% signal measurements provide a conservative estimate of the noise at zero power [20] (i.e., noise amplitudes are slightly smaller than at zero power). The same is expected for the BFN2 unit. At this level there are no significant acoustic sources. To compensate for the non-acoustic noise source represented in the 1000# data, the CLTP MSL inlet pressure signals are modified according to [20]:

$$P(f) = P_0(f) * \max \left[\beta, 1 - \frac{\bar{N}(f)}{\bar{P}_0(f)} \right], \quad \beta=0.5 \quad (8)$$

where f is the frequency (in Hz), $P_0(f)$ is the MSL inlet pressure (monopole or dipole) at CLTP conditions before correction, $P(f)$ is the corresponding post-correction pressure and $\bar{N}(f)$ and $\bar{P}_0(f)$ are averaged pressure amplitudes associated with the 1000 psig data and CLTP data respectively. Specifically,

$$\bar{P}_0(f) = \frac{1}{2} \int_{f-1}^{f+1} |P_0(f)| df \quad (9)$$

where $|P_0(f)|$ denotes the absolute value of the complex quantity. Hence $\bar{P}_0(f)$ is the average amplitude of the CLTP pressure in the ± 1 Hz interval about frequency, f . The same definition, but using the 1000 psig pressure signal, is used for $\bar{N}(f)$. Note that this modification leaves the phase information in the original CLTP signal unchanged.

The applied load includes all biases and uncertainties for both the ACM (summarized in [2]) and the FEM. For the latter there are three main contributors to the bias and uncertainty. The first is an uncertainty (25.26%) that accounts for modeling idealizations (e.g., vane bank mass model), geometrical approximations and other discrepancies between the modeled and actual dryer such as neglecting of weld mass and stiffness in the FEA. The second contributor is a bias (9.53% - note that this has been increased from the 5.72% value previously used in [3] accounting for discretization errors associated with using a finite size mesh, upon computed stresses. The third contributor is also a bias and compensates for the use of a finite discretization schedule in the construction of the unit solutions. The frequencies are spaced such that at 1% damping the maximum (worst case) error in a resonance peak is 5%. The average error for this frequency schedule is 1.72%.

It is important to note that the loads and associated biases and uncertainties used here pertain to the existing BFN2 installation prior to the installation of ASBs planned for EPU operation. When these are installed the bias and uncertainty in the frequency range 109 to 113 Hz are

reduced resulting in a reduction in the limiting stresses. These are indicated and discussed further in the text below.

5.1 General Stress Distribution and High Stress Locations

The maximum stress intensities obtained by post-processing the ANSYS stress histories for CLTP at nominal frequency and with frequency shift operating conditions are listed in Table 7. Contour plots of the stress intensities over the steam dryer structure are shown on Figure 11 (nominal frequency) and Figure 12 (maximum stress over all nine frequency shifts including nominal). All plots here and in the following section pertain to Model 1 (see section 3.1 and Appendix A). Corrections using Model 2 are made in the Table as indicated. The figures are oriented to emphasize the high stress regions. Note that these stress intensities *do not* account for weld factors but include end-to-end bias and uncertainty. Further, it should be noted that since the allowable stresses vary with location, stress intensities do not necessarily correspond to regions of primary structural concern. Instead, structural evaluation is more accurately made in terms of the stress ratios which compare the computed stresses to allowable levels with due account made for stress type and weld factors and also account for stress corrections obtained using high-detail substructure models. Comparisons on the basis of stress ratios are made in Section 5.2.

The maximum stress intensities in most areas are low (less than 500 psi). For the membrane stresses (P_m) the high stress regions tend to occur at: (i) the restraint locations for the upper support ring; (ii) the upper edges of the closure plates and (iii) junctions connecting the bottoms of the hood supports. The first location experiences high stresses since the entire weight of the structure is transmitted through relatively small pads to the external structure. The stress is dominated by the static component as the stress intensities at this location do not vary significantly with frequency shift. However alternating stress intensities (1605 psi or less) are also present since the net acoustic loads integrated over the entire drier are transferred through the support locations. The closure plates experience high stresses since they restrain displacements in the adjacent vane banks. The junctions where the hoods, hood supports and base or cover plates meet also experience high stresses.

The membrane + bending stress (P_m+P_b) distributions evidence a more distinguished modal response especially on the outer hoods. The first three regions showing high stress intensities are the same as for membrane stresses. (Note that for the first two nodes, 123931 and 123865, $P_m=P_m+P_b$ because these stresses occur in solid elements for which no distinction between membrane and bending stresses is made.) In addition stress concentrations are now more pronounced on welds where the outer hoods and underlying hood supports meet, especially near the bottom where these welds meet the cover plate as seen in Figure 12b and c. Stress concentrations are also observed on: (i) the tie bar bases (ii) the closure plates where they connect to the hoods or vane bank end plates; (iii) the skirt/drain channel welds; (iv) the outer cover plates connecting to the upper support ring and bottom of the outer hoods; and (v) the outer hood end plates.

The alternating stress, S_{alt} , distributions are more localized, higher values being obtained on the outer hoods and their end plates. The contour plots with and without frequency shifts are similar. When all frequency shifts are considered (Figure 12d) there is a stronger response on

the outer hood end plates; also a weak modal response along the periphery of the submerged lower skirt is evident.

Comparing the nominal results (Table 7a) and results with frequency shifting it can be seen that maximum stress intensities, P_m and P_m+P_b , do not differ significantly. The alternating stresses however, can be as much as 47% higher when frequency shifts are considered. As shown in the next section, all stresses are well within allowable levels.

Table 7a. Locations with highest predicted stress intensities for CLTP conditions with no frequency shift. Signal noise has been partially removed using 19% power data.

Stress Category	Location	Weld	Location (in) ^(a)			node ^(b)	Stress Intensities (psi)		
			x	y	z		Pm	Pm+Pb	S _{alt}
Pm	Upper Support Ring (USR)/Support Block/Support	No	7	122.3	-9.5	123931	6571	6571	1411
"	USR/Seismic Block/Support Block	No	-122.1	10	-9.5	123865	6038	6038	1178
"	Top Cover Inner Hood/Middle Closure Plate/Inner Hood	Yes	-31.5	-108.4	88.9	100549	5352	6206	878
"	Splice Bar/USR	Yes	2.2	119	0	123619	5330	5330	<500
"	Middle Cover Plate/Hood Support/Inner Hood	Yes	39.8	-59.8	0	98774	4809	4907	1609
Pm+Pb	USR/Support Block/Support	No	7	122.3	-9.5	123931	6571	6571	1411
"	Top Cover Inner Hood/Middle Closure Plate/Inner Hood	Yes	-31.5	-108.4	88.9	100549	5352	6206	878
"	USR Seismic Block/Support Block	No	-122.1	10	-9.5	123865	6038	6038	1178
"	Submerged Drain Channel/Skirt	Yes	91	-76.7	-100.5	104142	1063	5719	1762
"	Splice Bar/USR	Yes	2.2	119	0	123619	5330	5330	<500
S _{alt}	Outer Hood/Gusset Pad Thin/Top Cover Outer Hood ^(c)	Yes	-93.5	-57.5	88.9	108730	337	4692	1616
"	Outer Hood/Gusset Pad Thin/Top Cover Outer Hood ^(c)	Yes	-93.5	-0.8	88.9	108664	336	3679	1715
"	Old tie bar/top cover plate ^(c)	Yes	-81.5	31.4	88.9	134490	3508	3508	878
"	Top Cover Middle Hood/Middle Hood/Shell Tie Bar ^(c)	Yes	-62.5	25.2	88.9	107158	1397	3770	2068
"	Dam Plate/New Gusset	Yes	-77	0	104.4	101769	137	2441	2360

Notes for Table 7 and Table 8.

- (a) Spatial coordinates are in a reference frame whose origin is located at the intersection of the steam dryer centerline and the plane containing the base plates (this plane also contains the top of the upper support ring and the bottom edges of the hoods). The y-axis is parallel to the hoods, the x-axis is normal to the hoods pointing from MSL C/D to MSL A/B, and the z-axis is vertical, positive up.
- (b) Node numbers are retained for further reference.
- (c) Alternating stress intensities modified using Model 2 as described in Appendix A.

Table 7b. Locations with highest predicted stress intensities taken over all frequency shifts CLTP conditions. Signal noise has been partially removed using 19% power data.

Stress Category	Location	Weld	Location (in) ^(a)			node ^(b)	Stress Intensities (psi)			% Freq. Shift
			x	y	z		Pm	Pm+Pb	Salt	
Pm	USR/Support Block/Support	No	7	122.3	-9.5	123931	6774	6774	1602	-10
"	USR/Seismic Block/Support Block	No	-122.1	10	-9.5	123865	6437	6437	1492	10
"	Top Cover Inner Hood/Middle Closure Plate/Inner Hood	Yes	31.5	108.4	88.9	98291	5561	6121	995	10
"	Splice Bar/USR	Yes	2.2	119	0	123619	5409	5409	<500	7.5
"	Middle Cover Plate/Hood Support/Inner Hood	Yes	-39.8	59.8	0	99801	5394	5415	2100	10
Pm+Pb	USR/Support Block/Support	No	7	122.3	-9.5	123931	6774	6774	1602	-10
"	USR/Seismic Block/Support Block	No	-122.1	10	-9.5	123865	6437	6437	1492	10
"	Top Cover Inner Hood/Middle Closure Plate/Inner Hood	Yes	-31.5	-108.4	88.9	100549	5507	6393	1084	10
"	Submerged Drain Channel/Skirt	Yes	-91	-76.7	-100.5	110570	1353	5971	2328	10
"	Outer Hood/Gusset Pad Thin/Top Cover Outer Hood ^(c)	Yes	-93.5	-57.5	88.9	108730	413	5848	2515	-5
Salt	Outer Hood/Gusset Pad Thin/Top Cover Outer Hood ^(c)	Yes	-93.5	-57.5	88.9	108730	413	5848	2379	-5
"	Outer Hood/Gusset Pad Thin/Top Cover Outer Hood ^(c)	Yes	-93.5	-0.8	88.9	108664	500	5743	2179	-10
"	Top Cover Middle Hood/Middle Hood/Shell Tie Bar ^(c)	Yes	-62.5	25.2	88.9	107158	1613	4958	2322	-5
"	Old tie bar/top cover plate ^(c)	Yes	-81.5	31.4	88.9	134490	3598	3598	878	0
	Outer Side Panel/Vane Bank Thin/Vane Bank Thick/Outer End Wall	Yes	86	85	12.1	102701	551	2863	2647	7.5

See Table 7a for notes (a)-(c).

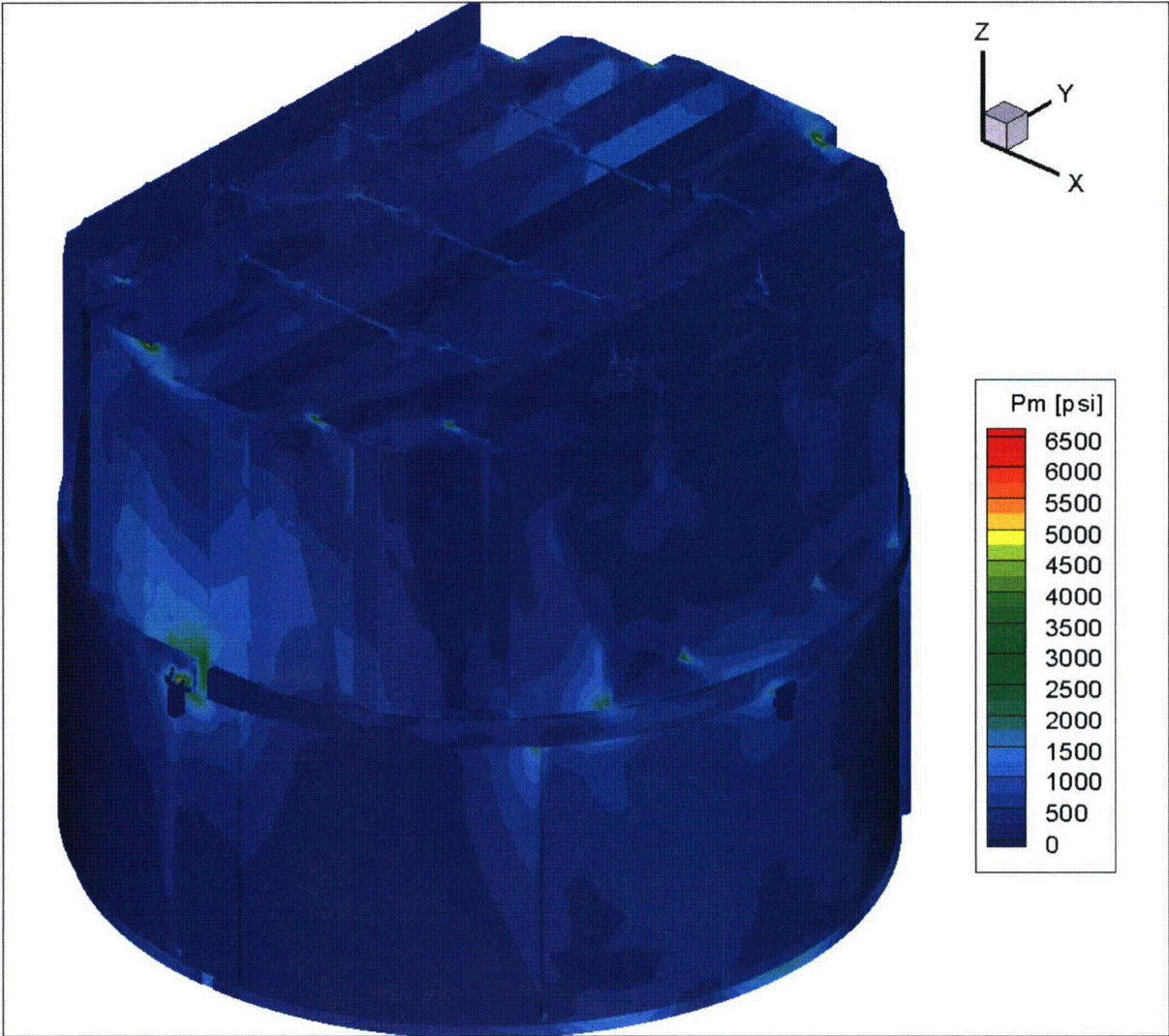


Figure 11a. Contour plot of maximum membrane stress intensity, P_m , for CLTP load. The maximum stress intensity is 6571 psi.

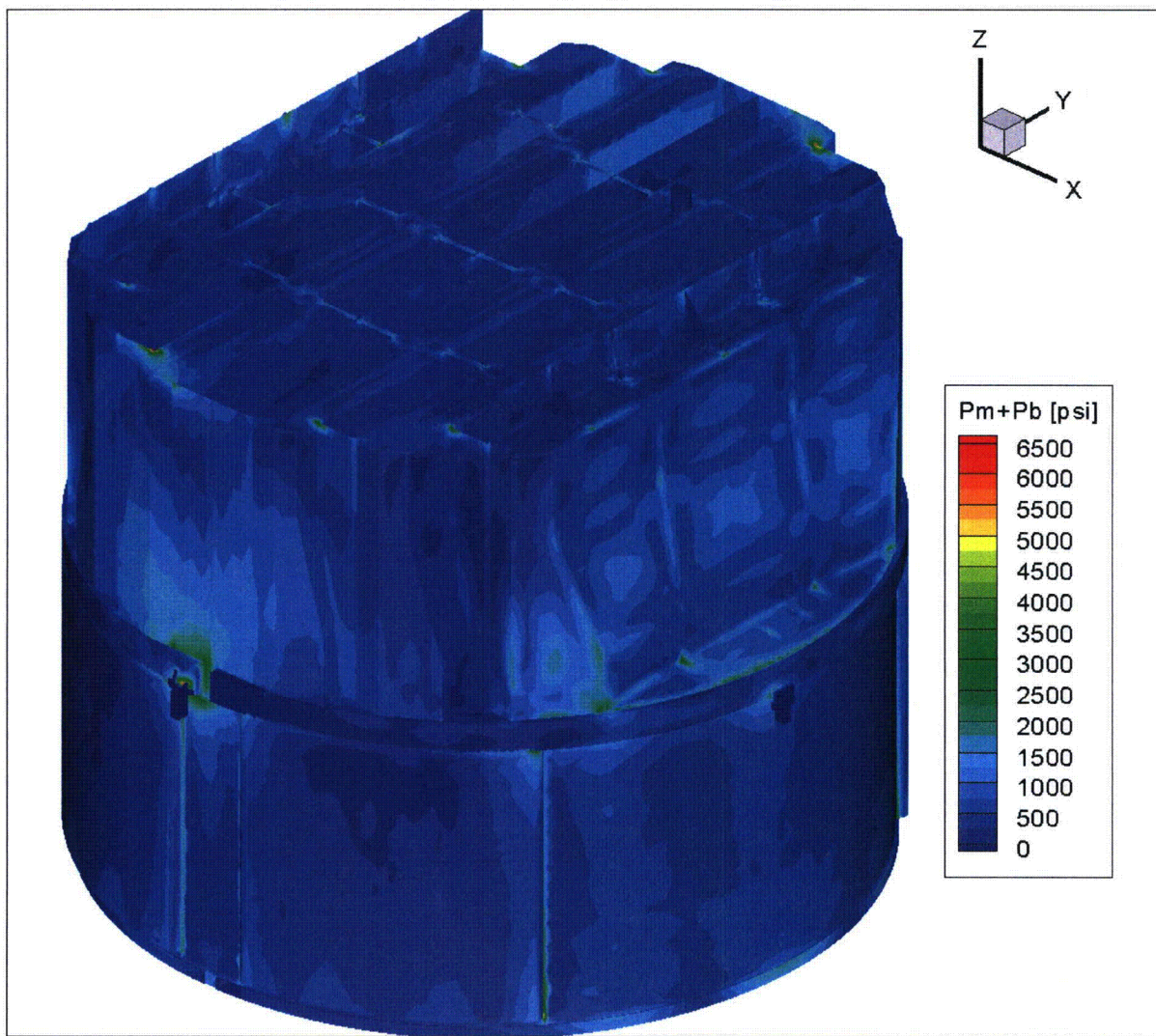


Figure 11b. Contour plot of maximum membrane+bending stress intensity, P_m+P_b , for CLTP load. The maximum stress intensity is 6571 psi. First view.

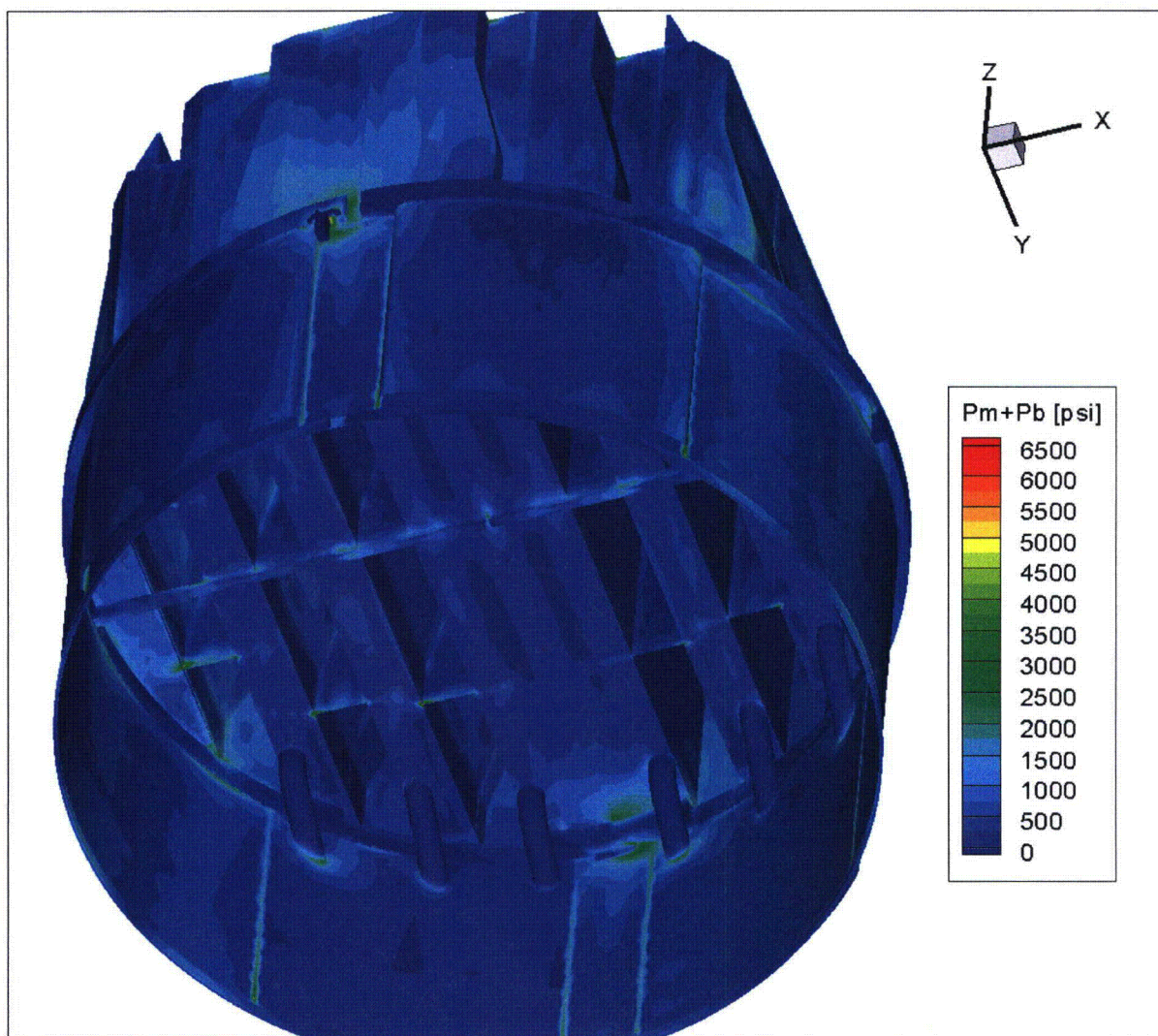


Figure 11c. Contour plot of maximum membrane+bending stress intensity, P_m+P_b , for CLTP load. This second view from below shows the high stress intensities at the bottom of the outer and middle hood supports, support beam, central base plates and drain pipe/skirt welds.

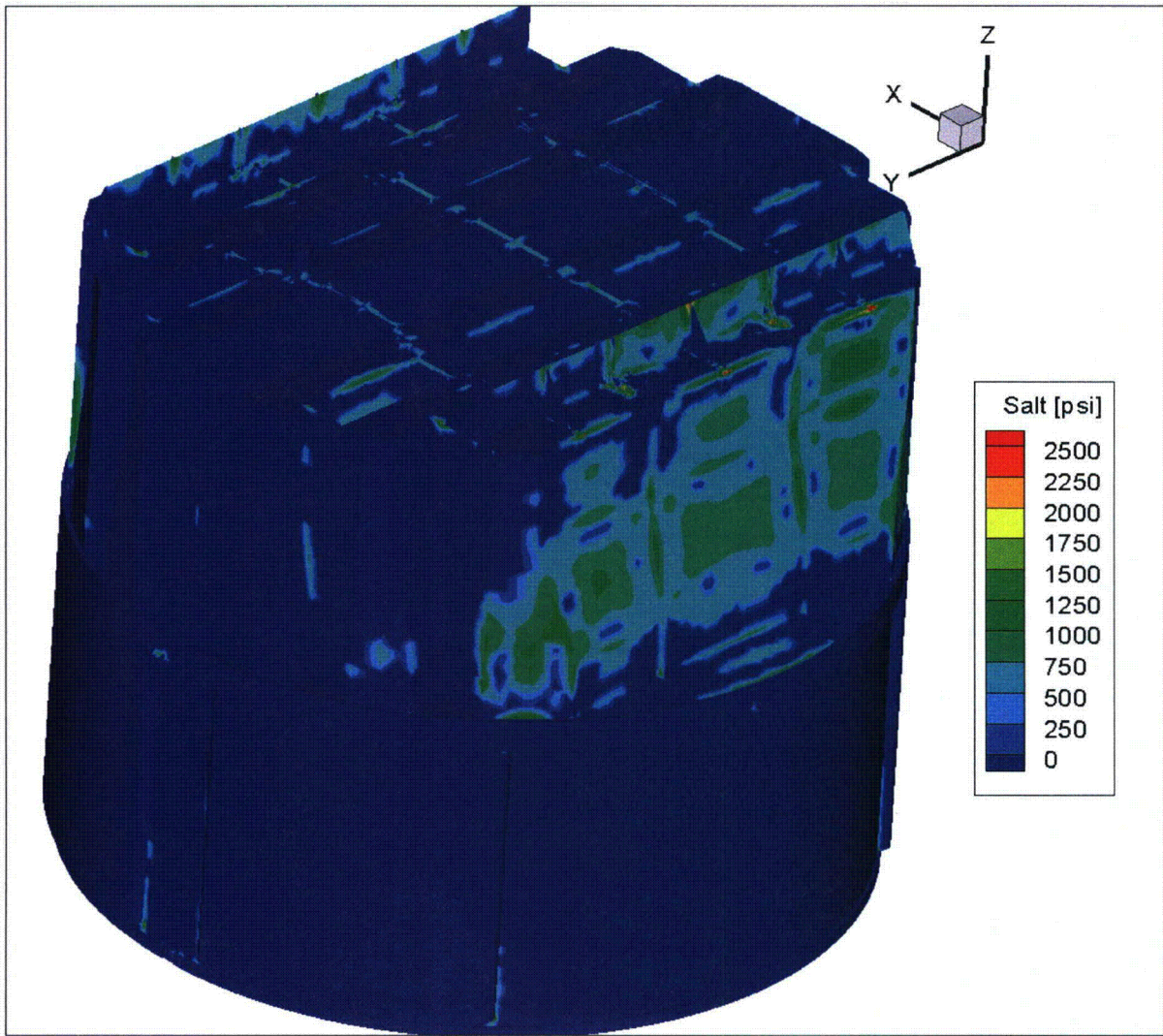


Figure 11d. Contour plot of alternating stress intensity, S_{alt} , for CLTP load. The maximum alternating stress intensity is 2388 psi.

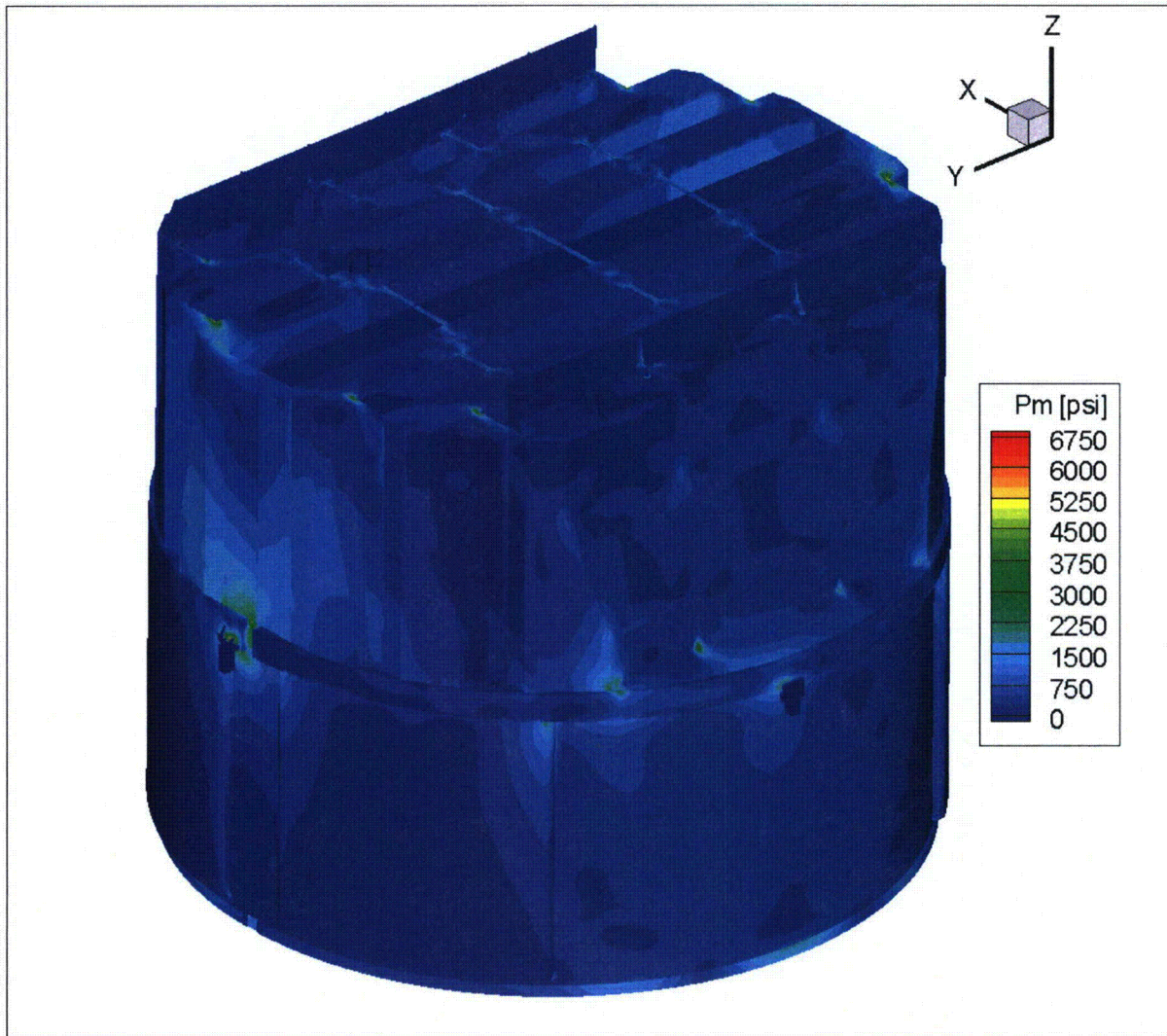


Figure 12a. Contour plot of maximum membrane stress intensity, P_m , for CLTP operation with frequency shifts. The recorded stress at a node is the maximum value taken over all frequency shifts. The maximum stress intensity is 6774 psi.

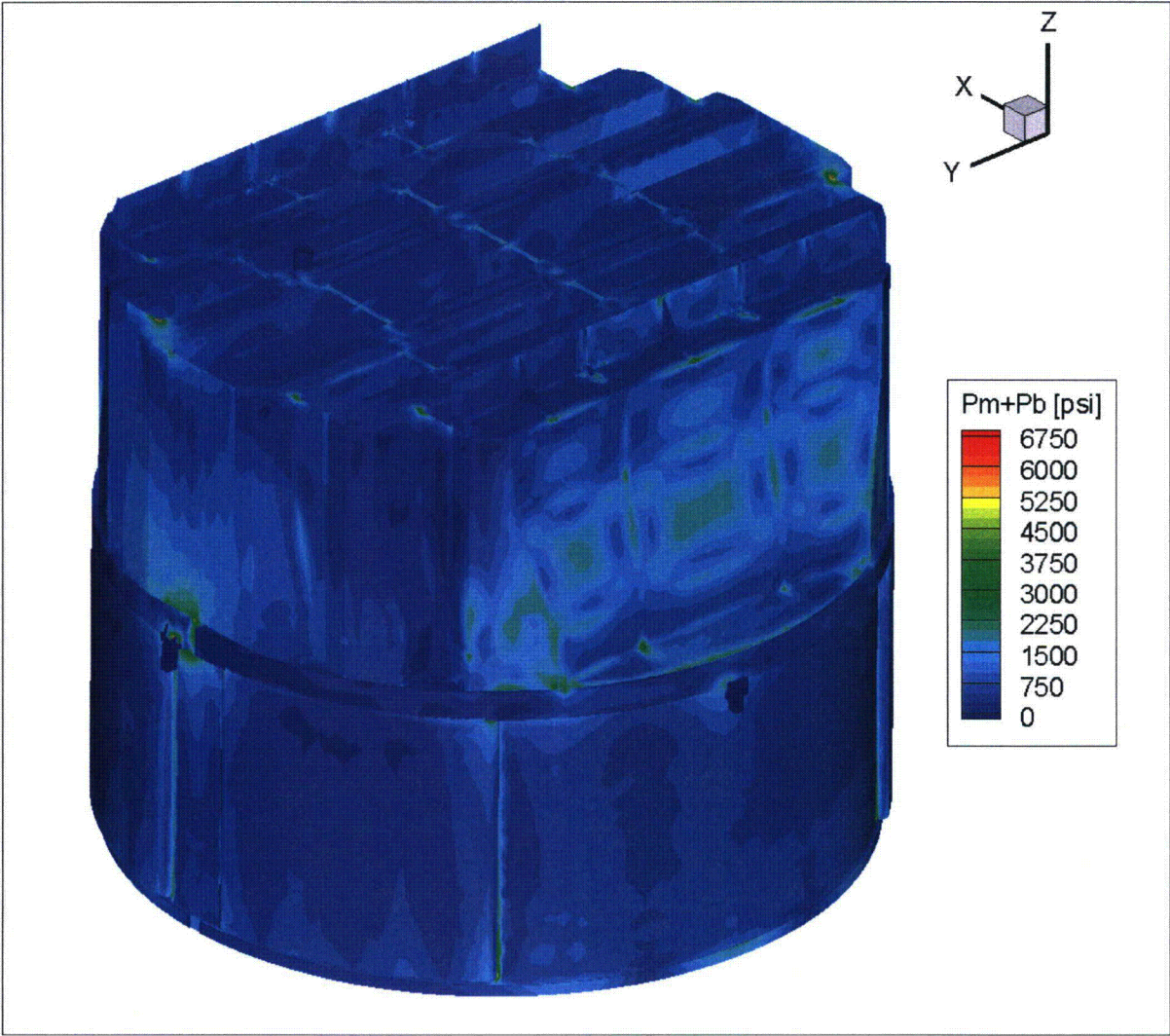


Figure 12b. Contour plot of maximum membrane+bending stress intensity, P_m+P_b , for CLTP operation with frequency shifts. The recorded stress at a node is the maximum value taken over all frequency shifts. The maximum stress intensity is 6774 psi. First view.

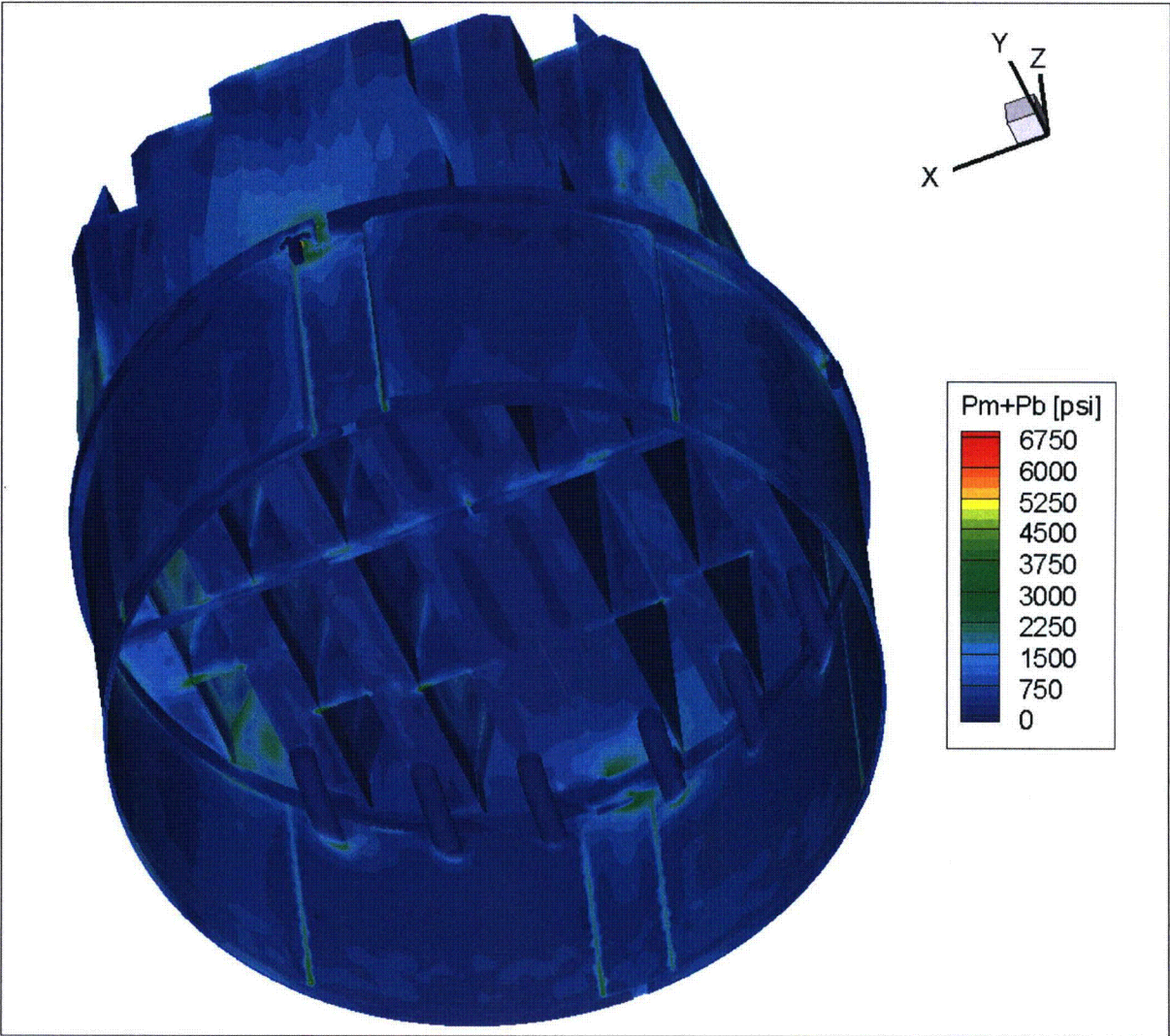


Figure 12c. Contour plot of maximum membrane+bending stress intensity, P_m+P_b , for CLTP operation with frequency shifts. This second view from beneath reveals stresses on the hood supports, support bar, inner base plates and drain pipe/skirt welds.

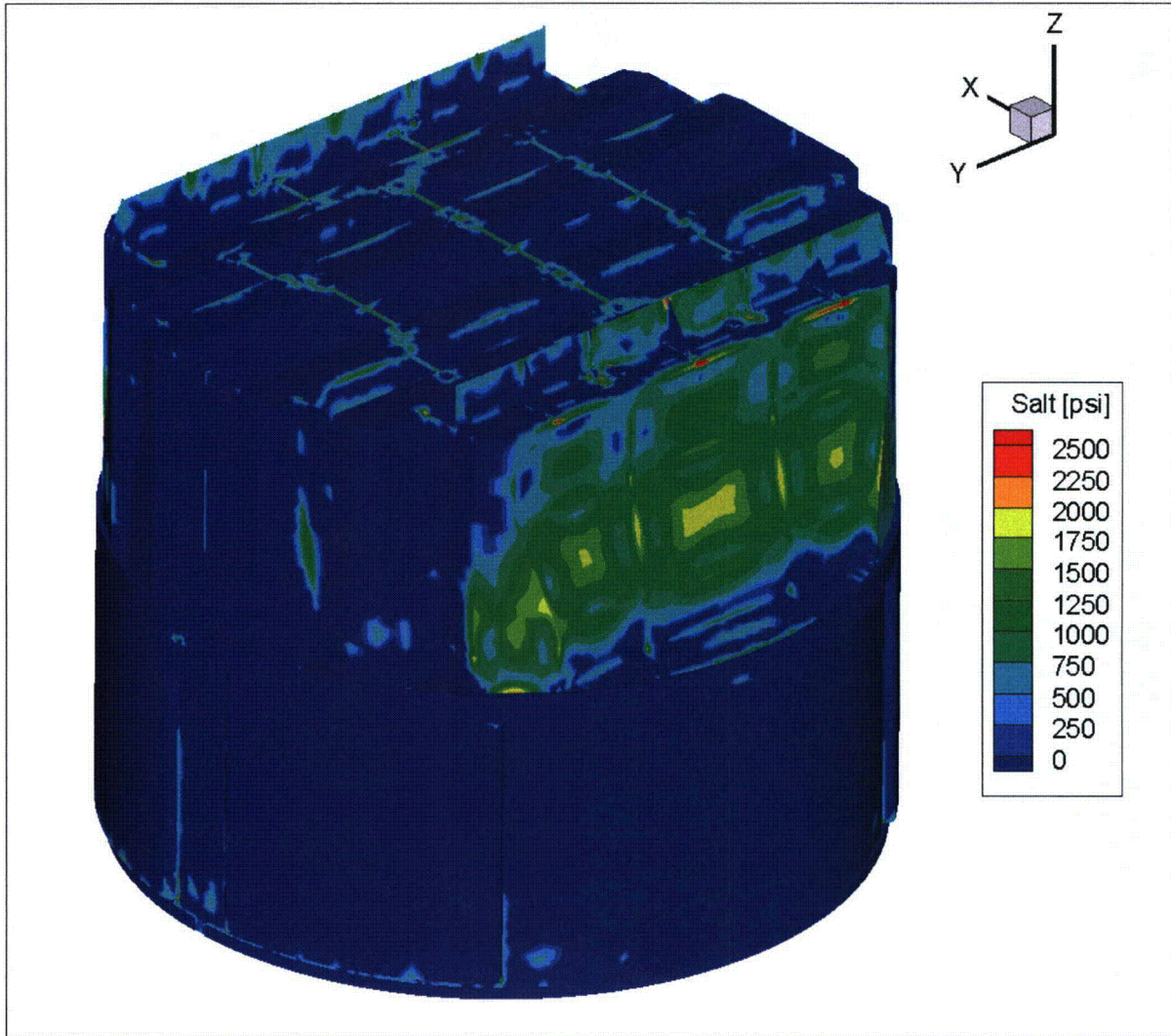


Figure 12d. Contour plot of alternating stress intensity, S_{alt} , for CLTP operation with frequency shifts. The recorded stress at a node is the maximum value taken over all frequency shifts. The maximum alternating stress intensity is 2647 psi. First view.

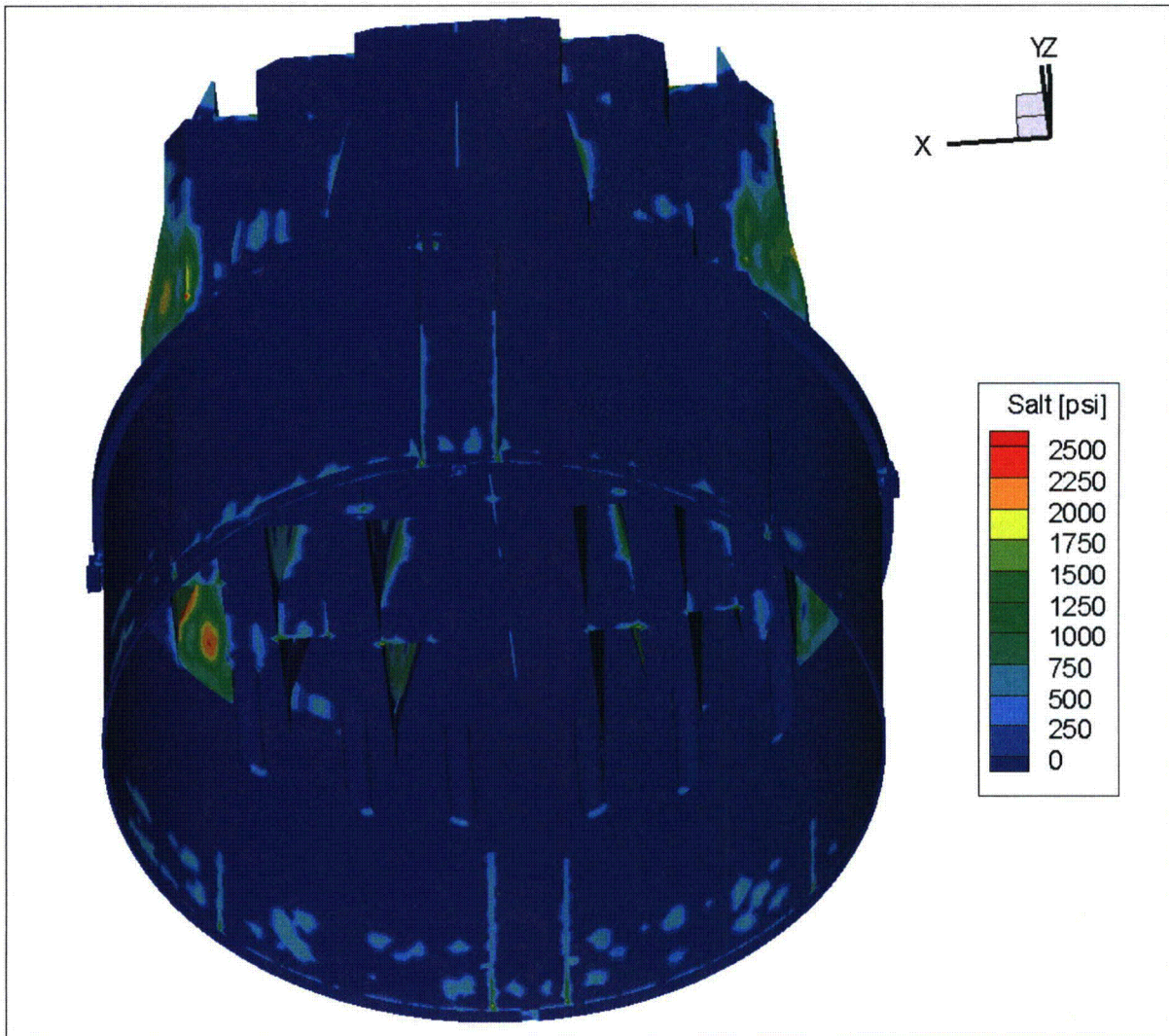


Figure 12e. Contour plot of alternating stress intensity, S_{alt} , for CLTP operation with frequency shifts. The recorded stress at a node is the maximum value taken over all frequency shifts. Second view from below.

5.2 Load Combinations and Allowable Stress Intensities

The stress ratios computed for CLTP at nominal frequency and with frequency shifting are listed in Table 8. The stress ratios are grouped according to type (SR-P for maximum membrane and membrane+bending stress, SR-a for alternating stress) and location (away from welds or on a weld). The tabulated nodes are also depicted in Figure 13 (no frequency shift) and Figure 14 (all frequency shifts included). The plots corresponding to maximum stress intensities depict all nodes with stress ratios $SR-P \leq 4$, and the plots of alternating stress ratios display all nodes with $SR-a \leq 4$.

For CLTP operation at nominal frequency the minimum stress ratio is identified as a maximum stress, $SR-P=1.88$, and is recorded on the top of the middle closure plate where it connects to the inner hood. However, this location is only weakly responsive to acoustic loads as can be seen from the high alternating stress ratio at this location ($SR-a > 6$ at all frequency shifts). The minimum alternating stress ratio, $SR-a=2.91$, occurs on the steam dam plate/gusset junction. The next lowest alternating stress ratio occurs at the bottom of the drain channel/skirt weld (note that no adjustment of nominal stresses on the basis of substructuring has been made at these locations since stress ratios were already above target levels. Based on substructuring studies in [21] and used in [22], one expects that stresses would be lower than reported here).

The effects of frequency shifts can be conservatively accounted for by identifying the minimum stress ratio at every node, where the minimum is taken over all the frequency shifts considered (including the nominal or 0% shift case). The resulting stress ratios are then processed as before to identify the smallest stress ratios anywhere on the structure, categorized by stress type (maximum or alternating) and location (on or away from a weld). The results are summarized in Table 8b and show that the lowest stress ratio, $SR-P=1.81$, occurs at the same location (strictly, at a mirror location) as in the nominal case. Moreover, the next two lowest SR-P locations are the same as in Table 8a. The two lowest alternating stress ratios, $SR-a=2.59$ and 2.70 , both lie on the outer vane bank end wall and assume their minimum values at the +7.5% frequency shift. The third lowest alternating stress ratio is 2.82 and occurs at the junction between the middle hood, hood support and base plate.

Compared to previous stress analysis of the BFN2 steam dryer [3], the addition of the modified tie bars with widened and tapered ends has eliminated virtually all of the high stress areas previously associated with old tie bar bases and nearly doubled the limiting alternating stress ratio associated with tie bars.

These stress predictions are based on the CLTP loads for the current BFN2 configuration. One of the modifications to be implemented for EPU operation is to install acoustic side branches to address potential flow-induced vibration (FIV) in the 109-113 Hz range. As is shown further in Section 5.3, the dominant frequency (109.2 Hz) for the two limiting nodes (i.e., those with the lowest alternating stress ratios) is in this range so one expects further stress reduction when the ASBs are installed. When the stresses are recomputed using the load and associated bias+uncertainty with ASBs accounted for, the minimum alternating stress ratio increases to $SR-a=2.81$.

In summary, the lowest stress ratio value at any frequency shift is associated with a maximum stress intensity and has the value $SR-P=1.81$ indicating that stresses are well below allowable levels. The lowest stress ratio associated with an alternating stress *prior to installation of ASBs* is $SR-a=2.59$. After ASBs are installed the lowest alternating stress ratio is $SR-a=2.81$. Since loads scale roughly with the square of the steam flow when acoustic resonance is not anticipated, it is reasonable to anticipate that under EPU conditions (where steam flow increases by 15%) the stresses would increase by approximately $(115\%)^2=1.32$. Under this assumption the minimum alternating stress ratio would reduce from 2.81 to $2.81/1.32=2.13$, which given that the applied loads already account for all end-to-end biases and uncertainties, still contains sufficient margin for sustained EPU operation.

Table 8a. Locations with minimum stress ratios for CLTP conditions with no frequency shift. Stress ratios are grouped according to stress type (maximum – SR-P; or alternating – SR-a) and location (away from a weld or at a weld). Bold text indicates minimum stress ratio of any type on the structure. Signal noise has been partially removed using 19% power data. Locations are depicted in Figure 13.

Stress Ratio	Weld	Location	Location (in.) (a)			node(b)	Stress Intensity (psi)			Stress Ratio	
			x	y	z		Pm	Pm+Pb	S _{alt}	SR-P	SR-a
SR-P	No	1. USR/Support Block/Support	7	122.3	-9.5	123931	6571	6571	1411	2.78	8.76
	"	2. USR/Seismic Block/Support Block	-122.1	10	-9.5	123865	6038	6038	1178	3.03	10.5
SR-a	No	<i>SR-a > 4 at non welds</i>									
SR-P	Yes	1. Top Cover Inner Hood/Middle Closure Plate/Inner Hood	-31.5	-108.4	88.9	100549	5352	6206	878	1.88	7.82
"	"	2. Splice Bar/USR	2.2	119	0	123619	5330	5330	<500	1.89	>13
"	"	3. Middle Cover Plate/Hood Support/Inner Hood	39.8	-59.8	0	98774	4809	4907	1609	2.09	4.27
"	"	4. Middle Cover Plate/Hood Support/Middle Hood	-70.8	54.6	0	100927	3893	4561	2008	2.59	3.42
"	"	5. Submerged Drain Channel/Skirt	91	-76.7	-100.5	104142	1063	5719	1762	2.64	3.9
"	"	6. Hood Support/Outer Hood/Outer Cover Plate	-102	28.7	2	106790	3769	4802	1778	2.67	3.86
"	"	7. Top Cover Middle Hood/Outer Closure Plate/Middle Hood	-62.5	85	88.9	100843	3550	4062	1827	2.83	3.76

See Table 7a for notes (a)-(c).

Table 8a (cont.). Locations with minimum stress ratios for CLTP conditions with no frequency shift. Stress ratios are grouped according to stress type (maximum – SR-P; or alternating – SR-a) and location (away from a weld or at a weld). Bold text indicates minimum alternating stress ratio on the structure. Signal noise has been partially removed using 19% power data. Locations are depicted in Figure 13.

Stress Ratio	Weld	Location	Location (in.) (a)			node(b)	Stress Intensity (psi)			Stress Ratio	
			x	y	z		Pm	Pm+Pb	S _{alt}	SR-P	SR-a
SR-a	Yes	1. Dam Plate/New Gusset	-77	0	104.4	101769	137	2441	2360	6.19	2.91
"	"	2. Submerged Drain Channel/Skirt	11.5	-118.4	-100.5	104169	1016	4680	2101	3.23	3.27
"	"	3. Middle Cover Plate/Hood Support/Middle Hood	-70.8	54.6	0	100927	3893	4561	2008	2.59	3.42
"	"	4. Top Cover Middle Hood/Middle Hood/Shell Tie Bar ^(c)	-62.5	25.2	88.9	107158	1397	3770	2068	4	3.32
"	"	5. Outer Side Panel/Vane Bank Thin/Vane Bank Thick/Outer End Wall	86	85	12.1	102701	500	2079	1897	7.26	3.62
"	"	6. Top Cover Middle Hood/Outer Closure Plate/Middle Hood	62.5	85	88.9	97204	2951	3054	1892	3.41	3.63

See Table 7a for notes (a)-(c).

Table 8b. Locations with minimum stress ratios for CLTP conditions with frequency shifts. Stress ratios at every node are recorded as the lowest stress ratio identified during the frequency shifts. Stress ratios are grouped according to stress type (maximum – SR-P; or alternating – SR-a) and location (away from a weld or at a weld). Bold text indicates minimum stress ratio of any type on the structure. Signal noise has been partially removed using 19% power data. Locations are depicted in Figure 14.

Stress Ratio	Weld	Location	Location (in.) (a)			node(b)	Stress Intensity (psi)			Stress Ratio		% Freq. Shift
			x	y	z		Pm	Pm+Pb	S _{alt}	SR-P	SR-a	
SR-P	No	1. USR/Support Block/Support	7	122.3	-9.5	123931	6774	6774	1602	2.7	7.72	-10
		2. USR/Seismic Block/Support Block	-122.1	10	-9.5	123865	6437	6437	1492	2.84	8.28	10
SR-a	No	1. Outer Hood	93.5	-58.2	88.6	43101	283	3343	3241	8.21	3.81	-10
"	"	2. Gusset Pad Thin	-93	-0.2	88.9	88782	238	3137	3094	8.75	4	-10
SR-P	Yes	1. Top Cover Inner Hood/Middle Closure Plate/Inner Hood	31.5	108.4	88.9	98291	5561	6121	995	1.81	6.9	10
"	"	2. Splice Bar/USR	2.2	119	0	123619	5409	5409	<500	1.86	>13	7.5
"	"	3. Middle Cover Plate/Hood Support/Inner Hood	-39.8	59.8	0	99801	5394	5415	2100	1.87	3.27	10
"	"	4. Hood Support/Outer Hood/Outer Cover Plate	-102	28.7	2	106790	4275	4802	1963	2.35	3.5	10
"	"	5. Middle Cover Plate/Hood Support/Middle Hood	-70.8	54.6	0	100927	4146	4561	2008	2.43	3.42	7.5
"	"	6. Top Cover Middle Hood/Outer Closure Plate/Middle Hood	-62.5	85	88.9	100843	4061	4657	2333	2.48	2.94	10
"	"	7. Submerged Drain Channel/Skirt	-91	-76.7	-100.5	110570	1353	5971	2328	2.53	2.95	10
"	"	8. Outer Hood/Gusset Pad Thin/Top Cover Outer Hood ^(c)	-93.5	-57.5	88.9	108730	413	5848	2379	2.58	2.89	-5
"	"	9. Outer Hood/Gusset Pad Thin/Top Cover Outer Hood ^(c)	-93.5	-0.8	88.9	108664	500	5743	2179	2.63	3.15	-10

See Table 7a for notes (a)-(c).

Table 8b (cont.). Locations with minimum stress ratios for CLTP conditions with frequency shifts. Stress ratios at every node are recorded as the lowest stress ratio identified during the frequency shifts. Stress ratios are grouped according to stress type (maximum – SR-P; or alternating – SR-a) and location (away from a weld or at a weld). Bold text indicates minimum alternating stress ratio. Signal noise has been partially removed using 19% power data. Locations are depicted in Figure 14.

Stress Ratio	Weld	Location	Location (in.) (a)			node(b)	Stress Intensity (psi)			Stress Ratio		% Freq. Shift
			x	y	z		Pm	Pm+Pb	S _{alt}	SR-P	SR-a	
SR-a	Yes	1. Outer Side Panel/Vane Bank Thin/Vane Bank Thick/Outer End Wall(d)	86	85	12.1	102701	551	2863	2647 (2441)	5.27	2.59 (2.81)	7.5
"	"	2. Outer End Wall Ext/Outer End Wall(d)	93.4	-75.4	0	103411	631	2753	2540 (2272)	5.48	2.70 (3.02)	7.5
"	"	3. Middle Cover Plate/Hood Support/Middle Hood	70.8	54.6	0	97294	2493	3150	2433	4.04	2.82	5
"	"	4. Dam Plate/New Gusset	-77	0	104.4	101769	137	2457	2426	6.14	2.83	2.5
"	"	5. Outer Hood/Outer End Wall	100.7	-65.9	25.1	103405	867	2760	2416	5.47	2.84	7.5
"	"	6. Outer Hood/Gusset Pad Thin/Top Cover Outer Hood(c)	-93.5	-57.5	88.9	108730	413	5848	2379	2.58	2.89	-5
"	"	7. Top Cover Middle Hood/Outer Closure Plate/Middle Hood	62.5	85	88.9	97204	3178	3446	2353	3.17	2.92	10
"	"	8. Submerged Drain Channel/Skirt	-91	-76.7	-100.5	110570	1353	5971	2328	2.53	2.95	10
"	"	9. Outer Hood/Top Cover Outer Hood	-93.5	-47.4	88.9	108710	356	2344	2328	6.44	2.95	-5
"	"	10. Top Cover Middle Hood/Middle Hood/Shell Tie Bar(c)	-62.5	25.2	88.9	107158	1613	4958	2322	3.05	2.96	-5
"	"	11. Submerged Drain Channel/Skirt	11.5	118.4	-100.5	104115	1440	2905	2289	5.2	3	10

See Table 7a for notes (a)-(c).

Note (d): Values in parentheses correspond to stress intensities and ratios with ASBs installed.

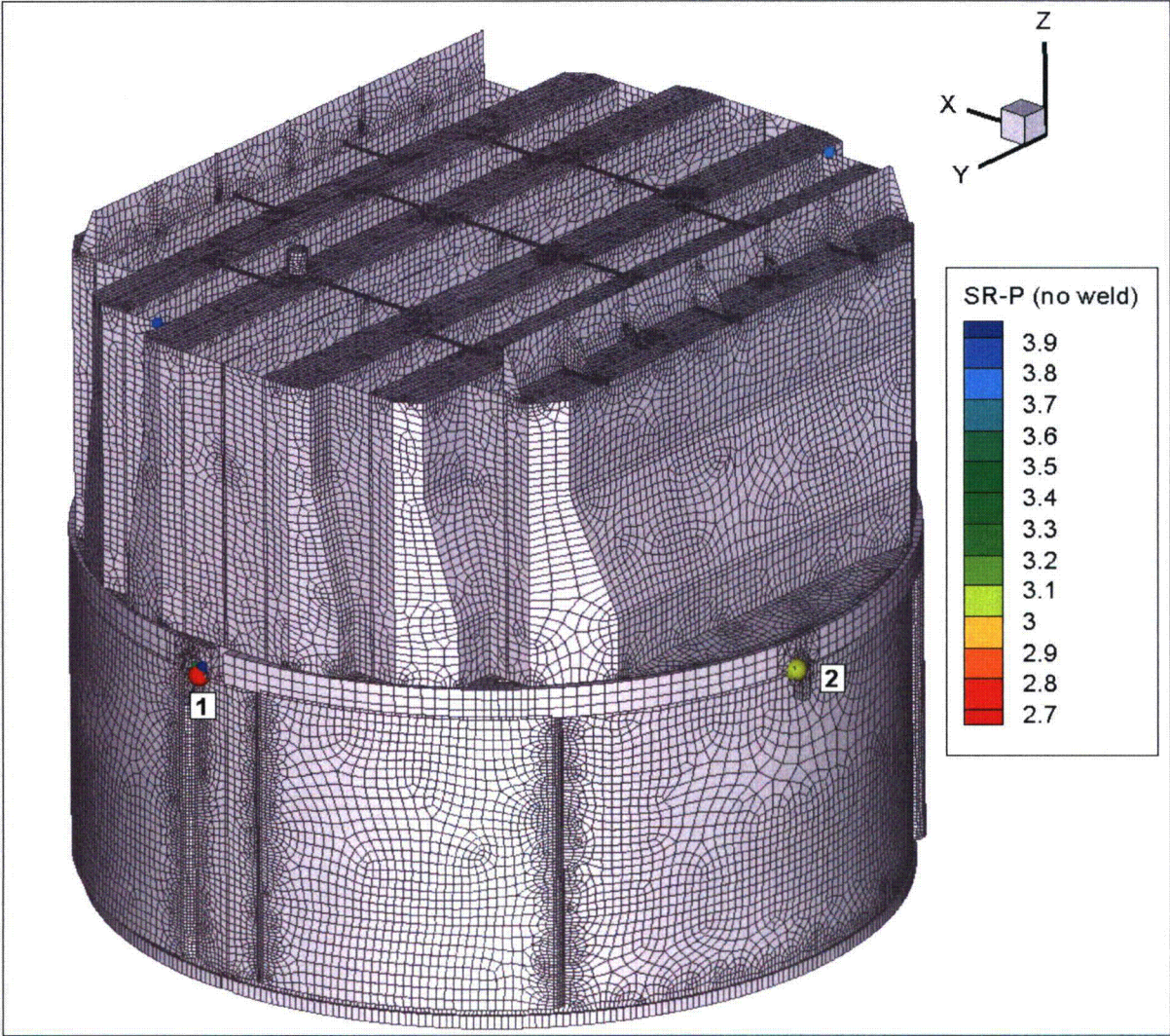


Figure 13a. Locations of nodes with stress ratios, $SR-P \leq 4$, associated with a maximum stress at non-welds for nominal CLTP operation. Numbers refers to the enumerated locations for SR-P values at non-welds in Table 8a.

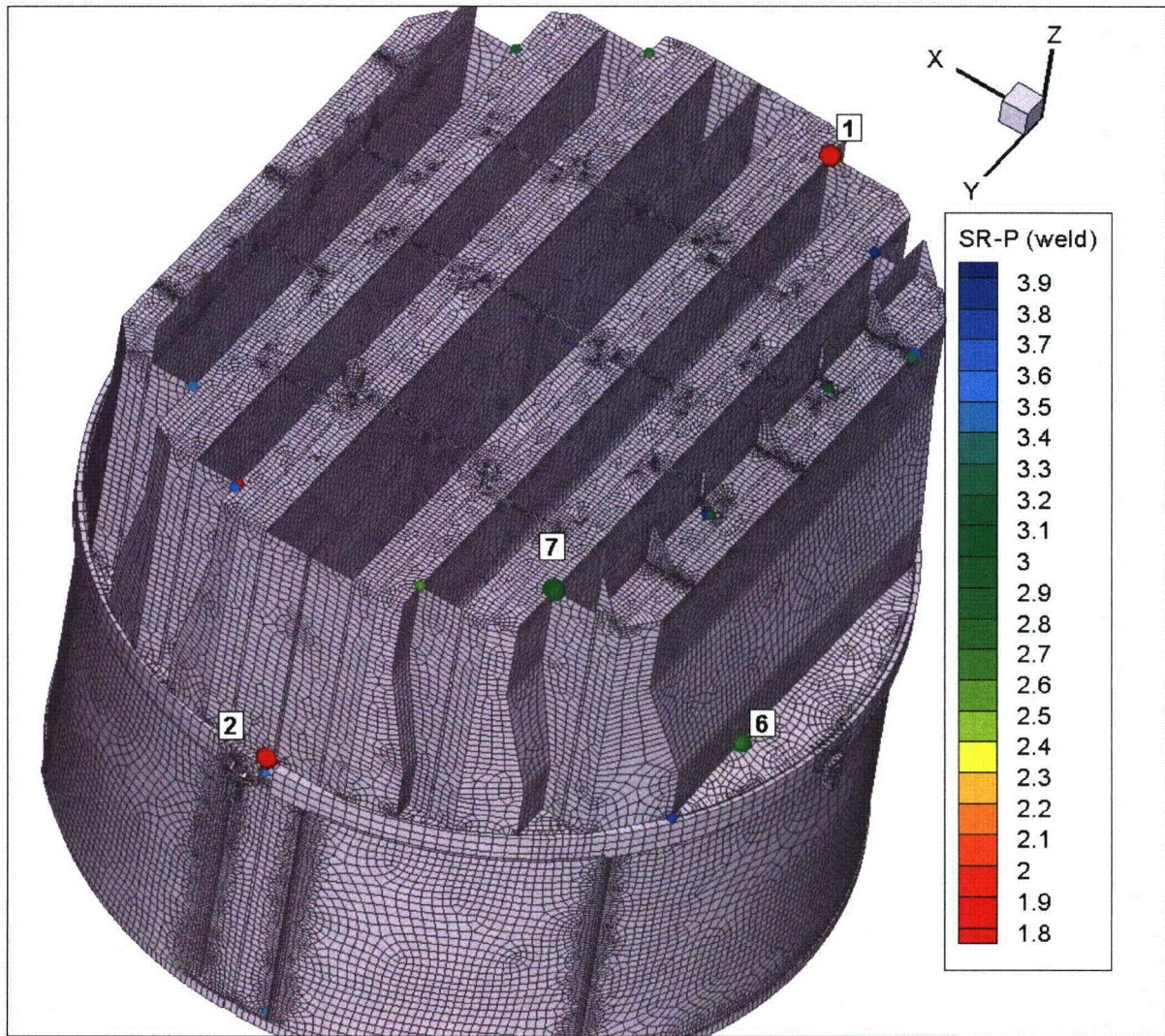


Figure 13b. Locations of smallest stress ratios, $SR-P \leq 4$, associated with maximum stresses at welds for nominal CLTP operation. Numbers refer to the enumerated locations for SR-P values at welds in Table 8a. This view shows locations 1, 2, 6 and 7.

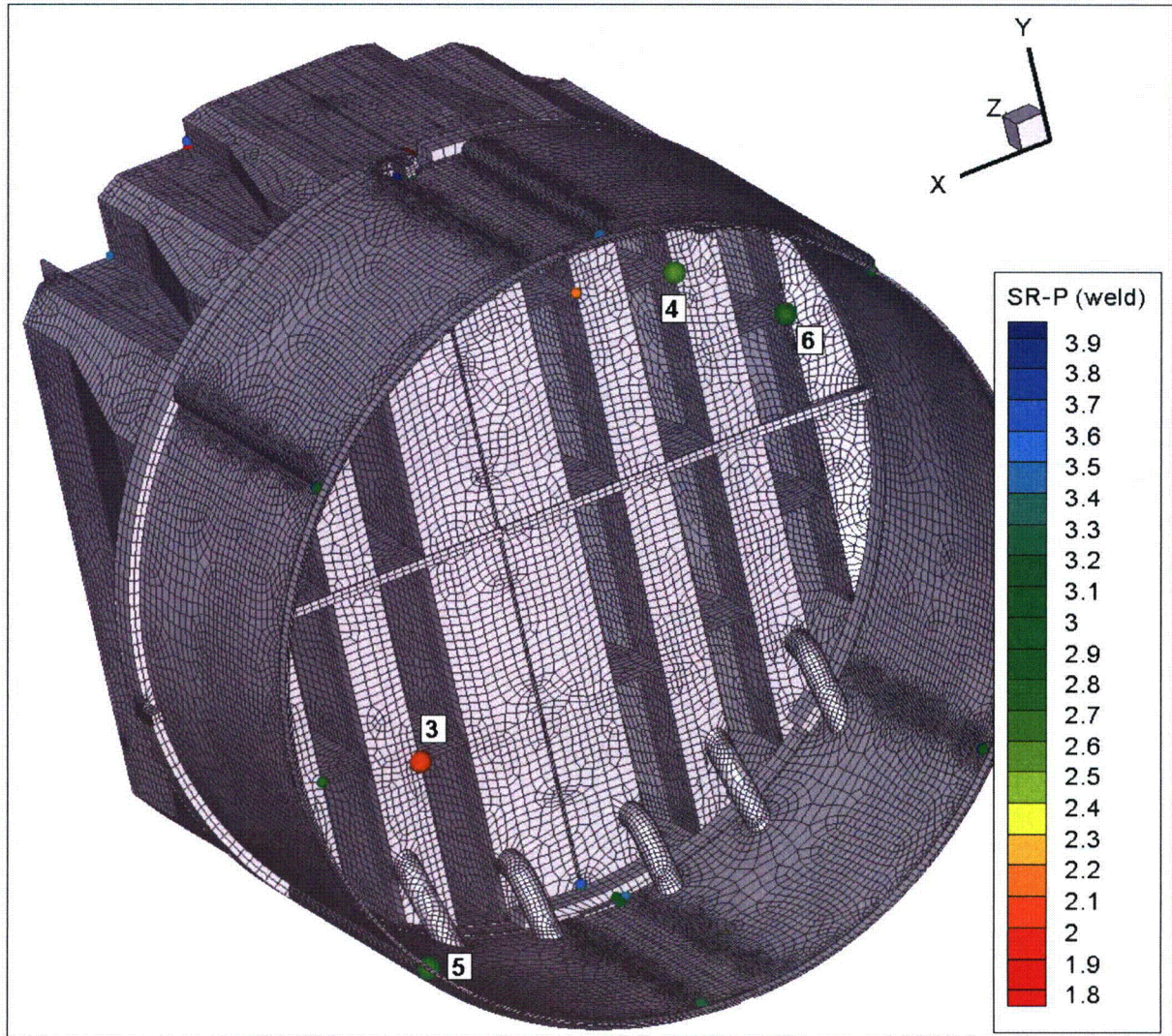


Figure 13c. Locations of minimum stress ratios, $SR-P \leq 4$, associated with maximum stresses at welds for nominal CLTP operation. Numbers refer to the enumerated locations for SR-P values at welds in Table 8a. This view shows locations 3-6.

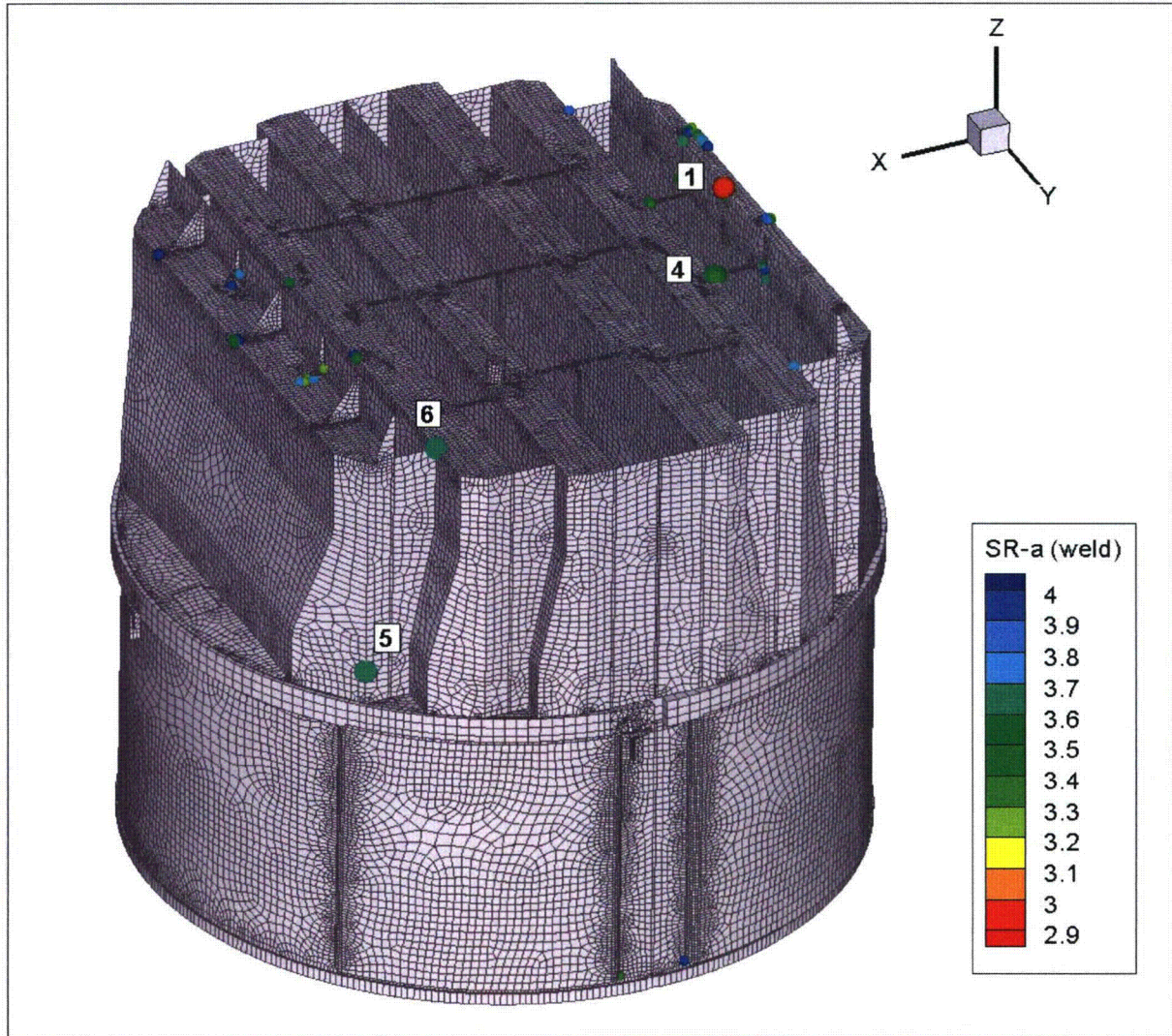


Figure 13d. Locations of minimum alternating stress ratios, $SR-a \leq 4$, at welds for nominal CLTP operation. Numbers refer to the enumerated locations for $SR-a$ values at welds in Table 8a. Locations 1 and 4-6 are shown.

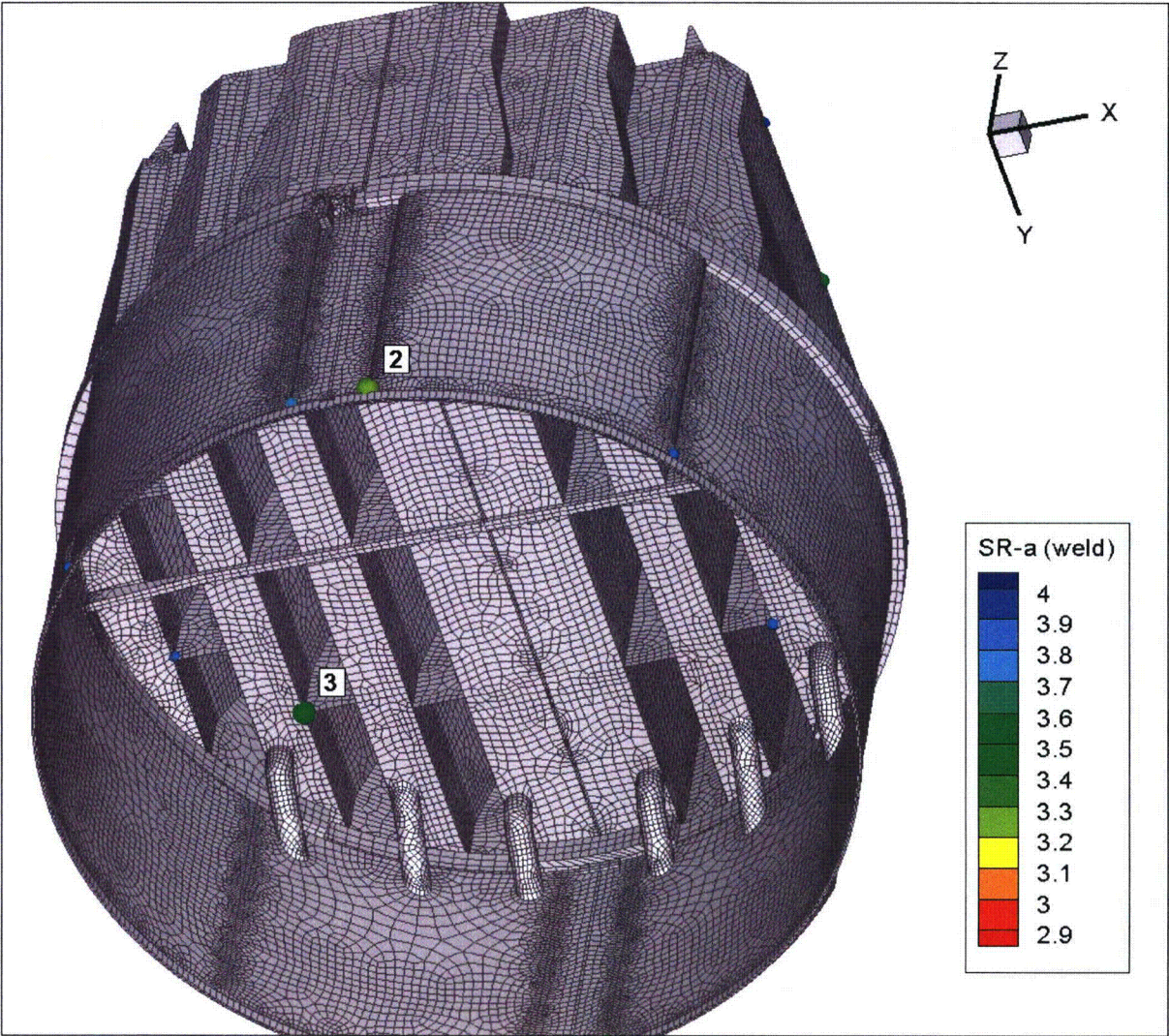


Figure 13e. Locations of minimum alternating stress ratios, $SR-a \leq 4$, at welds for nominal CLTP operation. Numbers refer to the enumerated locations for SR-a values at welds in Table 8a. Locations 2 and 3 are shown.

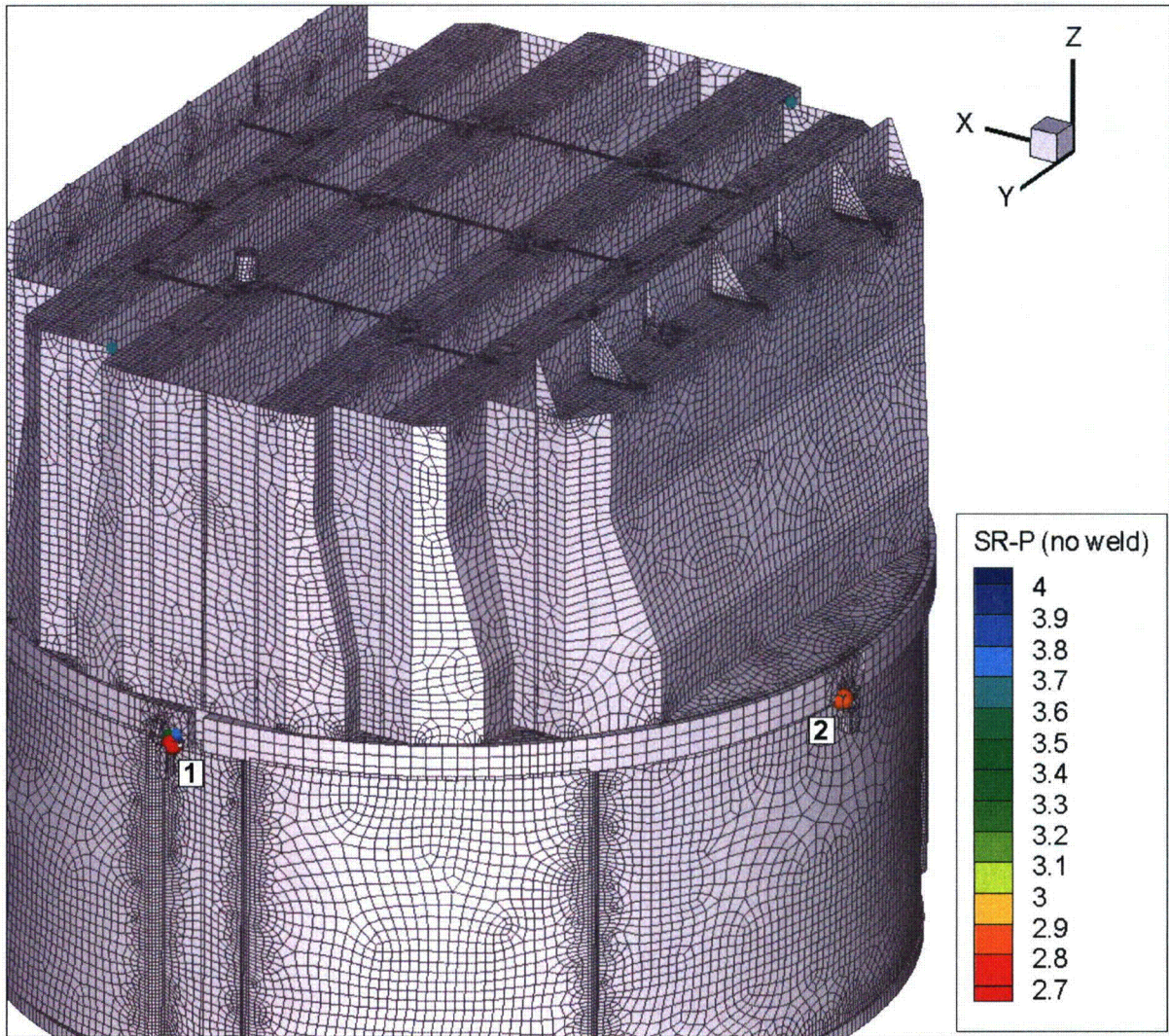


Figure 14a. Locations of minimum stress ratios, $SR-P \leq 4$, associated with maximum stresses at non-welds for CLTP operation with frequency shifts. The recorded stress ratio is the minimum value taken over all frequency shifts. The numbers refers to the enumerated location for SR-P values at non-welds in Table 8b.

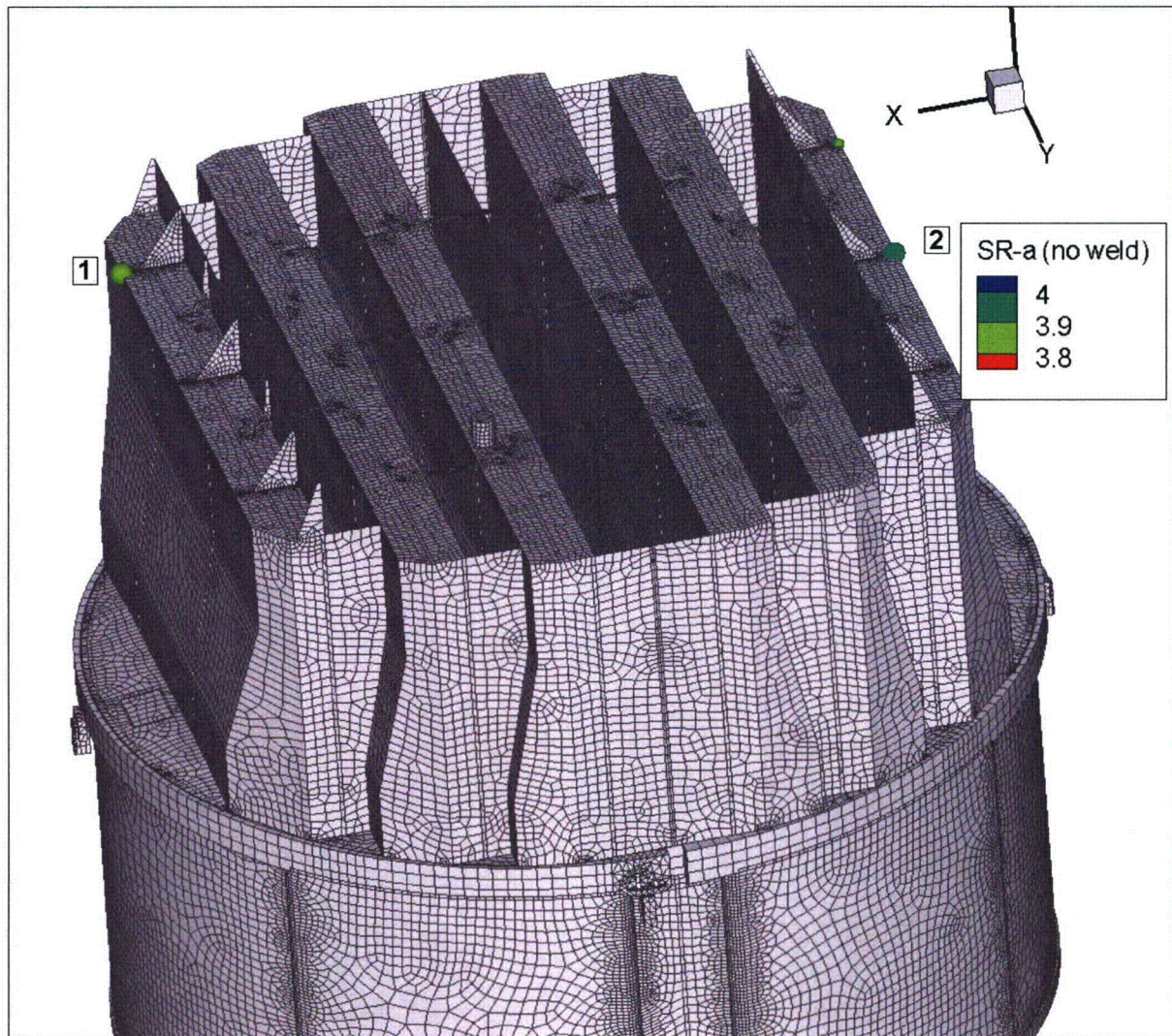


Figure 14b. Locations of minimum alternating stress ratios, $SR-a \leq 4$, at non-welds for CLTP operation with frequency shifts. The recorded stress ratio at a node is the minimum value taken over all frequency shifts. Numbers refer to the enumerated locations for SR-a values at non-welds in Table 8b.

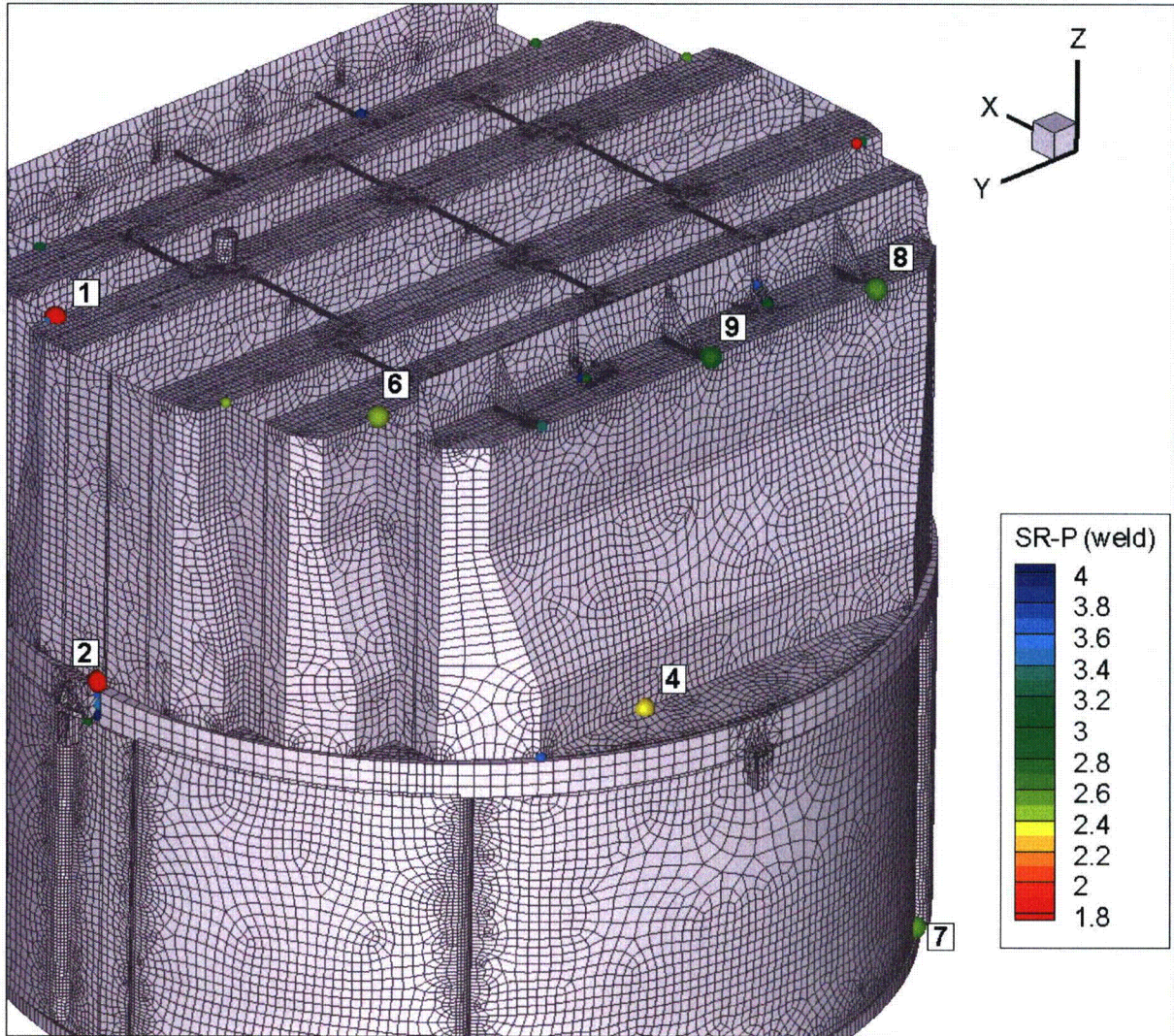


Figure 14c. Locations of minimum stress ratios, $SR-P \leq 4$, associated with maximum stresses at welds for CLTP operation with frequency shifts. The recorded stress ratio at a node is the minimum value taken over all frequency shifts. Numbers refer to the enumerated locations for SR-P values at welds in Table 8b. This view shows locations 1, 2, 4 and 6-9.

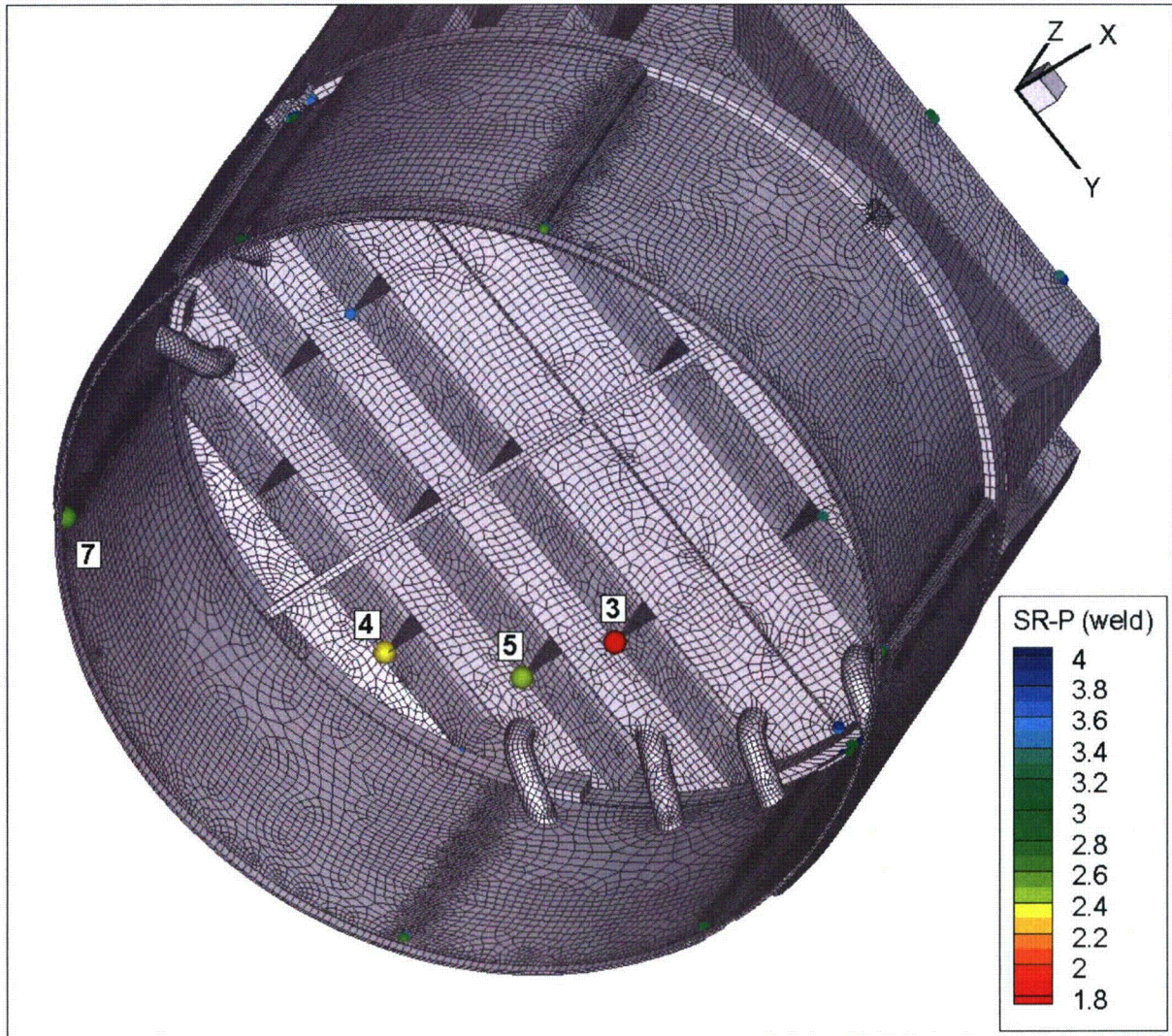


Figure 14d. Locations of minimum stress ratios, $SR-P \leq 4$, associated with maximum stresses at welds for CLTP operation with frequency shifts. The recorded stress ratio at a node is the minimum value taken over all frequency shifts. Numbers refer to the enumerated locations for SR-P values at welds in Table 8b. This view shows locations 3-5 and 7.

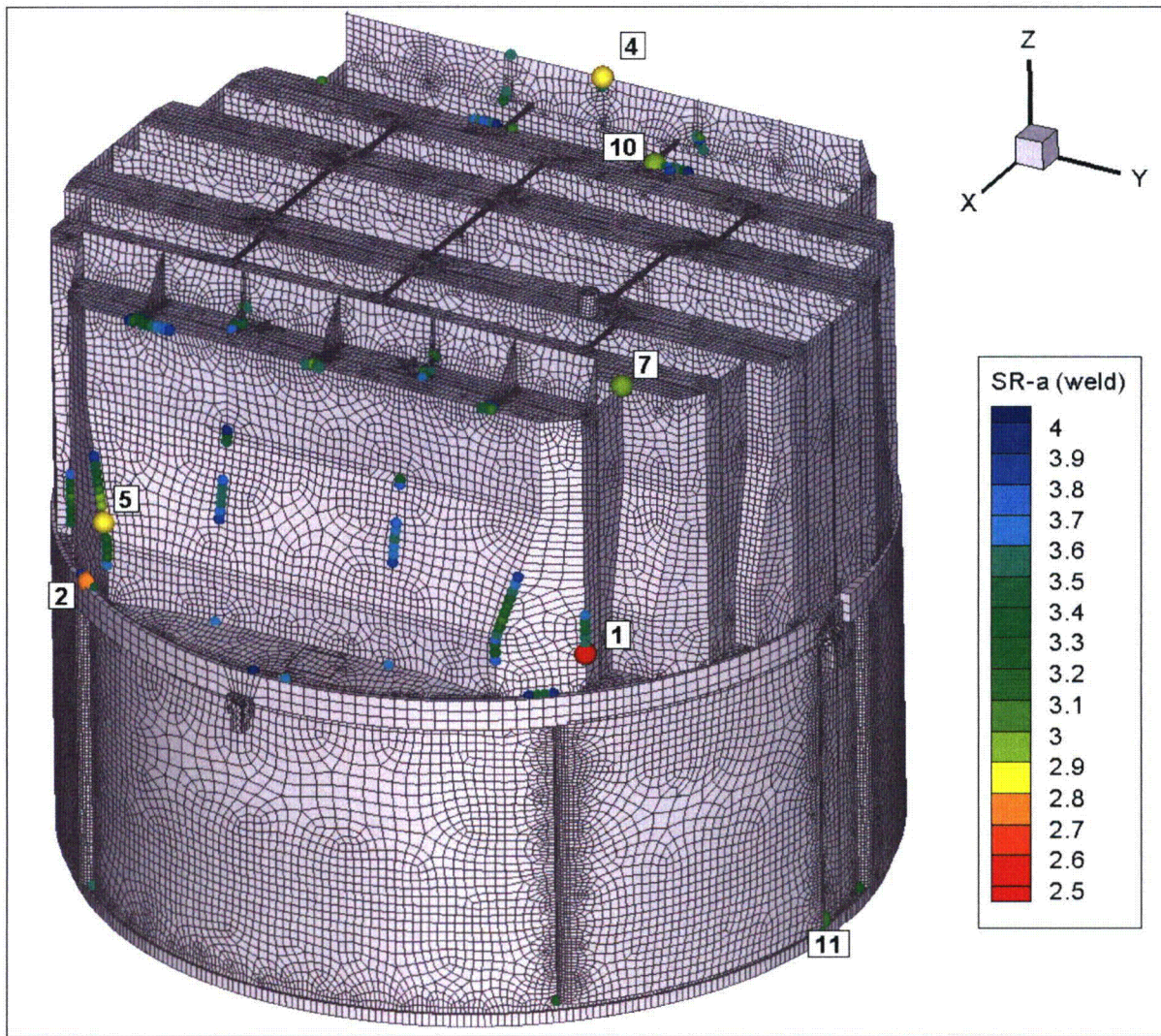


Figure 14e. Locations of minimum alternating stress ratios, $SR-a \leq 4$, at welds for CLTP operation with frequency shifts. The recorded stress ratio at a node is the minimum value taken over all frequency shifts. Numbers refer to the enumerated locations for SR-a values at welds in Table 8b. This view shows locations 1, 2, 4, 5, 7, 10 and 11.

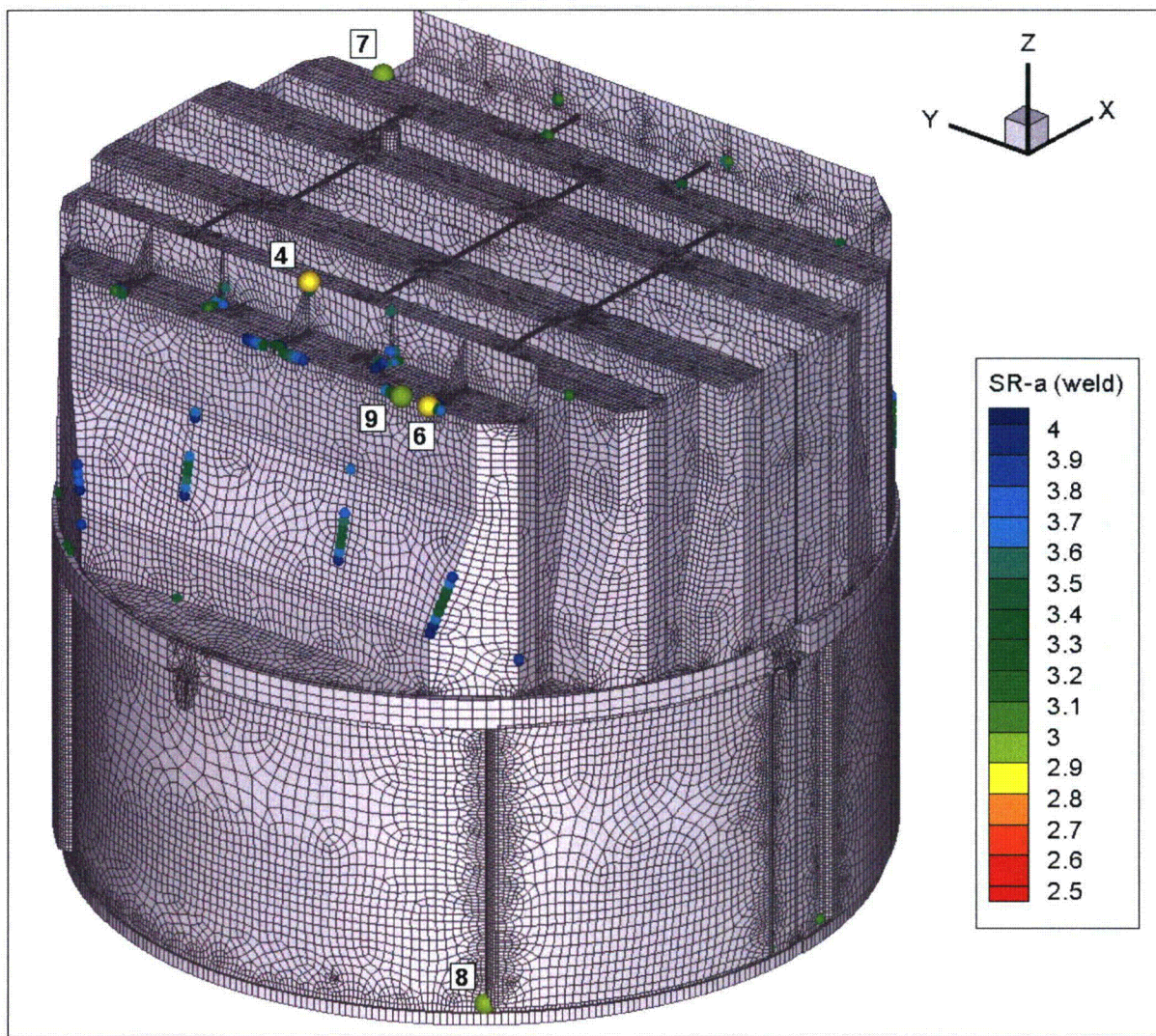


Figure 14f. Locations of minimum alternating stress ratios, $SR-a \leq 4$, at welds for CLTP operation with frequency shifts. The recorded stress ratio at a node is the minimum value taken over all frequency shifts. Numbers refer to the enumerated locations for SR-a values at welds in Table 8b. This view shows locations 4 and 6-9.

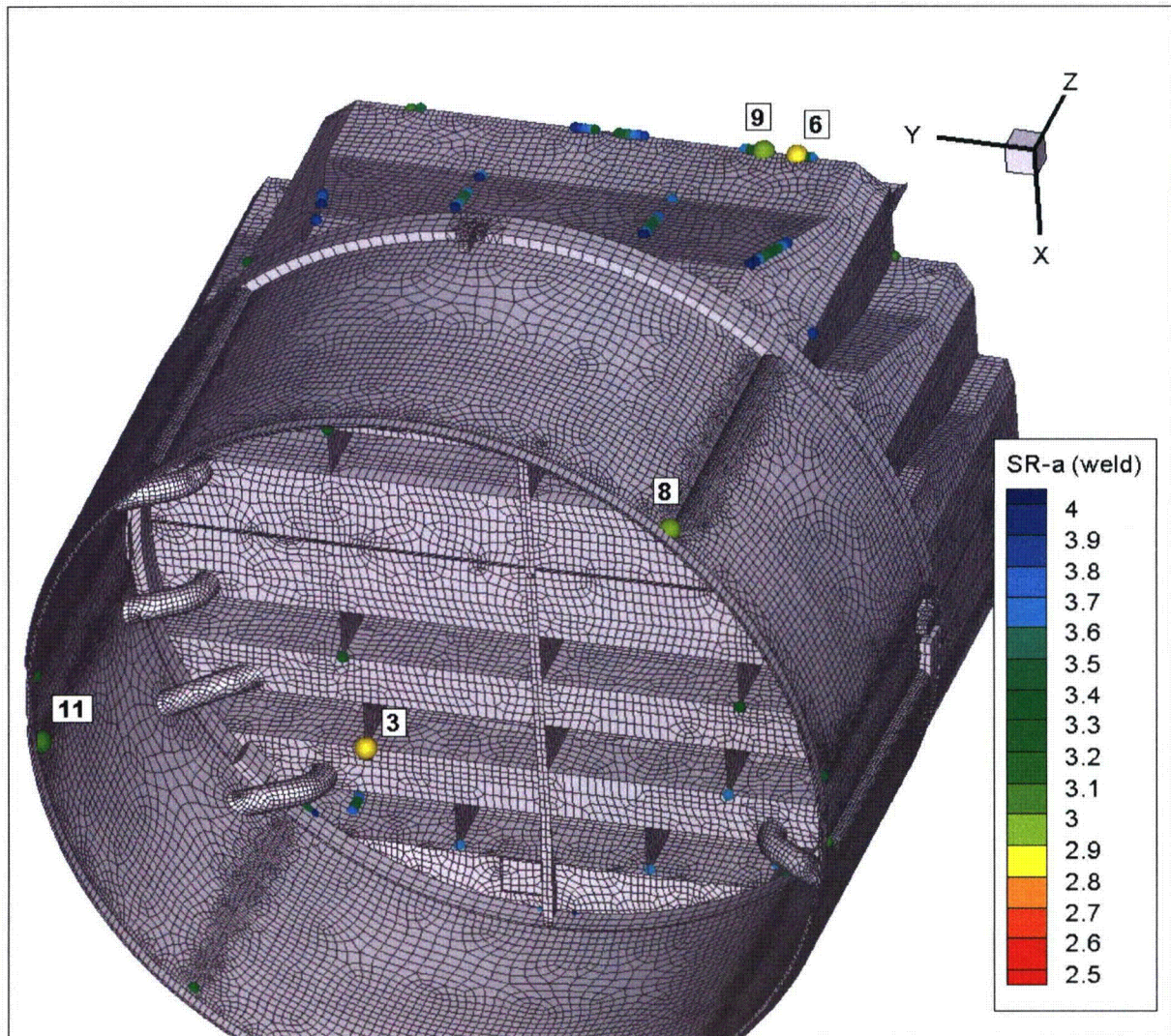


Figure 14g. Locations of minimum alternating stress ratios, $SR-a \leq 4$, at welds for CLTP operation with frequency shifts. The recorded stress ratio at a node is the minimum value taken over all frequency shifts. Numbers refer to the enumerated locations for SR-a values at welds in Table 8b. This view shows locations 3, 6, 8, 9 and 11.

5.3 Frequency Content and Filtering of the Stress Signals

The frequency contribution to the stresses can be investigated by examining the power spectral density (PSD) curves and accumulative PSDs for selected nodes having low alternating stress ratios. The accumulative PSDs are computed directly from the Fourier coefficients as

$$\Sigma(\omega_n) = \sqrt{\sum_{k=1}^n |\tilde{\sigma}(\omega_k)|^2}$$

where $\tilde{\sigma}(\omega_k)$ is the complex stress harmonic at frequency, ω_k . Accumulative PSD plots are useful for determining the frequency components and frequency ranges that make the largest contributions to the fluctuating stress. Unlike PSD plots, no “binning” or smoothing of frequency components is needed to obtain smooth curves. Steep step-like rises in $\Sigma(\omega)$ indicate the presence of a strong component at a discrete frequency whereas gradual increases in the curve imply significant content over a broader frequency range. From Parseval’s theorem, equality between $\Sigma(\omega_N)$ (where N is the total number of frequency components) and the RMS of the stress signal in the time domain is established.

The selected nodes are the ones having the lowest alternating stress ratios (at a weld) in Table 8b. These are:

- Node 102701 – located on the weld connecting the outer vane bank end plate to the outer end wall. The associated PSDs are shown in Figure 15a.
- Node 103411 - located on the weld at the bottom of the outer vane bank end wall on the upper support ring. The associated PSDs are shown in Figure 15b.
- Node 97294 – located on the weld at the middle hood/hood support/base plate junction. The associated PSDs are shown in Figure 15c.
- Node 101769 – located on the top of the weld connecting the new gusset base to the steam dam plate. The associated PSDs are shown in Figure 15d.

In each case, since there are six stress components and up to three different section locations for shells (the top, mid and bottom surfaces), there is a total of 18 stress histories per component. Moreover, at junctions there are at least two components that meet at the junction. The particular stress component that is plotted is chosen as follows. First, the component and section location (top/mid/bottom) is taken as the one that has the highest alternating stress. This narrows the selection to six components. Of these, the component having the highest Root Mean Square (RMS) is selected.

For nodes 102701 and 103411, the PSD curves are qualitatively similar and are marked by a large increase at 117.4 Hz (this corresponds to the +7.5% shift; at zero shift this forcing frequency would correspond to 109.2 Hz) and a smaller one about 68.2 Hz (63.4 at zero shift). This similarity is not surprising given that both nodes reside on the same component (the outer vane bank end plate). The shifted 109.2 Hz peak lies within the 109-113 Hz frequency range addressed by ASBs that will be installed for EPU operation to suppress FIV. Therefore, the installed ASBs will reduce the loads and associated stress peaks in this frequency range. The effects on stress intensities and alternating stress ratios are indicated in Table 8b. For node

97294, the dominant frequency is 196.8 Hz whereas for the last node, 101769, the dominant frequency is 86.6 Hz. Shifting the frequency of the applied load appears to shift the peaks, which is indicative of a peak in the applied forcing signal.

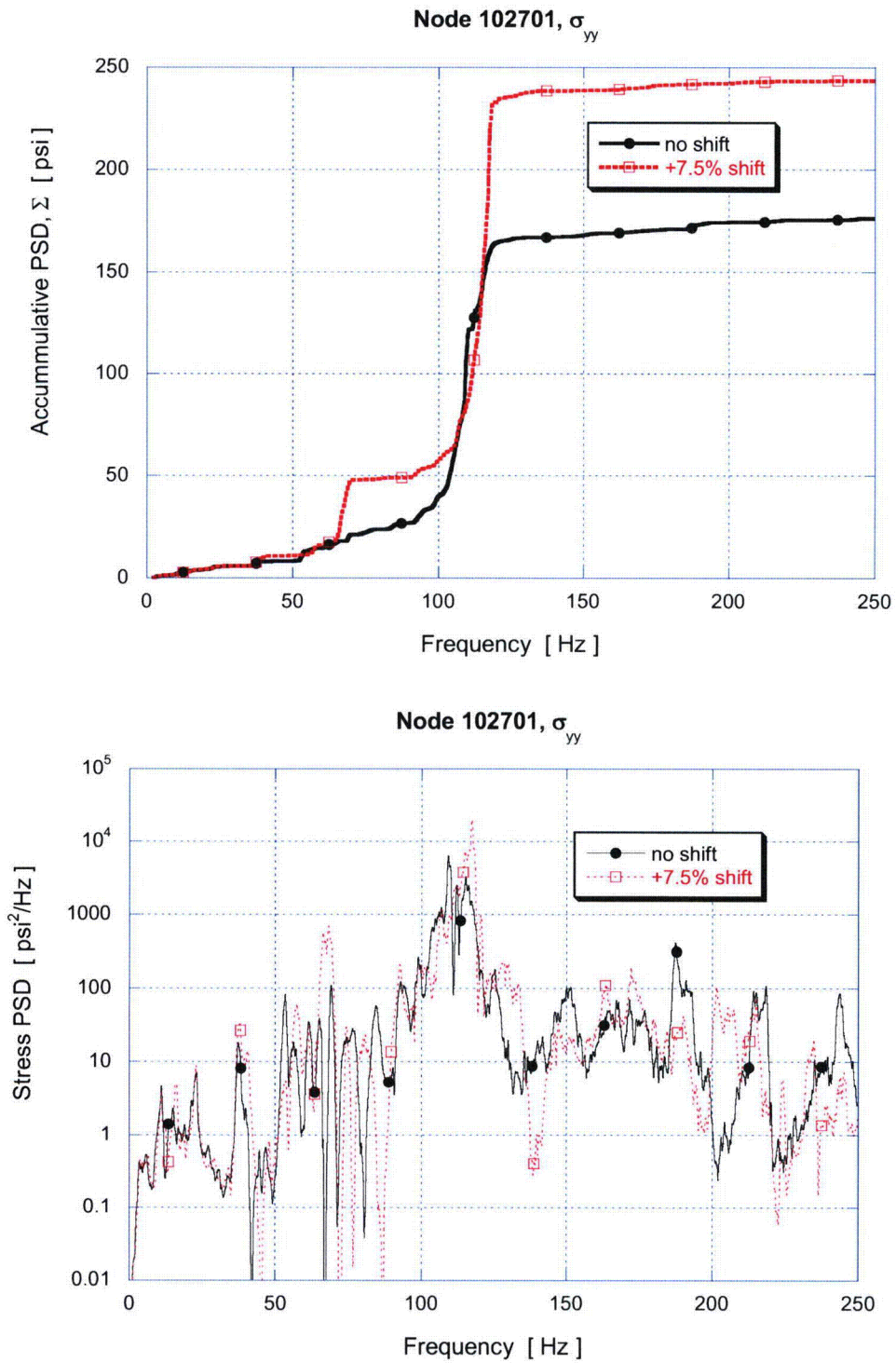


Figure 15a. Accumulative PSD and PSD curves of the σ_{yy} stress response at node 102,701.

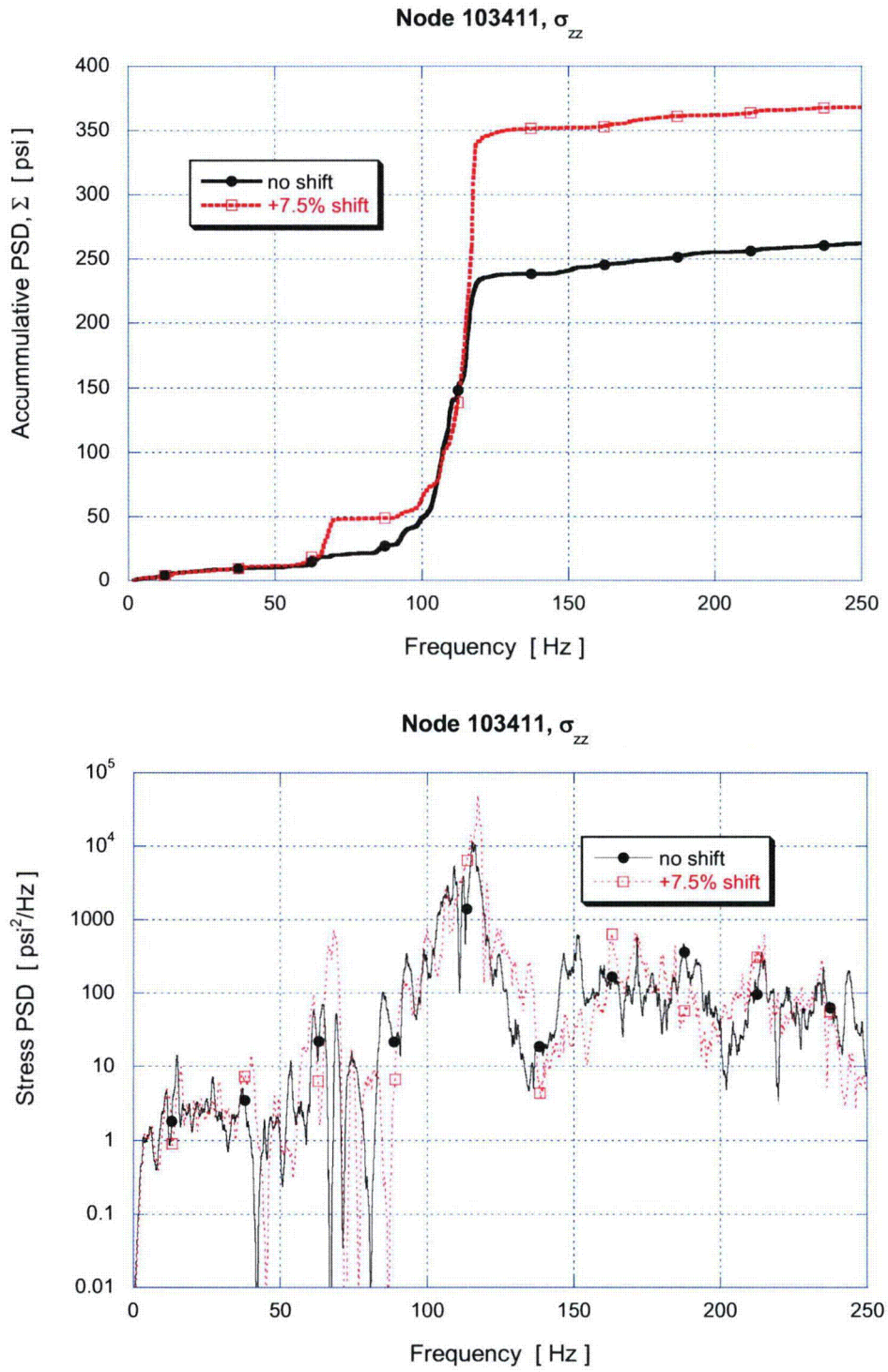


Figure 15b. Accumulative PSD and PSD of the σ_{zz} stress response at node 103,411.

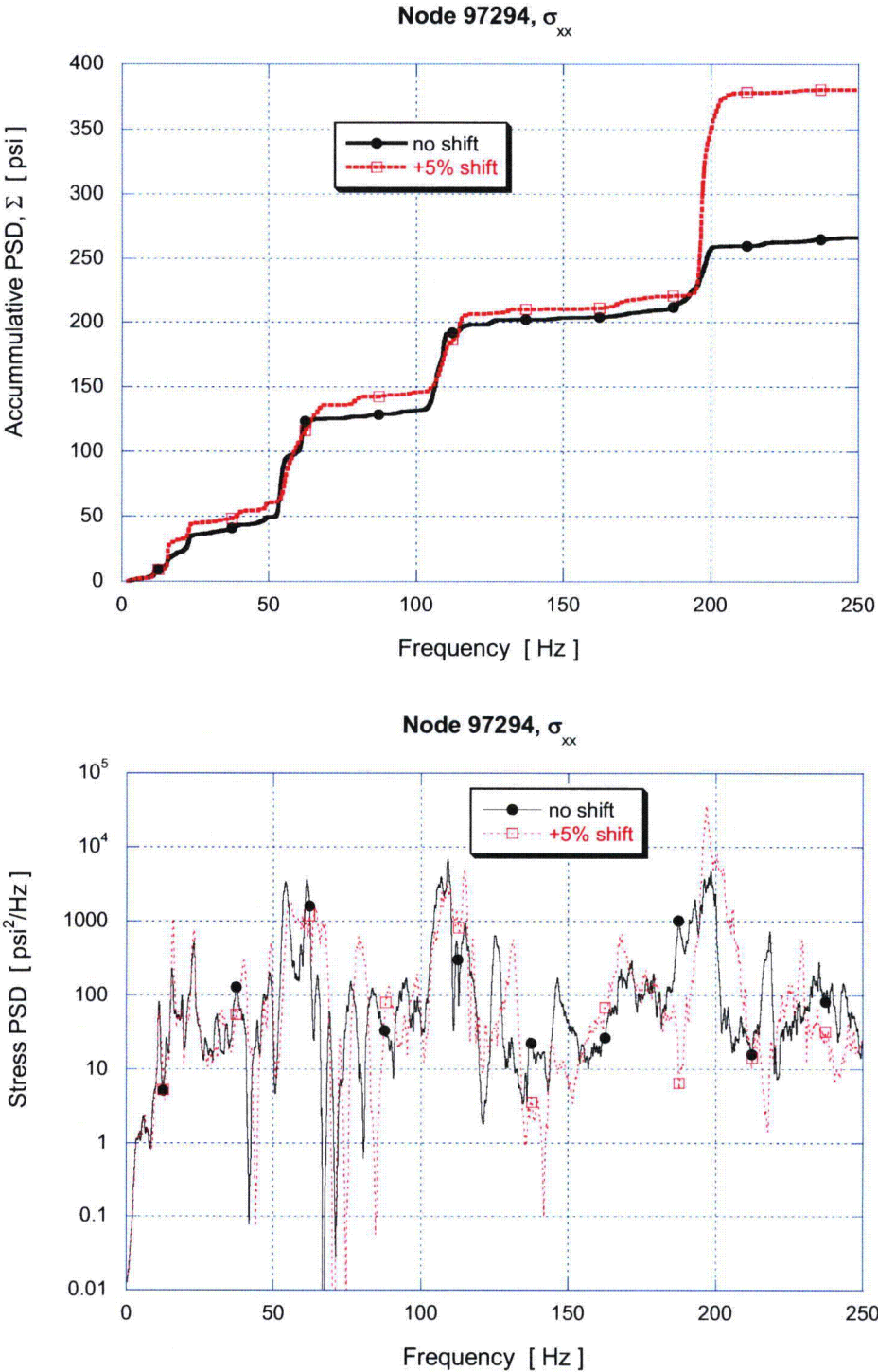


Figure 15c. Accumulative PSD and PSD of the σ_{xx} stress response at node 97,294.

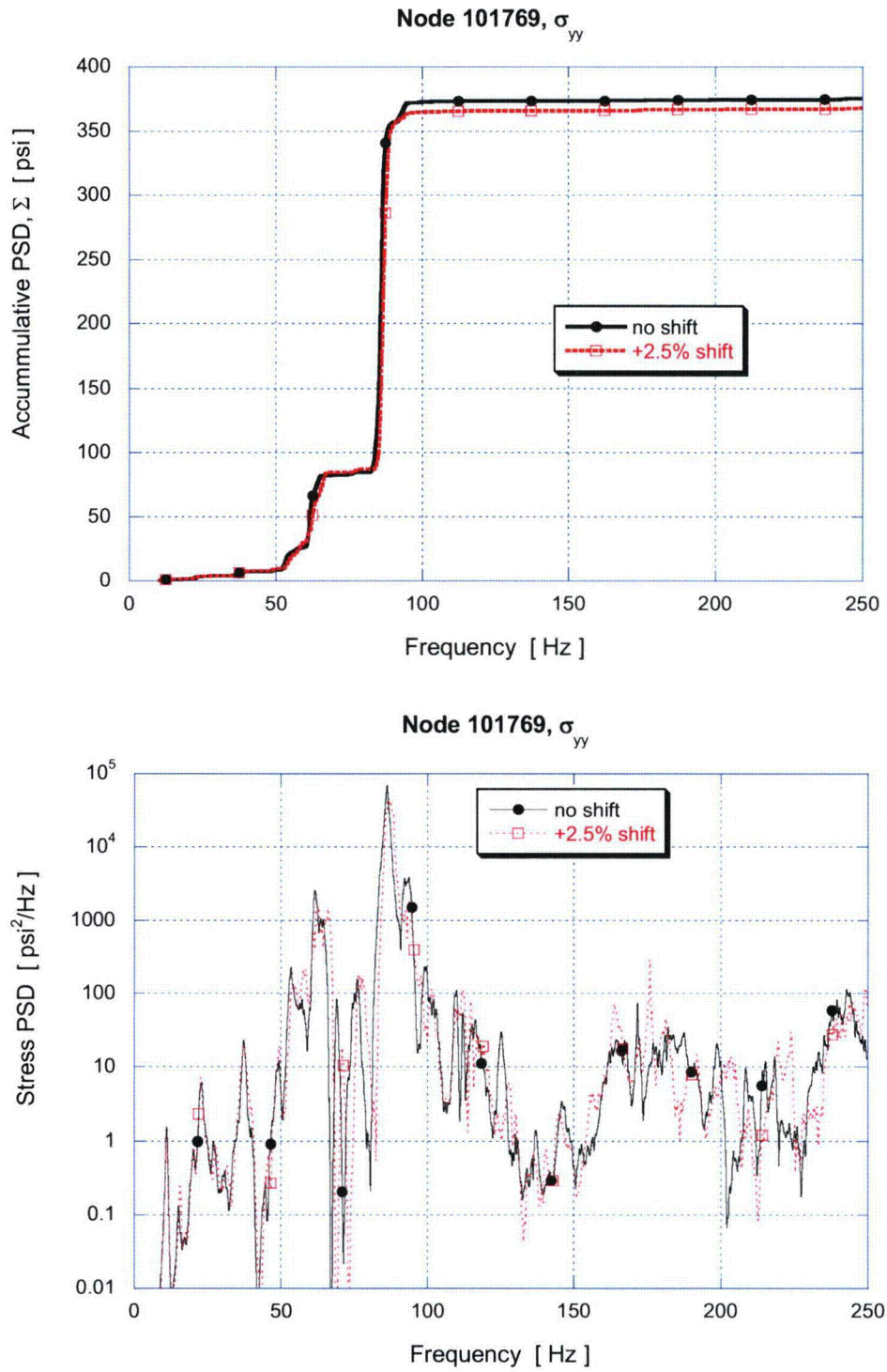


Figure 15d. Accumulative PSD and PSD of the σ_{yy} stress response at node 101,769.

6. Conclusions

A frequency-based steam dryer stress analysis has been used to calculate high stress locations and calculated / allowable stress ratios for the Browns Ferry Unit 2 steam dryer at CLTP load conditions using plant measurement data. A detailed description of the frequency-based methodology and the finite element model for the BFN Unit 2 steam dryer is presented. The CLTP loads obtained in a separate acoustic circuit model [2] including end-to-end bias and uncertainty for both the ACM [2] and FEA were applied to a finite element model of the steam dryer consisting mainly of the ANSYS Shell 63 elements, brick continuum elements and beam elements.

The measured CLTP loads are applied with compensation for background noise based on 1000 psig data taken at 19% power. The resulting stress histories were analyzed to obtain maximum and alternating stresses at all nodes for comparison against allowable levels. These results are tabulated in Table 8 of this report. The minimum alternating stress ratio at nominal operation is $SR-a=2.91$ and the minimum alternating stress ratio taken over all frequency shifts is $SR-a=2.59$. The maximum stress ratio associated with maximum stress intensities varies weakly with frequency shift and assumes a minimum value of $SR-P=1.88$ at zero shift and $SR-P=1.81$ when all frequency shifts are considered.

As part of the power uprate program ASBs will be installed to address the potential onset of FIV in the 109-113 Hz range. When these ASBs are accounted for in the acoustic load and applied to the steam dryer, the minimum alternating stress ratio at any frequency shift increases to $SR-a=2.81$. Assuming that alternating stresses scale approximately with the square of the steam flow speed, then at 115% CLTP the minimum alternating stress ratio is estimated as $SR-a=2.13$ which exceeds the EPU target of $SR-a=2.0$.

7. References

1. Continuum Dynamics, Inc. (2005). "Methodology to Determine Unsteady Pressure Loading on Components in Reactor Steam Domes (Rev. 6)." C.D.I. Report No. 04-09 (Proprietary).
2. Continuum Dynamics, Inc. (2008). "Acoustic and Low Frequency Hydrodynamic Loads at CLTP Power Level on Browns Ferry Nuclear Unit 2 Steam Dryer to 250 Hz with Noise Removed, Rev. 2" C.D.I. Report No. 08-05P (Proprietary)
3. Continuum Dynamics, Inc. (2008). "Stress Assessment of Browns Ferry Nuclear Unit 2 Steam Dryer, Rev. 1," C.D.I. Report No. 08-07P (Proprietary).
4. Continuum Dynamics, Inc. (2007). "Methodology to Predict Full Scale Steam Dryer Loads from In-Plant Measurements, with the Inclusion of a Low Frequency Hydrodynamic Contribution," C.D.I. Report No. 07-09P (Proprietary).
5. Structural Integrity Associates, Inc. 2006. Main Steam Line 100% CLTP Strain Data Transmission. SIA Letter Report No. GSZ-06-017. Files No. 20061128172906 (CLTP), 20061128172419 (Electrical Noise), and 20061022082630 (19% Power Level).
6. ANSYS Release 10.0. URL <http://www.ansys.com>. Documentation: ANSYS 10.0 Complete User's Manual Set.
7. Continuum Dynamics, Inc. (2007). Response to NRC Request for Additional Information on the Hope Creek Generating Station, Extended Power Uprate, RAI No. 14.110
8. Continuum Dynamics, Inc. (2008). "Stress Assessment of Browns Ferry Nuclear Unit 1 Steam Dryer, Rev. 0," C.D.I. Report No. 08-06P (Proprietary).
9. Press, W. H., S. A. Teukolsky, et al. (1992). *Numerical Recipes*, Cambridge University Press.
10. O'Donnell W.J. (1973). "Effective Elastic Constants For the Bending of Thin Perforated Plates With Triangular and Square Penetration Patterns," ASME Journal of Engineering for Industry, Vol. 95, pp. 121-128.
11. Idel'chik, I E. and Fried, E. (1989). *Flow Resistance, a Design Guide for Engineers*, Taylor & Francis, Washington D.C., p 260.
12. DeSanto, D.F. (1981). "Added Mass and Hydrodynamic Damping of Perforated Plates Vibrating in Water," Journal of Pressure Vessel Technology, Vol. 103, p. 176-182.
13. Continuum Dynamics, Inc. (2007). "Dynamics of BWR Steam Dryer Components," C.D.I. Report No. 07-11P

14. U.S. Nuclear Regulatory Commission, (2007). Regulatory Guide 1.20 "Comprehensive Vibration Assessment Program for Reactor Internals During Preoperational and Initial Startup Testing," March 2007.
15. WRC Bulletin 432 (1998). "Fatigue Strength Reduction and Stress Concentration Factors For Welds In Pressure Vessels and Piping," WRC, NY, p.32
16. Pilkey W.D. (1997). *Peterson's Stress Concentration Factors*, 2nd ed., John Wiley, NY, p.139.
17. Lawrence F.V., Ho N.-J., Mazumdar P.K. (1981). "Predicting the Fatigue Resistance of Welds," *Ann. Rev. Mater. Sci.*, vol. 11, pp. 401-425.
18. General Electric (GE) Nuclear Energy (2003). Supplement 1 to Service Information Letter (SIL) 644, "BWR/3 Steam Dryer Failure," September 5, 2003.
19. Tecplot 10 (2004). URL: <http://www.tecplot.com>. Documentation: *Tecplot User's Manual* Version 10 Tecplot, Inc. Bellevue, Washington October.
20. Continuum Dynamics, Inc., Response to NRC RAI EMCB 172, June 2008.
21. Structural Integrity Associates Calculation Package, 0006982.301, "Shell and Solid Sub-Model Finite Element Stress Comparison," June 04, 2008.
22. Continuum Dynamics, Inc. (2008). "Stress Assessment of Browns Ferry Nuclear Unit 1 Steam Dryer with Tie bar Modifications " C.D.I. Report No. 08-15P (Proprietary).

Appendix A. Local Stress Corrections Resulting from Finalized Modification Designs

In order to meet the target alternating stress ratios of $SR-a=2$ at EPU, it will be necessary to implement additional modifications to the existing steam dryers for all three Browns Ferry Units. These consisted chiefly of: (i) the modified tie bars with widened and tapered ends to alleviate stresses at the tie bar/top cover plate welds and (ii) the additional support for the steam dam. The BFN1 dryer design was used to develop the necessary design modifications since EPU will be implemented first. As reported in [22] the BFN1 design changes proved successful and the target stress ratios at EPU were met. The BFN2 /3 dryer design is different however, and additional design changes were necessary to eliminate localized stress concentrations identified on the new design.

For efficiency, these additional changes were analyzed over a reduced frequency range. As discussed below, this analysis is acceptable since these changes produce only localized changes in stresses (i.e., their influence on the global response and modal properties is negligible) and the frequency range considered (70.45 to 95.11 Hz) is responsible for virtually all of the stress contributions at these locations.

Additional Locations Reanalyzed Over Reduced Frequency Range

The modified locations were as follows:

- (i) Additional strengthening of the outermost tie bar/middle hood junction. The apparent cause for the higher stress in this tie bar than in the BFN1 unit appears to be different outer hood structures. In the BFN1 unit the hood supports were removed, the outer hood replaced with a thicker (1" thick) one and reinforcement channels added to the exterior of the hood for additional strength. This design isolates the response of the outer hood from the middle and inner vane bank. In the BFN2 dryer, the older design with interior hood supports and $\frac{1}{2}$ " thick hood more of the load applied on the outer hood face is transmitted to the neighboring middle hood via the tie bar. The stress analysis conducted on BFN2 showed high stress intensities where the tie bar lands on the middle hood cover plate. This is addressed by widening the tie bar where it crosses the vertical hood face from 2" to 3" and adding a vertical reinforcement pad on the middle hood immediately below the tie bar. This vertical pad is tapered and flared like the tie bar ends and is intended to distribute the load over a larger area and onto a stiffer structural component (i.e., the thicker $\frac{1}{2}$ " hood face rather than the $\frac{1}{4}$ " top cover plate).
- (ii) Retraction of the gusset bases and reinforcement of the outer hood top cover plate near the outer hood/top cover plate edge. The design calls for the installation of additional gussets to support the steam dam. In BFN2 five gussets are distributed along the length of the steam dryer (not including the existing smaller gussets at the ends of the steam dam). The original design followed that in BFN1 where the gusset base (located between the gusset above and the top cover plate underneath) extended from the steam dam all the way to the outer hood face. Analysis of this configuration for BFN2 predicted high stresses at the front of this gusset base (i.e., where it meets the outer hood face). Therefore it was decided to retract the gusset base by 2". Analysis of this configuration showed that stresses, while lower on the gusset base, remained high on the top cover

plate/outer hood edge. In the subsequent redesign, the gusset bases were retracted further so that the front of the gusset base is 3" from the vertical hood face. In addition a 3" strip was added along the top cover plate with one edge aligned with the vertical hood plane. This strip is intended to alleviate the stresses along this edge.

- (iii) Installation of steam gussets at the locations where tie bars had previously been planned. In BFN1 the thinner tie bars (denoted here by TB1) originally installed have been replaced by the currently installed thick tie bars (TB2). These thicker tie bars produced high stresses in the vicinity of the tie bar/top vane bank cover plate welds. Therefore it is planned to remove these tie bars and replace them with the new tie bars having flared/tapered ends (TB3) that distribute the stress more evenly. For BFN2, prior to the current suite of design modifications, it had been planned to remove the existing TB1 tie bars and replace them with thicker TB2 tie bars. Hence, all previous analyses had modeled the BFN2 dryer assuming that the TB2 tie bars are in place. Under the current design the TB1 tie bars are replaced directly by TB3 tie bars and there is no need for an intermediate set of TB2 tie bars. Nevertheless, the finite element model used here to analyze the BFN2 unit assumed that the TB2 tie bars were in place. This is of consequence for the tie bars that connect the outer and middle hoods. In the FE model first used in preparation of this report, these TB2 tie bars had been cut at the steam dam and the section extending from the steam dam to the top cover plate retained in place to support the steam dam by means of a lock gusset resting on this tie bar remnant. This model was not appropriate however since in the actual BFN2 dryer, the TB2 tie bars have not been installed. Therefore in the subsequent model revision, the gusset currently installed in the actual dryer is removed and replaced by the larger and extended gussets with a gusset base

In order to evaluate the stresses at these locations only, a revised structural FEA model with these modifications incorporated was developed and analyzed over the reduced frequency range, 70.45 - 95.11 Hz. The model is depicted in Figure 2 and Figure 3. The stress intensities at these locations only were then re-evaluated using the procedure described below and reported in Table 7 and Table 8.

Finite Element Model Summary

To clarify how the stresses at the modified locations (i) to (iii) above and also other locations on the dryer, it is useful to summarize the three finite element models that have been used for BFN2.

FEA Model 0 This refers to the BFN2 dryer model used in [3] before any of the modifications in the present report were made. It contains the thick TB2 tie bars which are currently installed in BFN1. It had previously been planned to install them in the BFN2 and BFN3 units also, but this is no longer the case since the TB2 designs have been superseded by the TB3 designs. This model is not used in the current report.

FEA Model 1 This model was derived from Model 0 by replacing the tie bars with ones having flared and tapered ends. Also, additional gussets were introduced to support the steam dam. A complete stress analysis over the complete 0-250 Hz frequency range was carried out using this model.

FEA Model 2. This model was derived from Model 1 by incorporating the additional design changes (i) to (iii) above. A stress analysis over the reduced frequency range was carried out using this model and combined with the Model 1 results to calculate the stresses at the redesigned locations.

Justification for Reduced Frequency Range Analysis

Justification for a reduced frequency range analysis to accurately analyze the stresses at the three locations (i) to (iii) above, rests on two observations. First, the modifications (i) to (iii) produce localized changes and redistributions of stress, but do not significantly affect the response elsewhere on the dryer. Secondly, most of the stress contribution originates from the 70.45-95.11 Hz frequency range. These observations are discussed next.

Each modification is highly localized and, importantly, does not significantly alter the modal properties of the overall steam dryer. This follows from the observation that each modification is both geometrically small and also is unlikely to significantly alter modal frequencies in the 0-250 Hz range of interest here. The latter can be inferred from simple integral relations for the frequency, ω_n , mass and stiffness matrices, \mathbf{M} and \mathbf{K} , and mode shapes, Φ_n :

$$\omega_n^2 = \frac{\Phi_n^T \mathbf{K} \Phi_n}{\Phi_n^T \mathbf{M} \Phi_n} \quad (\text{A.1})$$

For the modes of interest here (i.e., with lower frequencies of interest and participation by the modified parts), the mode shapes tend to involve significant portions of the dryer such as the hood. This indicates that for these modes the changes in mass and stiffness, $\delta\mathbf{M}$ and $\delta\mathbf{K}$, due to the localized modifications in (i) to (iii) above are such that $\Phi_n^T(\delta\mathbf{K})\Phi_n \ll \Phi_n^T \mathbf{K} \Phi_n$ and $\Phi_n^T(\delta\mathbf{M})\Phi_n \ll \Phi_n^T \mathbf{M} \Phi_n$. Another way to see this is that if the characteristic size of the design modification is c (for example, $c=2''$ in the case of the retracted gusset bases) and the characteristic wavelength of the mode, Φ_n , is L , then approximately the change in ω_n^2 is on the order of $(c/L)^2$. In the case of the hoods L is on the order of 60" so that $(c/L)^2$ is on the order of $(2''/60'')^2 < 0.12\%$. Additional evidence for the essential invariance of the modal frequencies, at least those of most relevance to the stress state, is found in the results below. The dominant frequency that contributes the most to the stresses at the locations (i) and (ii) above, is 81.5 Hz before the local modifications. After the modifications the dominant frequency remains at the same frequency.

The FEA analysis with the modifications (i) to (iii) in place is limited to the frequency range 70.45-95.11 Hz. To show that this range is the dominant stress contributor at these locations the stress intensities are calculated in the original model (i.e., prior to modifications (i) to (iii)) using the following modified loads:

- Load A: The complete MSL signals, $P(f)$, over the entire 0-250 Hz range.
- Load B: The same as Load A, but with the signals zeroed over the ranges 0-70.45 Hz and 95.11-250 Hz.

The alternating stress results for the components (i) – (iii) at welds are shown below in Table A1. These results show that for nodes involving the gusset pads (component (ii)) the reduced frequency range loads capture 95.7% of the limiting stress intensities obtained when applying the complete signal. Similarly, for the tie bar/middle vane bank cover plate location (location (i)) the reduced frequency range load reproduces 91.8% of the full stress intensity and at the lock gusset location (location (iii)) it reproduces 85.6% of the full stress intensity. From this one infers that the reduced frequency range signal adequately captures the stress intensities.

Table A1. Limiting alternating stresses intensities and ratios at any frequency shift calculated using: Load A (the full signal over the 0-250 Hz frequency range) and Load B (the signal over the 70.45 - 95.11 Hz frequency range).

Location	node	Alternating Stress Intensity (psi)		$\frac{(S_{alt})_{B1}}{(S_{alt})_{A1}}$	Alternating Stress Ratio		% Freq. Shift	
		Load A	Load B		Load A	Load B	Load A	Load B
1. Outer Hood/Gusset Pad Thin/Top Cover Outer Hood	108730	5816	5565	95.7	1.18	1.23	-5	-5
2. Outer Hood/Gusset Pad Thin/Top Cover Outer Hood	108664	5631	5172	91.8	1.22	1.33	-10	-10
3. Top Cover Middle Hood/Middle Hood/Shell Tie Bar	107158	4486	4377	97.6	1.53	1.57	-5	-5
4. Old tie bar/top cover plate	134490	3446	2950	85.5	1.99	2.33	0	0

Stress Calculations for Revised Components

For each of the modified locations (i) to (iii) the stress intensities are calculated by the formula:

$$S_{alt} = (S_{alt})_{B2} + \{ (S_{alt})_{A1} - (S_{alt})_{B1} \} \tag{A.2}$$

where:

- $(S_{alt})_{A1}$ is the alternating stress intensity computed using Model 1 and the load over the entire frequency range (0-250 Hz);
- $(S_{alt})_{B1}$ is the alternating stress intensity computed using Model 1 and the load over the reduced frequency range (70.45-95.11 Hz);
- $(S_{alt})_{B2}$ is the alternating stress intensity computed using Model 2 at the same location using the load over the reduced frequency range.

This effectively takes the Model 1 stress prediction, and replaces the stress contribution over the 70.45-95.11 Hz range by the Model 2 prediction. It is conservative since the contribution from the remaining frequency range (0 to 70.45 Hz and 95.11 to 250 Hz) is left at the Model 1 prediction whereas in actuality one expects this stress contribution to also be reduced since the changes in (i) to (iii) above involve thickening of the higher stress regions which reduces stress contributions at all frequencies. Finally, since the models are different locally at the places of

interest, the task of matching nodes in the preceding formula must be addressed. This is done as follows. The low stress ratio nodes are first identified using Model 1 for which the full frequency solution is available. $(S_{alt})_{A1}$ and $(S_{alt})_{B1}$ are computed at each such node, n_1 . The correction, $(S_{alt})_{B2}$ is then obtained by calculating the stress intensities at a collection of nodes $\{n_2\}$ in Model 2 that are on welds and that are closest to the high stress intensity node, n_1 , of Model 1. Of this collection of Model 2 nodes, $\{n_2\}$, the one having the highest stress intensity is selected to represent $(S_{alt})_{B2}$ in the preceding formula (A.2).

ENCLOSURE 11

**TENNESSEE VALLEY AUTHORITY
BROWNS FERRY NUCLEAR PLANT (BFN)
UNITS 1, 2, AND 3**

**TECHNICAL SPECIFICATIONS (TS) CHANGES TS-431 AND TS-418
EXTENDED POWER UPRATE (EPU)**

**CDI REPORT NO. 08-05NP, "ACOUSTIC AND LOW FREQUENCY HYDRODYNAMIC LOADS
AT CLTP POWER LEVEL ON BROWNS FERRY NUCLEAR UNIT 2 STEAM DRYER TO
250 HZ"**

(NON-PROPRIETARY VERSION)

Attached is the **Non-Proprietary Version** of CDI Report No. 08-05, "Acoustic and Low Frequency Hydrodynamic Loads at CLTP Power Level on Browns Ferry Nuclear Unit 2 Steam Dryer to 250 Hz."